MASTERARBEIT | MASTER'S THESIS

Titel | Title

Investigation of host and environmental microbiomes and the mercury detoxification strategies of two Caiman species in French Guiana.

verfasst von | submitted by

Mason Hanson Scarpa BSc

angestrebter akademischer Grad | in partial fulfilment of the requirements for the degree of

Master of Science (MSc)

Wien | Vienna, 2025

Studienkennzahl lt. Studienblatt | Degree programme code as it appears on the student record sheet:	UA 066 220
Studienrichtung lt. Studienblatt | Degree programme as it appears on the student record sheet:	Joint-Masterstudium Evolutionary Genomics and Systems Biology
Betreut von | Supervisor:	Assoz. Prof. Maria Filipa Baltazar de Lima de Sousa PhD

Table of Contents

1 Abstract (German)

Die Belastung mit Schwermetallen gehört weltweit zu den am weitesten verbreiteten Gefahren für Umwelt und menschliche Gesundheit (Briffa et al., 2020). Der kleingewerbliche und handwerkliche Goldbergbau (ASGM) erhöht die Quecksilber-Belastung (Hg) in Französisch-Guayana, doch die Folgen für mit Wildtieren assoziierte Mikrobiome und das mikrobielle Hg-Entgiftungspotenzial sind bislang unzureichend verstanden. Wir untersuchten Boden-, Haut- und Kloakenmikrobiome zweier Kaimanarten, *Melanosuchus niger* und *Paleosuchus trigonatus*, die entlang eines Umwelt-Hg-Gradienten beprobt wurden, und erfassten das Quecksilberreduktase-Gen (merA), um das Entgiftungspotenzial zu beurteilen. Die Zusammensetzung der Mikrobiome wurde vor allem durch das Umweltkompartiment und die Geographie bestimmt, mit dem stärksten Wirteinfluss in Kloaken-Gemeinschaften. Hg war ein zusätzlicher Treiber für Verschiebungen der Bodengemeinschaften, während wirtassoziierte Gemeinschaften entlang des Gradienten vergleichsweise geringe Änderungen der Zusammensetzung zeigten. Die Alpha-Diversität unterschied sich zwischen Gruppen mit niedriger und hoher Hg-Belastung nicht konsistent; bei höherer Hg-Exposition beobachteten wir jedoch eine Tendenz zu verminderter Diversität in Kloakenmikrobiomen und erhöhtem Artenreichtum in Hautmikrobiomen. Netzwerkanalysen deuteten darauf hin, dass Bodengemeinschaften an Standorten mit hoher Hg-Belastung weniger vernetzt waren und mutmaßliche Schlüssel-Taxa verloren, im Einklang mit einer stressbedingten Vereinfachung. Im Gegensatz dazu blieben Haut- und Kloaken-Netzwerke über den Gradienten hinweg topologisch stabil. Über alle Kompartimente hinweg detektierten wir merA-Varianten aus mehreren bakteriellen Phylen, was auf wiederholte Aneignung über verschiedene Abstammungslinien hindeutet. Das Auftreten von merA war zwischen den Umwelten unregelmäßig und folgte nicht den gemessenen Hg-Konzentrationen, was eher auf Selektion im Maßstab des Mikrohabitats und eine heterogene Bioverfügbarkeit von Hg als auf eine einheitliche Anpassung an Hg-Stress schließen lässt. Diese Ergebnisse zeigen, dass Böden sensibel auf Hg-Störungen reagieren, während kaimanassoziierte Mikrobiome unter den derzeitigen Expositionsbedingungen relativ stabil bleiben.

2 Abstract

Heavy metal contamination is one of the most widespread threats to both environmental and human health worldwide (Briffa et al., 2020). Artisanal and small-scale gold mining (ASGM) elevates mercury (Hg) exposure in French Guiana, yet its consequences for wildlife-associated microbiomes and microbial Hg detoxification potential are not well understood. We examined soil, skin, and cloacal microbiomes of two caiman species, *Melanosuchus niger* and *Paleosuchus trigonatus*, sampled along an environmental Hg gradient, and surveyed the mercuric reductase gene (*merA*) to evaluate resistance potential. Microbiome composition was structured chiefly by environment and geography, with the strongest host signal in cloacal communities. Hg was an additional driver of community shifts in soils, whereas host-associated communities exhibited comparatively modest compositional changes across the gradient. Alpha diversity did not differ consistently between low- and high-Hg groups; however, we observed a tendency toward reduced cloacal diversity and increased skin richness at higher Hg exposure. Network analyses indicated that soil communities in high-Hg sites became less connected and lost putative keystone taxa, consistent with stress-induced simplification. In contrast, skin and cloacal networks remained topologically stable across the gradient. Across compartments, we recovered *merA* variants spanning multiple bacterial phyla, suggesting repeated acquisition across lineages. *merA* occurrence was irregular among environments and did not track measured Hg, pointing to microhabitat-scale selection and patchy Hg bioavailability rather than uniform adaptation to Hg stress. These findings identify soils as sensitive to Hg disturbance while indicating relative stability of caiman-associated microbiomes under current exposure regimes.

3 Introduction

3.1 Mercury as a Global Contaminant

Heavy metal contamination is one of the most widespread threats to both environmental and human health worldwide (Briffa et al., 2020). Heavy metals are broadly defined as elements with high atomic density or weight that can be toxic even at low levels (Järup, 2003; Lenntech, 2004). While some metals like zinc (Zn), copper (Cu), and manganese (Mn) are essential micronutrients and serve as enzyme cofactors (Mildvan, 1970; Sharma & Agrawal, 2005), others, such as mercury (Hg), cadmium (Cd), arsenic (As), and lead (Pb), have no known biological role in humans and are toxic even at trace amounts (Holum, 1983; Fosmire, 1990).

Mercury (Hg) is a highly toxic heavy metal and due to its persistence, bioaccumulation, and neurotoxicity it is ranked among the top three most hazardous substances (ATSDR 2024). Although naturally present in the Earth's crust, anthropogenic activities have greatly expanded its global distribution and risk; major sources include coal combustion, non-ferrous metal production, waste incineration, cement production, and especially artisanal and small-scale gold mining (ASGM) (Pirrone et al., 2010; Kocman et al., 2017). In ASGM, Hg is used for amalgamation and is released via volatilization and discharge to soils and waters, driving persistent contamination of terrestrial and aquatic ecosystems (Esdaile & Chalker, 2018). In South America, ASGM emits over 1,600 tons of Hg annually, contaminating river systems such as the Amazon Basin and the Guiana Shield (Veiga et al., 2014; Legg et al., 2015). Globally, ASGM is the largest single source of anthropogenic Hg (38% of atmospheric emissions), with impacts amplified in tropical forests where high rainfall and acidic, organic-rich soils enhance Hg mobility and methylation (AMAP, 2021). Once released, Hg undergoes atmospheric transport, deposition, re-volatilization, and transformation, increasing the global Hg pool by transferring Hg from lithospheric to atmospheric and aquatic compartments (Driscoll et al., 2013). Secondary re-emissions from land and oceans complicate source attribution (Mason & Sheu, 2002; Selin, 2009) and enable long-range transport and deposition, including in seemingly pristine regions.

The toxicity and ecological threat of mercury are not solely a function of total mercury concentrations but depend on chemical speciation. Elemental mercury (Hg^0), while volatile and mobile, is less toxic than its oxidized (Hg^{2+}) and organic forms (e.g. methylmercury). Inorganic divalent mercury (Hg^{2+}) can be transformed by anaerobic microbes, especially sulfate-reducing, iron-reducing, and methanogenic bacteria, into methylmercury (MeHg), a highly bioavailable and neurotoxic compound (Ullrich et al., 2001; Parks et al., 2013). When formed, MeHg can readily enter aquatic food webs where it bioaccumulates in organisms and biomagnifies with each trophic level (Lavoie et al., 2013; Eagles-Smith et al., 2018). This leads to apex predators such as large fish, birds, and reptiles exhibiting the highest tissue concentrations. The risk is increased by the slow excretion rates of MeHg, its strong

binding to thiol groups in proteins, and its ability to cross the blood-brain and placental barriers, causing neurodevelopmental damage in both wildlife and humans (Clarkson et al., 2006; Eagles-Smith et al., 2018).

3.2 Study Site and Focal Species

3.2.1 Study Site

This study was carried out in French Guiana, part of the Guiana Shield, which is heavily affected by ASGM, a predominant source of mercury contamination in soils and waterways (Veiga et al., 2014; Legg et al., 2015; AMAP, 2021). The tropical climate, high rainfall, acidic soils, and wetlands increase mercury mobility and methylation, causing spatial variation in mercury exposure (Driscoll et al., 2013). Two caiman species found in French Guiana are the focus of this study: the Black Caiman (*Melanosuchus niger*), which inhabits coastal swamps, and the Smooth-fronted Caiman (*Paleosuchus trigonatus*), found in closed-canopy forest streams and terrestrial edges (Lemaire et al., 2022).

3.2.2 Current Research on Heavy Metals and Crocodilians

Research on heavy metal accumulation in crocodilians is well established, with numerous studies documenting contaminant exposure across species and regions. As long-lived, apex predators in aquatic ecosystems, crocodilians are frequently exposed to non-essential trace metals such as mercury, arsenic, cadmium, and lead, and have been widely used as bioindicators of environmental pollution. Exposure occurs primarily through ingestion of contaminated prey, dermal contact with sediments, and, in some cases, maternal transfer to offspring (Smith et al., 2007). Trophic position has been shown to be the main source of variation in mercury contamination in *M. niger* (Lemaire et al., 2020). Much of the foundational work has focused on the American alligator (*Alligator mississippiensis),* which has been used extensively to monitor Hg contamination in wetlands. Studies have shown that alligators from polluted habitats accumulate high concentrations of mercury in liver, kidney, and muscle tissues, and that Hg levels tend to increase with age (Heaton-Jones et al., 1997; Yanochko et al., 1997; Khan & Tansel, 2000). Longitudinal comparisons in the Florida Everglades even suggest temporal changes in contamination levels, likely linked to regional remediation efforts (Rumbold et al., 2002). Similar patterns of bioaccumulation have been observed in other species. In *Crocodylus moreletii*, mercury concentrations correlate positively with body size, and in some Mexican populations, levels of Hg and other metals in eggs and scutes exceed regulatory thresholds (Buenfil-Rojas et al., 2015; Cedillo-Leal et al., 2018). In Brazil, free-ranging *Caiman crocodilus* individuals from the Rio Negro exhibited elevated levels of As, Pb, and Ni compared to captive conspecifics, underscoring the influence of habitat and local contamination (Barbosa et al., 2003).

3.2.3 Mercury Contamination in Neotropical Caimans of French Guiana

Mercury contamination in aquatic ecosystems has been documented in French Guiana, where both *M. niger* and *P. trigonatus* have been the subject of recent research (Lemaire, 2023; Lemaire et al., 2024a). These studies have shown that mercury accumulates in caiman tissues and that exposure varies by species, sex, body size, and trophic level (Lemaire et al., 2021a; Lemaire et al., 2022; Lemaire et al., 2024a). Non-invasive sampling methods, such as caudal scutes, have been validated as reliable indicators of individual mercury burden (Lemaire, 2023). In addition to accumulation patterns, mercury and other trace elements such as lead and selenium have been associated with physiological effects in wild caimans, including altered blood parameters and body condition indices (Lemaire et al., 2021b). Mercury has also been shown to transfer from females to their offspring, resulting in detectable levels in neonates and raising concerns about early-life exposure (Lemaire, 2023).

A well-established vertebrate detoxification pathway involves selenium (Se), a trace element with antioxidant and endocrine roles that binds Hg to form biologically inert Se-Hg complexes, reducing Hg bioavailability and toxicity (Beijer & Jernelöv, 1978; Ralston et al., 2008; Ralston & Raymond, 2010). In French Guiana caimans, species-specific Se:Hg molar ratios differ; *M. niger* shows lower Se:Hg than *P. trigonatus*, suggesting contrasts in dietary exposure and detoxification capacity (Lemaire et al., 2022). These interspecific differences indicate *M. niger* may be employing alternative detoxification methods motivating the evaluation of additional detoxification pathways, including microbiome-mediated mechanisms. Across hosts and environments, pollutants such as Hg alter microbial community composition, reduce diversity, and select for resistant taxa, including those carrying detoxification pathways like the *mer* operon (Barkay et al., 2003; Handy et al., 2023). Few studies have examined metal effects on crocodilian microbiota; for example, work in *Alligator mississippiensis* investigated dietary Se impacts on gut and cloacal communities (Kieran et al., 2020). Comparable field studies for Hg in neotropical caimans are lacking. This gap is interesting because microbiome shifts at the host-environment interface can modulate contaminant processing and thereby influence toxicity. While Hg exposure in *M. niger* and *P. trigonatus* has been documented in French Guiana, the responses of associated microbiomes to Hg contamination and the potential contribution of microbial resistance determinants to Hg handling remain unknown. This study addresses this gap by characterizing the taxonomic composition and detoxification potential of host-associated (cloaca and skin) and environmental (associated soils) microbiomes in both species.

3.3 Roles of Microbes in Hg Transformation

3.3.1 Mercury Methylation

Microorganisms play a central role in the environmental transformation and toxicity of mercury (Barkay et al., 2003; Ullrich et al., 2001). While elemental mercury (Hg^0) and divalent inorganic mercury (Hg^{2+}) can persist in the abiotic environment, it is the microbial conversion of Hg^{2+} to methylmercury (MeHg)

that generates the most ecologically and toxicologically significant form of mercury (Driscoll et al., 2013; Gilmour et al., 2013). Methylmercury is more soluble, more readily assimilated by organisms, and far more neurotoxic than its inorganic precursors (Clarkson et al., 2006; Sanfeliu et al., 2003). As such, the process of mercury methylation is the critical step that determines mercury's entry into aquatic food webs and its subsequent biomagnification (Ullrich et al., 2001; Eagles-Smith et al., 2018). Methylation of mercury is primarily a biological process that occurs under anoxic or suboxic conditions, typically in sediments, flooded soils, and biofilms (Compeau & Bartha, 1985; Kerin et al., 2006).

The genetic basis for microbial mercury methylation was found with the discovery of the *hgcAB* gene cluster (Parks et al., 2013). The *hgcA* gene encodes a corrinoid protein that facilitates methyl group transfer to Hg^{2+}, while *hgcB* encodes a ferredoxin that regenerates the reduced state of the corrinoid cofactor (Smith et al., 2015; Gilmour et al., 2013). Together, these genes form a conserved operon for the methylation of Hg^{2+} in laboratory and environmental settings (Parks et al., 2013; Podar et al., 2015). Phylogenomic surveys have detected *hgcAB* across diverse taxonomic groups, including DeltaPseudomonadota, Bacillota (e.g., Clostridia), and Methanobacteriota (e.g., Methanomicrobia), indicating that mercury methylation potential is both phylogenetically and ecologically widespread (Gilmour et al., 2013; Podar et al., 2015; Christensen et al., 2016). Horizontal gene transfer is believed to have played a major role in spreading the *hgcAB* operon across evolutionary lineages (Ranchou-Peyruse et al., 2009; Bae et al., 2014). Methylators have now been detected in a wide array of ecosystems, including wetlands, peatlands, paddy soils, aquatic sediments, and, more recently, in animal-associated microbiomes (Podar et al., 2015; Yu et al., 2013).

In tropical freshwater systems, such as those found in the Guiana Shield, conditions frequently favor net Hg(II) methylation. High rainfall, low pH, abundant organic matter, and seasonally anoxic sediments promote microbial processes associated with Hg transformation (Oberkircher, 2019; Barbieri & Gardon, 2009). These habitats also receive high loads of inorganic Hg from ASGM, creating ideal conditions for microbial conversion to MeHg and subsequent entry into aquatic food webs (Legg et al., 2015; Veiga et al., 2014). Understanding the role of microbes in the mercury cycle is important when explaining spatial and temporal variations in MeHg production and the exposure of apex predators, such as caimans (Lemaire et al., 2021; Eagles-Smith et al., 2018).

3.3.2 Mercury detoxification

While mercury methylation increases toxicity and bioavailability, microorganisms have also evolved mechanisms to detoxify mercury and mitigate its cellular effects. The most well-characterized system for microbial mercury resistance is the mer operon, which encodes a suite of proteins that collectively convert toxic divalent mercury (Hg^{2+}) into less toxic elemental mercury (Hg^0), thereby reducing mercury's biological impact (Barkay et al., 2003; Mathema et al., 2011). This enzymatic detoxification

process enables mercury-resistant bacteria (MRB) to survive in contaminated environments, where they often dominate microbial communities (Müller et al., 2001; Nascimento & Chartone-Souza, 2003).

The central component of the mer operon is the gene merA, which encodes the flavin-dependent enzyme mercuric reductase (MerA) (Osborn et al., 1997). MerA catalyzes the reduction of Hg^{2+} to Hg^{0} using electrons from NADPH, a reaction that allows the volatile and lipid-soluble Hg^{0} to diffuse from the cell without a dedicated efflux system (Barkay et al., 2003; Mathema et al., 2011). Alternative mechanisms to enzymatic detoxification via the mer operon involve membrane-bound efflux systems that actively transport divalent mercury (Hg^{2+}) out of the cell, thereby lowering intracellular concentrations and preventing damage to cellular components (Nies, 1999; Silver & Phung, 2005). Some bacteria also produce extracellular polymeric substances (EPS), which can bind heavy metals at the cell surface, limiting their entry into the cytoplasm and reducing toxic effects (Gupta & Diwan, 2017). MerA is therefore distinct from other heavy metal resistance strategies that rely on sequestration or efflux, as it directly alters mercury speciation and thereby its toxicity (Barkay et al., 2003; Nies, 1999).

In addition to merA, the mer operon can include genes for mercury uptake and regulation. These include merP, a periplasmic mercury-binding protein; merT and merC, inner membrane transport proteins; and merR, a regulatory protein that induces operon expression in the presence of Hg^{2+} (Narita et al., 2003; Barkay et al., 2003). Variants can also contain merB, an organomercurial lyase that cleaves carbon-mercury bonds in compounds such as methylmercury, allowing merA to complete the detoxification process (Lal & Lal, 2009; Krout et al., 2022). There are two categories of mercury resistance. Broad-spectrum mercury resistance is based on the presence of merB, allowing organisms to degrade both inorganic and organic mercury species (Clark et al., 1977; Mathema et al., 2011). Narrow-spectrum mercury resistance means that the organism is resistant to inorganic Hg^{2+} but sensitive to organomercurials (Clark et al., 1977). MerB has been found in the absence of merA; however, demethylation of MeHg, which occurs without *merA* present, has been shown to result in greater cytotoxicity and increased cell lysis (Krout et al., 2022). Phylogenetic analysis suggests that *merB* was recruited recently, which is consistent with the dependence of *merB* on *merA* (Christakis et al., 2021).

The mer operon has been identified across a broad array of bacterial and archaeal lineages. It is particularly prevalent in Pseudomonadota (Alpha-, Beta-, and Gamma-classes), Actinomycetota, and Bacillota , including genera such as Pseudomonas, Shewanella, Bacillus, Staphylococcus, and Streptomyces (Barkay et al., 2010; Nascimento & Chartone-Souza, 2003). Among the Archaea, *merA* has been identified in thermophilic lineages, such as Thermoproteota and Methanobacteria, suggesting that resistance mechanisms evolved under naturally high-mercury conditions, including geothermal or hydrothermal systems, but also extend to mesothermal environments with moderate temperatures (Christakis et al., 2021). In aquatic environments, mer genes are commonly detected in biofilms,

estuarine sediments, and contaminated riverbeds (von Canstein et al., 1999; Ghosh et al., 2015). Importantly, the mer operon is often located on mobile genetic elements, such as plasmids, transposons, and integrative conjugative elements, which facilitate horizontal gene transfer and enable the rapid spreading of resistance traits within microbial communities (Barkay et al., 2003; Osborn et al., 1997). This helps explain the wide phylogenetic distribution of the operon and its presence in environmental samples from various habitats, including agricultural soils, wastewater, marine sediments, and animal gut microbiomes (Pal et al., 2015; Yu et al., 2025).

Microbial detoxification also plays a key role in modulating net methylmercury production at the ecosystem level. By reducing the local availability of Hg^{2+}, merA activity can inhibit microbial methylation and thus lower MeHg concentrations in aquatic systems (Barkay et al., 2003; Ravichandran, 2004). Experimental and field studies have demonstrated a negative correlation between MRB abundance and MeHg accumulation, supporting this antagonistic interaction (Schaefer et al., 2004; Kane et al., 2016; Panahi et al., 2022). Due to the central role that merA plays, it is widely used as a molecular marker for mercury resistance; however, its presence alone does not guarantee phenotypic resistance. The effectiveness of mercury detoxification in situ depends on several factors, including gene expression levels, operon organization, regulatory mechanisms, and the availability of required cofactors (Trojańska et al., 2022; Sotero-Martins et al., 2008).

3.3.3 Effect of Mercury on Microbiomes

Mercury exposure alters microbial communities across environments, with documented effects in soils, aquatic sediments, and animal and human gastrointestinal tracts (Frey & Rieder, 2013; Frossard et al., 2018; Li et al., 2022; Chen et al., 2018; Conteville et al., 2023; Rowland et al., 2018). As a selective stressor, Hg often reduces overall diversity and enriches taxa carrying mercury resistance genes such as merA (Barkay et al., 2003; Mathema et al., 2011). Reported taxonomic shifts increases in *Pseudomonadota, Bacillota , Bacteroidetes*, and other opportunistic or resistant groups (Liu et al., 2018; Mahbub et al., 2017) in addition to negative impact on ammonium oxidizers and nitrifiers (Mahbub et al., 2017). Functionally, Hg disrupts key processes, including ammonia oxidation, methanogenesis, and sulfate and iron cycling (Liu et al., 2010; Achá et al., 2011; Yu et al., 2013). Sulfate-reducing and iron-reducing bacteria involved in methylmercury formation are inhibited at high Hg but can persist under chronic exposure through acquisition of resistance genes (Cabral et al., 2016; Parks et al., 2013).

However, most work mentioned above addresses free-living communities; host-associated microbiomes are less studied despite evidence that metal contamination shifts these assemblages with consequences for host health and contaminant processing (Conteville et al., 2023; Handy et al., 2023). Experimental models show that Hg exposure can drive gut communities toward taxa harboring metal resistance operons (Zhang et al., 2022).

3.3.3.1 Soil Microbiome

Soils host diverse microbial communities that mediate carbon and nitrogen cycling and transform trace elements, including mercury (Fierer, 2017; Islam et al., 2020). Across contamination gradients, Hg typically reduces taxonomic richness and shifts community composition toward tolerant or resistant taxa (Frey and Rieder, 2018; Frossard et al., 2017; Liu et al., 2018; Li et al., 2022). Under anoxic conditions, sulfate- and iron-reducing Deltaproteobacteria increase and are implicated in methylmercury production, linking community change to enhanced Hg bioavailability (Kerin et al., 2006; Gilmour et al., 2013). The magnitude and direction of these shifts depend on total Hg, speciation, and site geochemistry, with threshold responses reported (Frossard et al., 2017; Zheng et al., 2022; Frey & Rieder, 2013).

3.3.3.2 Skin Microbiome

Vertebrate skin hosts dynamic microbial communities that are primarily shaped by environmental factors, alongside host physiology and geography (Ross et al., 2019; Grice et al., 2008; Kueneman et al., 2014). Among these, the environment exerts the strongest influence on skin community structure, often overriding phylogenetic constraints such as host order or broad geographic location. This is particularly evident in amphibians, where local ecology and infection can dominate, reducing microbial diversity regardless of the species' evolutionary history (Ross et al., 2018; Kirsch et al., 2024). Environmental complexity is also linked to increased microbial richness and enhanced resistance to disturbance, underscoring its central role in maintaining diverse and resilient skin microbiomes (Harrison et al., 2017).

External skin microbiomes respond to pollutants, including heavy metals, through shifts in taxonomic composition and functional traits that promote stress resistance and detoxification. For example, metal exposure in amphibians is associated with an increased relative abundance of taxa carrying antibiotic and detoxification genes, as well as microbial community changes that may reduce arsenic permeability at the host-microbe interface (Su et al., 2023; Cordeiro et al., 2024). These findings motivate investigations into similar adaptive microbial responses to mercury and other contaminants in reptilian skin microbiomes.

Crocodilians are semi-aquatic and experience variable physical and chemical conditions; their dorsal skin bears ridges and ossified scutes, whereas the ventral surface is flatter, creating distinct microhabitats influenced by light, water column, and sediment contact (Kieran et al., 2020). Despite clinical reports of pathogens in captive or diseased individuals, baseline composition and functions of healthy crocodilian skin microbiomes remain poorly characterized (Isberg et al., 2018; Turutoglu et al.,

2005). Mercury-exposed river and sediment biofilms often show reduced diversity and enrichment of mercury-resistant taxa, including carriers of mer operons (Cabral et al., 2016; Chen et al., 2018). Given the extensive sediment contact of caiman skin, it likely harbors microbiomes shaped by local mercury levels. Our study examines whether mercury contamination decreases microbial diversity and promotes the selection of mercury-resistant bacteria on the caiman skin surface.

3.3.3.3 Cloacal Microbiome

The cloaca is a shared exit for digestive, urinary, and reproductive tracts in reptiles and other vertebrates, functioning as a conduit for excretion, copulation, and oviposition (van Dongen et al., 2013; Silva et al., 2022). Because of its dual exposure to internal and external environments, the cloaca integrates microbial inputs from the gut and surroundings, resulting in a microbiome comprised of both host-associated and environmentally acquired taxa. While cloacal swabs are frequently used as non-invasive proxies for gut microbiomes in reptiles and birds, they may not capture the full diversity of the distal gastrointestinal tract, particularly obligate anaerobes (van Dongen et al., 2013; Silva et al., 2022). Bacterial genera identified in crocodilian cloacae include typical gut residents such as Clostridium, Bacteroides, and Fusobacterium (Lovely and Leslie, 2008; Silva et al., 2009; Charruau et al., 2012; Keenan et al., 2013). Fungal species, likely introduced via soil, water, or nest materials, further contribute to cloacal community complexity (Nuñez-Otaño et al., 2013). Taken together, these observations underscore the role of the cloaca as an ecological interface shaped by both host physiology and environmental exposures.

Mercury contamination has the potential to alter these cloacal microbial communities through several pathways. For instance, ingestion of contaminated prey can lead to gastrointestinal mercury accumulation, exerting selective pressure against sensitive taxa while promoting those with resistance traits (Lin et al., 2020; Tan et al., 2022). Furthermore, evidence from studies in humans and mice indicates that mercury exposure may reduce gut microbial diversity and increase the prevalence of Pseudomonadota and other mercury-resistant taxa, including strains carrying the mer operon (Conteville et al., 2023; Yu et al., 2025). In addition, direct contact of the cloaca with polluted sediments and soils may introduce environmental mercury-resistant bacteria. Since the cloaca integrates both dietary and habitat-related exposures, its microbiome may reflect a combination of ingestion-based and environmental influences. Thus, characterizing mercury-associated shifts in the cloacal microbiome can provide insight into how host-associated communities respond to local contamination.

3.4 Research Objectives

This study builds on prior research that documents mercury accumulation and physiological effects in *M. niger* and *P. trigonatus* from French Guiana, by investigating the contribution of host-associated and environmental microbiomes to mercury resistance in these species. The analysis centers on the role of mercury-resistant bacteria (MRB), particularly those harboring the mercury reductase gene *merA*, in mediating microbial responses to mercury contamination. The central hypothesis is that MRB are present in the skin and cloacal microbiota of caimans and that microbial community composition varies between contaminated and less-contaminated sites due to environmental filtering by mercury.

To address this, we aim to:

- Describe the taxonomic composition of skin, cloacal, and soil microbiomes associated with both caiman species.
- Identify the main factors structuring microbiome composition, including host species, sample type, site, and environmental variables such as mercury concentration.
- Assess the influence of mercury on microbial community structure and diversity to determine whether variations in mercury levels correspond to measurable shifts in community composition.
- Evaluate whether microbial communities show a functional response to mercury exposure, including the detection of *merA* and the relative abundance of taxa known to tolerate or transform mercury.

4 Materials and Methods

4.1 Study area.

Samples were collected within the Kaw-Roura National Nature Reserve (*Réserve Naturelle Nationale de Kaw-Roura*) in French Guiana (4°36′ N, 52°07′ W), a protected area encompassing 94,700 ha located approximately 90 km southeast of Cayenne, and within the Nouragues Nature Reserve (*Réserve Naturelle des Nouragues*; 4°05′ N, 52°41′ W), a 105,000 ha primary rainforest reserve situated in the central eastern part of the country. Nine sampling sites were visited, and 17 individuals were captured between 20:00 and 01:00 h using a headlamp and a snare.

4.2 Microbiome sampling.

Sterile polyester-tipped swabs were used to collect skin microbiome samples. 9 swabs were run over the entire body surface of each individual, and a single swab was inserted into the cloaca and rotated. Swabs were immediately placed into sterile 2 mL Eppendorf tubes. Soil samples were collected at the location where individuals were captured by scooping soil directly into sterile 2 mL Eppendorf tubes. Water samples were collected upriver from the capture site using sterile 50 mL Falcon tubes. Blood samples were taken from the occipital sinus vein using a heparinized (heparin sodium) needle of 27 gauge and 16 mm for neonates, and 25 gauge to 25 mm for adults. Each individual was measured for Total Length (TL) and weighed. All samples were stored in a dry shipper at -196 °C until laboratory analyses at the University of Vienna, Austria.

P. trigonatus and *M. niger* are protected by the French law and a permission to capture individuals and draw blood was granted by the French authorities (Direction Generale des Territoires et de la Mer) after evaluation by the CSRPN, the regional scientific committee (Permit: R03-2022-10-20-00004, www.guyane.developpem ent-durable.gouv.fr).

4.3 Processing of Blood Samples: Mercury and Blood Biochemistry

Whole Blood Mercury Quantification. 1 mL of each total blood sample was freeze-dried for 48 hours and grounded to a fine powder. Total Hg concentration (hereafter Hg) in the blood was determined by direct measurement using a Direct Mercury Analyzer (DMA-80 Evo III, Milestone®). Analyses were made on at least two replicates of ~2.0 mg dry weight (dw) for each individual. The reproducibility for duplicate samples was approved when Relative Standard Deviation (RSD) was below 10%. The method was validated by the analyses of certified reference material (CRM) produced by the National Research Council of Canada: TORT-3 (Lobster hepatopancreas; certified Hg concentration: 0.292 ± 0.022 mg g^{-1} dw). CRMs were analyzed at the beginning and at the end of the analytical cycle, and between every 10 samples. Recovery rates of certified reference material were 101.0 ± 1.5% for TORT3 (n = 20).

Blanks were included at the beginning of each analytical run, and the limit of quantification was 0.01 ng. Hg concentrations in caiman blood are presented in $ug.g^{-1}$ dw.

Soil mercury content was determined using the same method as "Whole Blood Mercury Quantification" except drying occurred for 72 h at 45°C in an oven and not freeze drying.

Blood biochemistry analysis. Approximately 4 h after sampling, blood parameters were analyzed using VetScan VS2 Chemistry Analyzer (Abaxis, Inc., Union City, California, USA) by applying 100 µL of whole blood on “Avian-Reptilian” and/or “Preventive Care Profile Plus” designated rotors to measure alkaline phosphatase (ALP).

4.4 DNA Extraction.

Between 19 November 2024 and 5 February 2025, DNA was extracted from 177 samples: 29 soil samples, 115 skin swabs, 12 cloacal swabs, 21 water samples, and three blanks. Extractions were performed using the DNeasy PowerSoil HTP 96 Kit (QIAGEN, Hilden, Germany) following the manufacturer’s protocol, except that lysing was performed in 2 mL Lysing Matrix E tubes (MPBio, Eschwege, Germany). DNA concentration and quality were first assessed by measuring 1 µL of extract on a NanoPhotometer (Implen GmbH, Munich, Germany) and then on a Qubit 2.0 fluorometer (Thermo Fisher Scientific, Waltham, MA, USA). Clean-up was performed using the Monarch PCR & DNA Cleanup Kit (New England Biolabs, Ipswich, MA, USA) following the manufacturer’s protocol, with the elution buffer pre-heated to 75°C.

Skin swabs collected in the field were stored either individually, in pairs, or in triplicate in 2 mL Eppendorf tubes. DNA was initially extracted from all swabs in the same tube; however, bead-beating two or three swabs simultaneously resulted in absorption of most of the lysis buffer, leaving too little for effective extraction. Therefore, each swab was processed separately, and eluates were pooled onto a single MB Spin Column at the elution step (Step 6) of the manufacturer’s protocol (DNeasy PowerSoil HTP 96 Kit).

Water samples were processed using two methods: (1) centrifugation at 4 °C for 30 min at 4,500 rpm, with 600 µL of pellet used for extraction, and (2) direct extraction of 1,800 µL uncentrifuged water divided into three 600 µL aliquots, each processed separately and pooled onto a single MB Spin Column at the elution step (Step 6). All isolates were eluted in 10 µL of elution buffer.

Preliminary NanoPhotometer readings showed 4.9 ng/µL for Method 1 and 1.05 ng/µL for Method 2. After cleanup and 10 µL elution, concentrations increased to 39.15 ng/µL (A260/280 = 1.710; A260/230 = 0.538) for Method 1 and 45.0 ng/µL (A260/280 = 1.768; A260/230 = 0.520) for Method 2. For

reference, pure DNA typically exhibits A260/280 near 1.8 and A260/230 between 1.8 and 2.2; the very low A260/230 values therefore indicate substantial co-extracted contaminants affecting UV absorbance (Thermo Fisher Scientific, 2012). Given comparable purity but higher yield after concentration, subsequent extractions used Method 2.

Across all water samples processed by Method 2, NanoPhotometer concentrations averaged 54.2 ± 53.1 ng/µL (n = 21) with poor purity (mean A260/230 = 0.16). Cleanup of four test extracts led to undetectable DNA by spectrophotometry, suggesting initial absorbance largely reflected contaminants rather than nucleic acids. Qubit fluorometry confirmed that DNA was below the detection limit (< 0.5 ng/µL) for most isolates, and all subsequent PCR attempts failed. Water-derived microbiomes were therefore excluded from downstream sequencing.

4.5 DNA Sequencing

Skin swabs from 12 individuals were pooled by host, yielding 13 composite samples, each submitted in triplicate (36 libraries total) along with 28 soil, 11 cloacal samples and 2 blanks. Water samples were excluded because DNA yields were consistently <0.1 ng μL^{-1}. For each retained sample, 15 µL of extracted DNA was submitted to the Joint Microbiome Facility for library preparation. The V4 region of the bacterial 16S rRNA gene was amplified with Earth Microbiome Project primers 515F (Parada) and 806R (Apprill) (forward 5′-GTGYCAGCMGCCGCGGTAA-3′; reverse 5′-GGACTACNVGGGTWTCTAAT-3′). Amplicons were sequenced on an Illumina MiSeq (2×300 bp), targeting ~50,000 reads per sample.

4.6 Qualitative PCR of the *merA* gene

Primers targeting the *merA* gene were synthesized by Microsynth based on published sequences. Stock solutions were prepared at 100 µM in DEPC-treated water, with working solutions at 10 µM. Gradient PCRs were conducted to optimize annealing temperatures and assess potential PCR inhibition at varying template DNA concentrations. Initial trials using Poulain et al. (2015) primers failed to yield amplicons. Control reactions with 16S rRNA primers verified DNA integrity and tested for inhibition. A nested PCR approach using primers from Wang et al. (2011) yielded successful amplification and was adopted for all *merA* PCRs (Nlf F: CCA TCG GCG GCA CYT GCG TYA A, Nlf R: CGC YGC RAG CTT YAA YCY YTC RRC CAT YGT; Nsf F: ATC CGC AAG TNG CVA CBG TNG G, Nsf R: CGC YGC RAG CTT YAA YCY YTC RRC CAT YGT). Cycling conditions: 98 °C for 3 min; 30 cycles of 98 °C for 10 s, 56 °C for 30 s, 72 °C for 30 s; followed by 72 °C for 5 min. Final concentrations: 1X of 5X Phire Green Hot Start II PCR Master Mix, 200 µM each dNTP, 0.5 µM of the forward primer, 0.5 µM of the reverse primer, 1 µL of undiluted template DNA, 0.4 µL Phire Hot Start II DNA Polymerase, and nuclease-free water to a final volume of 20 µL. DNA extracted from an agricultural soil sample from Montana, USA served as a positive control. PCRs used 1 µL of undiluted

template. Samples failing to amplify were re-run with diluted template (2.5-10 ng DNA) to mitigate potential inhibition. Products were visualized on 1% agarose gels in 0.5x TAE buffer, stained with SYBR Safe, and imaged under UV light.

4.7 Quantitative PCR of the *merA* gene.

Five primer pairs targeting conserved *merA* regions (**Fehler! Verweisquelle konnte nicht gefunden werden.**) were tested. Stock and working solution preparation matching the qualitative PCR protocol. Gradient PCRs were performed to optimize annealing temperatures and assess amplification efficiency. No primer sets produced successful amplification in DNA extracts from our samples; *merA* quantification by qPCR was therefore not possible.

4.8 Identification of merA variants via cloning.

PCR products from nested *merA* amplification were cloned into *E. coli* using the pJET1.2/blunt cloning vector system (Thermo Fisher Scientific). Ligation reactions were assembled at a 3:1 insert-to-vector molar ratio and incubated at room temperature for 5 min. Ligated products were transformed into chemically competent E. coli TOP10 cells via heat shock (42 °C, 45 s), recovered in SOC medium at 37 °C for 45 min, and plated on LB agar with ampicillin. Plates were incubated overnight at 37 °C. Colony PCR was conducting using the nested *merA* primers to screen for inserts. Amplicons were visualized on 1% agarose gels stained with SYBR Safe. Positive products were purified with the Monarch PCR & DNA Cleanup Kit. Colonies selected for sequencing included *merA* fragments from soil and cloacal samples of *M. niger*, and skin, cloacal, and soil samples of *P. trigonatus*. Purified products were submitted to Eurofins Genomics for Sanger sequencing.

4.9 Data Analysis

4.9.1 16S rRNA Gene Sequencing, Processing, and Data Preprocessing

Paired-end 16S rRNA gene reads were processed with QIIME 2 v2024.10.1 (Bolyen et al., 2019). Initial quality assessment used `qiime demux summarize`. Denoising, paired-end joining, amplicon sequence variant (ASV) inference, and chimera removal were performed with `qiime dada2 denoise-paired` with truncation lengths of 200 bp (forward) and 180 bp (reverse) (Callahan et al., 2016). Technical replicates were pooled by summing counts with `qiime feature-table group` based on biological sample IDs. To optimize taxonomic assignment, we compared Naïve Bayes classifiers trained on SILVA, Greengenes, and GTDB with alternative trimming windows (Quast et al., 2013; DeSantis et al., 2006; Parks et al., 2018). SILVA 138 trained on 200-180 bp reads was selected for its balance of classification depth and low unassigned reads, and taxonomy was assigned with the QIIME 2 `classify-sklearn` plugin (Bolyen et al., 2019). Putative contaminants (mitochondria, chloroplasts, Eukaryota, unassigned) were removed prior to downstream analyses. Raw ASV counts were converted to per-sample relative abundances and Hellinger-transformed using `vegan::decostand` to down-weight highly abundant taxa and accommodate zeros (Legendre & Gallagher, 2001; Oksanen et al., 2024). Bray-Curtis dissimilarities computed from the transformed data with `vegan::vegdist` were used for subsequent analyses (Bray & Curtis, 1957; Oksanen et al., 2024).

4.9.2 Definition of Variables: Body Condition Index (BCI) and Mercury Bins

4.9.2.1 Body Condition Index

Body condition index (BCI) was quantified using Fulton's condition factor (Fulton 1904), calculated for each individual as, where W is body mass and L is total length:

$$K = 100 * \frac{W(g)}{L^3(cm^3)}$$

4.9.2.2 Mercury Binning: Categorizing Samples based on Mercury Levels

To examine potential differences in microbiome composition across mercury exposure levels, samples were categorized into "High" and "Low" mercury groups based on the median mercury concentration within each dataset. For soil and skin microbiome datasets, binning was performed using soil mercury concentration (Soil_Hg), while for the cloacal microbiome dataset, binning was based on whole blood mercury concentration, described in section 2.3 (HG_WHOLE_BLOOD_.ppm.). For each dataset, the median value was calculated using median(na.rm = TRUE) in R, and samples with concentrations greater than the median were assigned to the "High" group, while those at or below the median were assigned to the "Low" group. Samples lacking mercury measurements were assigned an "NA" category and excluded from subsequent bin-based comparisons.

4.9.3 Taxonomic Composition Analysis and Diversity Analysis

Taxonomic profiles were aggregated at multiple taxonomic ranks including Phylum, Class, Order, Family, and Genus. Unassigned taxa were explicitly labeled to avoid ambiguity (e.g., p__Unclassified), and composite labels (e.g., p__Pseudomonadota; Gammaproteobacteria) were used to retain hierarchical context. For each rank, the top 20 most abundant taxa by summed relative abundance were selected for visualization. Zero values were imputed for missing taxon-sample combinations, and heatmaps were created using the pheatmap package with row-wise scaling (Kolde, 2019). Hierarchical clustering was applied to sample columns, with annotation for host species, environment, and geographic location.

Alpha diversity metrics included observed richness, Shannon diversity, and Pielou's evenness (computed via vegan::diversity; Shannon, 1948; Pielou, 1966; Oksanen et al., 2024), as well as Faith's phylogenetic diversity (Faith's PD). For Faith's PD, ASV representative sequences were aligned with DECIPHER::AlignSeqs (Wright, 2015), and a maximum-likelihood phylogeny was inferred under the GTR model using phangorn::optim.pml (Tavaré, 1986; Schliep, 2011). Faith's PD was then calculated with picante::pd (Kembel et al., 2010). Group differences in diversity metrics, including contrasts by environment or mercury exposure category, were tested with Kruskal-Wallis tests followed by pairwise Wilcoxon rank-sum tests with Benjamini-Hochberg correction for multiple comparisons (Kruskal & Wallis, 1952; Wilcoxon, 1945; Benjamini & Hochberg, 1995).

Beta diversity was assessed using Bray-Curtis dissimilarities computed on Hellinger-transformed relative abundances (Legendre & Gallagher, 2001; Bray & Curtis, 1957). Community differences were visualized with non-metric multidimensional scaling using vegan::metaMDS with k = 2 and with principal coordinates analysis (cmdscale), reporting axes by the percentage of variance explained (Kruskal, 1964; Gower, 1966; Oksanen et al., 2024). Differences in community composition between groups were tested by permutational multivariate analysis of variance with vegan::adonis2 using 999 permutations (Anderson, 2001). Homogeneity of multivariate dispersion was evaluated with vegan::betadisper, and permutation tests assessed group differences in dispersion (Anderson, 2006; Oksanen et al., 2024).

4.9.4 Association with Mercury: ASV Response, Differential Abundance, SIMPER, Network Analysis

ASV Response. For ASV-level responses to mercury, taxa detected in two or more samples within each environment were correlated against continuous mercury concentrations using Spearman's rank correlation (Spearman, 1904). ASVs with significant positive correlations ($p < 0.05$) were classified as Hg-tolerant, while those with significant negative correlations were considered Hg-sensitive. The

taxonomic composition of Hg-tolerant ASVs was summarized at the phylum and genus levels to reveal patterns of mercury-associated taxa.

Differential Abundance. Taxa present in at least four samples per environment, and taxonomic rank were tested for differential abundance between mercury exposure categories (Hg bins) using the DESeq2 package (Love, Huber, & Anders, 2014). Size factors were estimated with the "poscounts" method, and significance was determined at a false discovery rate (FDR) threshold of 0.05 (Benjamini & Hochberg, 1995). Results were visualized as volcano plots to display fold changes and statistical significance.

SIMPER. Similarity Percentage (SIMPER) analysis was performed to identify taxa that contributed most to community dissimilarity between mercury exposure categories (Clarke, 1993). SIMPER was run with 999 permutations to estimate the probability that a taxon's contribution to dissimilarity could be attributed to random variation. For each environment, taxa cumulatively explaining up to 70% of total Bray-Curtis dissimilarity were retained based on the cumulative sum of average contributions (Bray & Curtis, 1957). Statistical significance of contributing taxa was assessed using Benjamini-Hochberg correction of permutation p-values, and taxa with FDR < 0.05 were considered significant contributors (Benjamini & Hochberg, 1995).

Co-occurrence Network. For each environment, an abundance matrix was assembled with samples as rows and taxa as columns. Two resolutions were analyzed: Phylum level and Genus level. Abundances were aggregated to phylum or genus level and taxa with zero variance across samples were removed. For each environment per Hg bin, pairwise Spearman rank correlations were computed among taxa (Hmisc::rcorr) (Spearman, 1904; Harrell, 2024). Edges were retained when with absolute correlation coefficient $|\rho| \geq 0.65$ and Benjamini-Hochberg FDR $q < 0.05$. Edge sign was recorded as positive ($\rho > 0$) or negative ($\rho < 0$).

4.9.5 Environmental Drivers of Microbial Community Composition: RDA and Variation Partitioning

Redundancy Analysis. For each environment, Hellinger-transformed ASV data were analyzed by redundancy analysis (vegan::rda) to test associations with environmental predictors (e.g., mercury burden, sampling location) (Legendre & Gallagher, 2001; Oksanen et al., 2024). Model and term significance were assessed by permutation ANOVA (anova.cca, 999 permutations) and visualized as biplots (Oksanen et al., 2024).

Variance Partitioning Analysis (VPA). For each environment (cloaca, skin, soil), metadata were filtered to retain distinct SampleID entries with complete predictor information. Mercury burden values were log10-transformed to reduce right skew in the distribution, with a pseudocount of 0.001 added to

avoid undefined values at zero and to permit the inclusion of samples with very low or undetectable concentrations. The use of small constants before log transformation is a standard procedure in ecological analysis to stabilize variance while retaining zero values (Legendre & Gallagher, 2001; Quinn & Keough, 2002). Body condition index (BCI) was treated as a numeric predictor, and Place was treated as a categorical factor. Samples with missing values for any predictor were excluded. After alignment of community and metadata tables by intersecting sample IDs, environments with fewer than four samples were excluded. If Place contained fewer than two levels, it was removed from the predictor set. VPA was only performed when at least two predictor sets remained after filtering. Partitioning was implemented with redundancy analysis (RDA)-based adjusted R2 fractions (vegan::varpart) (Borcard, Legendre, & Drapeau, 1992; Peres-Neto, Legendre, Dray, & Borcard, 2006; Oksanen et al., 2024). Depending on the availability of predictors, either a two-set (Hg + Place, or Hg + BCI) or a three-set (Hg + Place + BCI) model was fitted. Unique contributions were further quantified using partial RDA (rda with Condition) and tested for significance by permutation (anova.cca, 999 permutations) (Legendre & Legendre, 2012; Oksanen et al., 2024). Visualization was performed with plot.varpart, modified for clarity. Negative fractions were retained in the diagrams (cutoff = -Inf).

4.9.6 Comparative Similarity Analysis of Skin, Cloaca, and Soil Microbiomes

To assess whether the skin microbiome is compositionally more similar to the cloacal microbiome or to the soil microbiome, a distance-based permutation testing approach was applied. Bray-Curtis dissimilarities were computed among all samples using Hellinger-transformed ASV abundance data to quantify compositional differences (Bray & Curtis, 1957; Legendre & Gallagher, 2001). The difference in mean Bray-Curtis dissimilarity between the skin-cloaca and skin-soil comparisons (denoted as Δ) was used as a summary statistic. Statistical significance of this difference was evaluated using a two-sided permutation test in which environment labels were randomly permuted across samples 9,999 times with a fixed seed (seed = 42) to ensure reproducibility (Good, 2005). For each permutation, the Δ statistic was recalculated to generate a null distribution. The empirical p-value was then calculated as the proportion of permuted absolute Δ values equal to or exceeding the observed absolute Δ. A 95% confidence interval for Δ was obtained by identifying the 2.5th and 97.5th percentiles of the permutation distribution. All distance calculations and permutation procedures were performed in R using functions from the vegan package (Oksanen et al., 2024).

4.9.7 Phylogenetic Analysis of *merA* Variants

Sanger-derived *merA* sequences were imported as DNAStringSet objects (Biostrings 2.76.0) and aligned with ClustalW (msa 1.40.0) (Pagès, Aboyoun, Gentleman, & DebRoy, 2024; Bodenhofer, Bonatesta, Horejš-Kainrath, & Hochreiter, 2015; Thompson, Higgins, & Gibson, 1994). The resulting multiple-sequence alignment was quality-filtered with Alignment Viewer (alignmentviewer.org): sequences containing more than 50% gap characters across their full length were excluded. The filtered

alignment was analyzed locally with IQ-TREE 2 (v2.3.6). Maximum-likelihood inference was performed with automatic model selection (ModelFinder), and node support was estimated with SH-aLRT (1,000 replicates) and ultrafast bootstrap (1,000 replicates) (Minh et al., 2020; Kalyaanamoorthy, Minh, Wong, von Haeseler, & Jermiin, 2017; Hoang, Chernomor, von Haeseler, Minh, & Vinh, 2018). The best-scoring tree was then uploaded to the Interactive Tree of Life (iTOL) for visualization and annotation (Letunic & Bork, 2021). In iTOL, the tree was midpoint-rooted, and tip labels/metadata tracks were added for downstream presentation.

5 Results: Taxonomic Composition of Skin, Cloacal, and Soil Microbiomes Associated with Caiman Species.

5.1 Sample Description and Demographics

Across 17 captures, we measured total length (TL) and body mass for 14 *P. trigonatus* and 3 *M. niger* individuals. One *P. trigonatus* (ID 298) lacked body mass measurement and was excluded from mass analyses; two individuals (IDs 295 and 343) lacked whole-blood mercury (Hg). In *P. trigonatus*, TL ranged from 26.4 to 140.0 cm (M = 100.6 SD =38.9; n = 14) and body mass from 70.0 to 15200.0 g (6048.8 ± 5069.6; n = 13). In *M. niger*, TL ranged from 109.0 to 146.0 cm (129.7 ± 18.9; n = 3) and body mass from 2600.0 to 8150.0 g (5700.0 ± 2831.5; n = 3). Whole-blood Hg averaged 0.68 ± 0.42 μg g^{-1} across all sampled individuals (n = 15), 0.53 ± 0.22 μg g^{-1} in *P. trigonatus* (n = 12), and 1.25 ± 0.60 μg g^{-1} in *M. niger* (n = 3). Across all soil samples, the mean Hg concentration was 0.144 μg g^{-1} (n = 9). By zone, Nouragues had a median of 0.163 μg g^{-1} (IQR = 0.051, n = 7), while Petit Saut and Kaw were represented by single samples (0.140 and 0.126 μg g^{-1}, respectively), precluding SD/IQR estimation. A Kruskal-Wallis test indicated no difference among zones ($\chi^2 = 1.15$, df = 2, p = 0.564).

5.2 Sequencing results and quality

Illumina MiSeq 2×300 bp sequencing produced 79 libraries with balanced paired-end yields (forward = reverse = 2,715,083 reads). Per-library depth ranged from 8 to 65,267 reads (median = 35,829; mean = 34,368). After DADA2 denoising/merging and ASV inference, 1,154,745 sequences were assigned to 12,214 ASVs using the SILVA-138 classifier. Taxonomic filtering removed non-target/ambiguous annotations: Unassigned (432,451 reads; 4,659 ASVs), Eukaryota (85,366; 604), mitochondria (34,115; 965), and chloroplasts (29,011; 148). The retained bacterial/archaeal fraction comprised 573,802 reads (49.7% of post-DADA2 reads) across 5,838 ASVs (47.8% of ASVs).

5.3 Microbiome samples separate clearly by environment and associated species

Non-metric multidimensional scaling (NMDS) of Hellinger-transformed ASV relative abundances showed clear separation by environment along NMDS1, with additional separation of skin and cloaca along NMDS2; soils spanned the range of both host-associated groups (Figure 1). Pairwise Bray-Curtis

dissimilarities quantified these patterns: the skin microbiome was equally dissimilar to soil and cloaca (mean distances 0.9971 and 0.9977; n(skin) = 15, n(soil) = 25, n(cloaca) = 11), with no significant difference between the two distances (p = 0.9832; 95% CI -0.0596 to 0.0594). In contrast, cloacal communities were more similar to soil than to skin (mean 0.915 vs 0.998; p = 0.0074; 95% CI -0.0568 to 0.0578).

Bray-Curtis PERMANOVA with 999 permutations showed that host species explained variation in all environments, with the clearest signal in the cloaca. In the cloaca, species explained 17.6% of compositional variance (R^2 = 0.176, p = 0.004) and dispersion did not differ among species (PERMDISP p = 0.751), indicating differences in location rather than spread. In skin and soil, species effects were significant (skin: R^2 = 0.128, p = 0.004; soil: R^2 = 0.135, p = 0.004) but coincided with heterogeneous dispersion (PERMDISP p = 0.001 in both cases), so these results should be interpreted with caution.

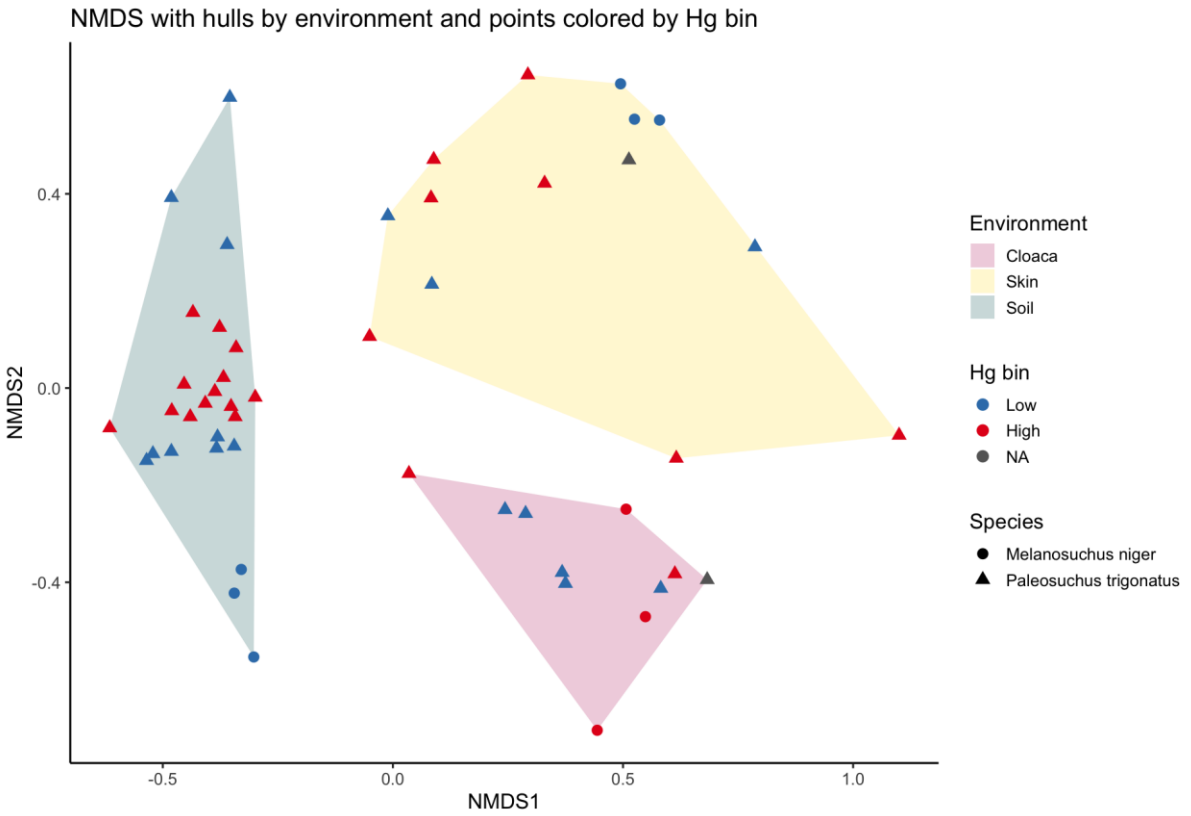

Figure 1: Non-metric multidimensional scaling (NMDS) ordination based on Bray-Curtis dissimilarities of ASV-level microbial communities. Stress = 0.17. Points represent individual samples, colored by mercury burden (Hg_bin: HighHg vs. LowHg, Soil and Skin= Soil Hg content, Cloaca = Whole Blood Hg) and shaped by host species. Shaded polygons indicate convex hulls grouping samples by environment.

5.4 Phylum-level community composition across environments, hosts, and space

Across all samples, 50 phylum-level taxa were detected; 41 named bacterial/archaeal phyla and 9 candidate/unclassified groups. By environment, cloaca samples were enriched in Pseudomonadota

(27%), Bacteroidota (23%), Bacillota (17%), and Actinomycetota (12%); skin harbored Pseudomonadota (30%), Cyanobacteriota (19%), and Actinomycetota (11.9%); soils were characterized by Pseudomonadota (25%), Acidobacteriota (14%), and Actinomycetota (12%). By host species, *M. niger* showed a Pseudomonadota-dominated profile (41%) with Cyanobacteriota (19%) and Actinomycetota (12%), whereas *P. trigonatus* had lower Pseudomonadota (24%) and higher Acidobacteriota (10%) and Bacteroidota (10%). Pseudomonadota dominated in all the environments (cloaca, skin and soil, 24.8-26.6%) as well as a large proportion of Actinomycetota (11.4-13%). Of the Pseudomonadota, Gammaproteobacteria represented one of the most abundant classes across all environments (Cloaca: 23.3%, Skin 9.4%, Soil: 9.02%), followed by Alphaproteobacteria, particularly in soil samples (Cloaca: 3.4%, Skin 9.2%, Soil: 14.92%). Bacteroidia (Phylum Bacteroidota) represented a substantial component of host-associated samples (Cloaca: 22.6%, Skin: 14.4%) while remaining minimal in environmental soils (3.5%). The skin and cloacal microbiomes of caimans exhibit a distinctive host-associated signature characterized by a core community dominated by Bacteroidia and Bacillota , with Fusobacteria serving as a defining crocodilian hallmark. Fusobacteria detection in cloacal and skin samples was 0.9% and 0.6% respectively. Bacillota also represented a consistent fraction of the communities (Cloaca: 16.0%, Skin: 5.3%, Soil: 8.1In addition to these major phyla, Synergistota were recovered in low abundance overall (Cloaca: 1.45%, Skin: 0.2%, Soil: not detected) but was found in over 50% of the cloacal samples. The skin microbiome included Pseudomonadota (29.5%), Cyanobacteriota (19.1%), and Actinomycetota (11.9%), but with an absence of the large Bacteroidota and Bacillota fractions found in the cloaca. Two specialized phyla, Deinococcota and Armatimonadota, were detected in over 50% of all skin samples.

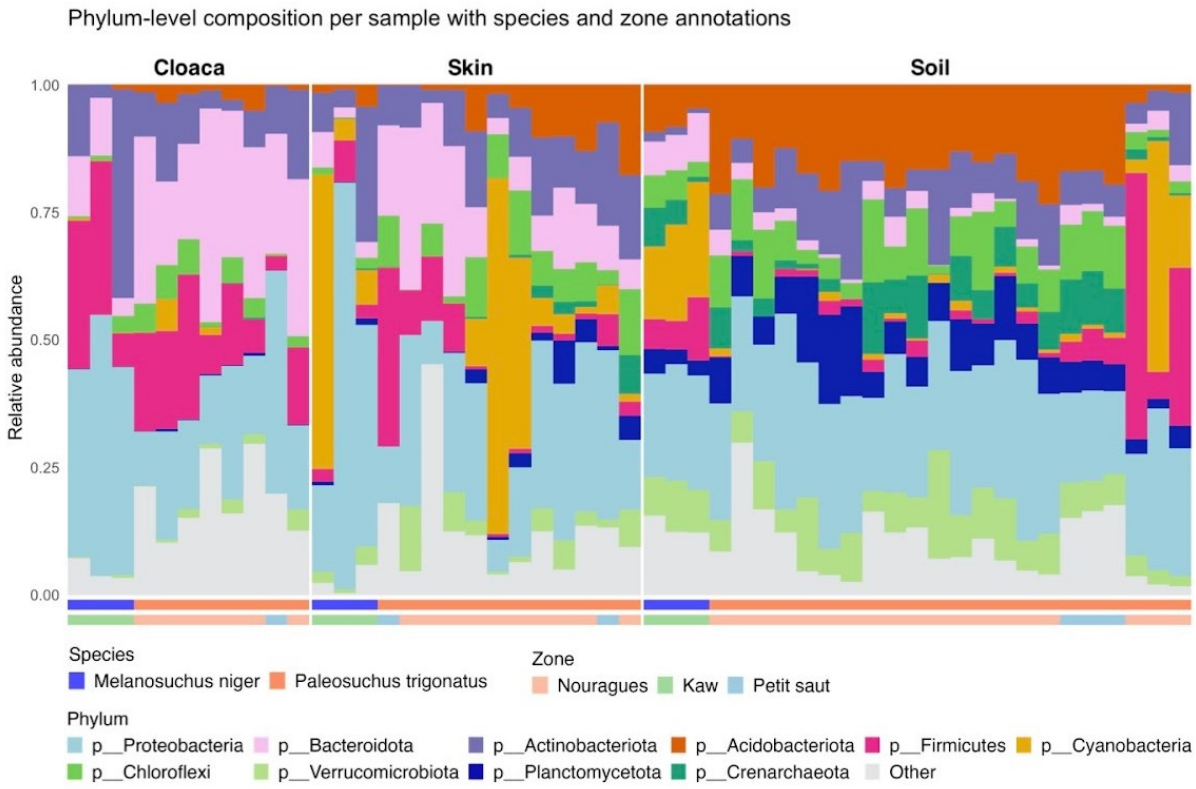

Figure 2: Phylum-level community composition per sample across three compartments (cloaca, skin, soil). Stacked bars show relative abundances for individual samples; colors denote phyla, with "Other" aggregating low-abundance taxa. Samples are annotated by host species (M. niger, P. trigonatus) and zone (Nouragues, Kaw, Petit Saut). Profiles differ by compartment, with soils enriched for Acidobacteriota/Actinomycetota and host sites dominated by Proteobacteria and Bacteroidota. Plot labels show legacy phylum names, in the text we use the updated NCBI nomenclature: Proteobacteria → Pseudomonadota, Actinobacteriota → Actinomycetota, Firmicutes → Bacillota, Cyanobacteria → Cyanobacteriota.

5.5 Environmental microbiomes are more diverse and even compared to host-associated microbiomes

Among the three environments, the skin microbiome showed the highest observed richness, with an average of 251 ± 134.8 ASVs, followed by soil with 166 ± 83.0 ASVs and cloaca with 131 ± 42.4 ASVs, none of the pairwise comparisons were statistically significant (cloaca vs skin: padj = 0.072; cloaca vs soil: padj = 0.595; skin vs soil: padj = 0.075). Shannon diversity was highest in soil (4.50 ± 0.65), intermediate in skin (4.09 ± 1.14), and lowest in cloaca (3.64 ± 0.59). Only the difference between soil and cloaca was statistically significant (padj = 0.004), indicating that soil communities are not only more species-rich but also more balanced in their composition than cloaca samples. Evenness followed a similar trend: soil communities were the most even (0.90 ± 0.088), while both skin (0.75 ± 0.161) and cloacal (0.75 ± 0.082) microbiomes were more uneven, reflecting a dominance of a few taxa. These differences were significant between soil and both host-associated compartments (soil vs cloaca: padj = 4.98×10^{-5}; soil vs skin: padj = 1.08×10^{-5}) but not between skin and cloaca (padj = 0.357). Taken together, these results show that soil microbiomes are the most diverse and compositionally balanced, whereas host-associated communities, particularly those of the cloaca, are less diverse and more uneven, likely reflecting stronger host filtering and specialized microbial associations.

5.5.1 Cloacal microbiomes differ by species: *P. trigonatus* enriched for Helicobacter, Turneriella, Mycoplasma; *M. niger* enriched only for *Lawsonella* sp.

Cloacal communities differed in phylum-level composition between host species. In *M. niger*, Pseudomonadota comprised 41.0% of reads, followed by Cyanobacteriota 19.1%, Actinomycetota 12.3%, Bacillota 8.7%, and Bacteroidota 5.2%. In *P. trigonatus*, Pseudomonadota were 24.0%, with higher contributions of Bacteroidota 9.9%, Acidobacteriota 9.6%, Actinomycetota 11.7%, and Bacillota 6.2%.

Differential abundance analysis using DESeq2 identified 8 genera and 2 phyla that significantly differed between the cloacal microbiomes of *M. niger* and *P. trigonatus* ($p_{adj} < 0.05$) (Figure 3). At the phylum level, Myxococcota (log_2 fold change = -7.10, padj = 0.004) and Nitrospirota (log_2 fold change = -5.99, padj = 0.011) displayed higher abundance in *P. trigonatus* compared to *M. niger*. The genera *Helicobacter* sp. (Campylobacterota; log_2 fold change = -24.17, padj = 1.29×10^{-10}), *Turneriella* sp. (Spirochaetota; log_2 fold change = -22.84, $p_{adj} = 9.48 \times 10^{-10}$), and *Mycoplasma* sp. (Bacillota ; log_2 fold change = -22.38, $p_{adj} = 1.55 \times 10^{-9}$) were more abundant in *P. trigonatus*. Other genera enriched in *P. trigonatus* included uncultured *Eubacterium* sp. (env.OPS_17; Bacteroidota), *Phascolarctobacterium* sp. (Bacillota), *Ca.* Competibacter (Pseudomonadota), and *Nitrospira* (Nitrospirota). In contrast, only *Lawsonella* sp. (Actinomycetota; log_2 fold change = 8.88, $p_{adj} = 0.045$) was significantly enriched in *M. niger*.

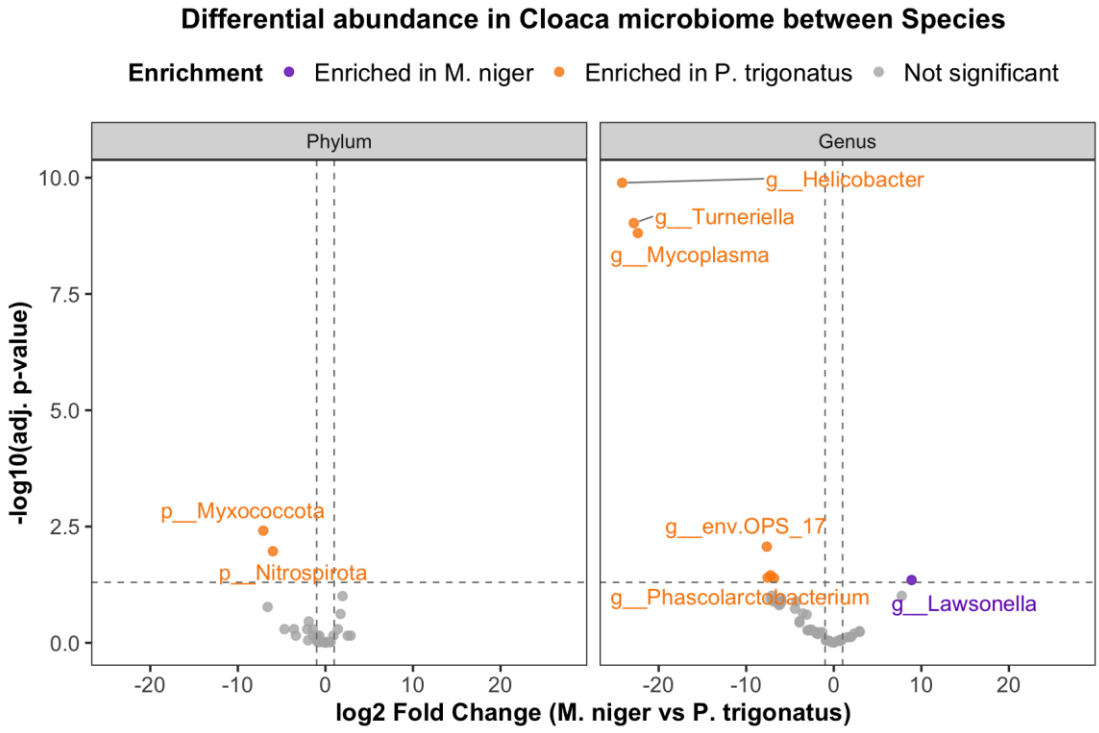

Figure 3: Differential abundance of cloacal microbiomes at the phylum and genus level between M. niger (purple) and P. trigonatus (orange). Volcano plot showing log_2 fold change (x-axis) and -log_{10} adjusted p-value (y-axis) from DESeq2 analysis. Positive values indicate enrichment in M. niger, negative values enrichment in P. trigonatus.

5.5.2 Composition of Skin Samples and comparison between species

Skin communities were summarized at the phylum level using per-sample normalized relative abundances and averaged within species. In *M. niger*, the ten most abundant phyla were Pseudomonadota 30.4%, Cyanobacteriota 12.5%, Actinomycetota 11.7%, Bacteroidota 11.3%, Acidobacteriota 5.57%, Bacillota 5.18%, Verrucomicrobiota 4.54%, Chloroflexota 3.33%, Planctomycetota 3.13%, and Nanoarchaeota 2.59%. In *P. trigonatus*, the ten most abundant phyla were Pseudomonadota 21.3%, Bacteroidota 15.05%, Actinomycetota 11.20%, Chloroflexota 10.30%, Bacillota 8.51%, Cyanobacteriota 6.00%, Acidobacteriota 5.87%, Planctomycetota 4.85%, Verrucomicrobiota 3.32%, and Spirochaetota 2.74%. Across species, nine phyla were shared among the respective top ten lists, with Pseudomonadota, Bacteroidota, Actinomycetota, Chloroflexota, Bacillota, Cyanobacteriota, Acidobacteriota, Planctomycetota, and Verrucomicrobiota contributing the largest fractions; Nanoarchaeota appeared only in *M. niger* and Spirochaetota only in *P. trigonatus*.

DESeq2 analysis identified five genera and three phyla significantly enriched in *P. trigonatus* skin samples compared to *M. niger* ($p_{adj} < 0.05$)(Figure 4). The genera *Blastocatella* sp. (Acidobacteriota; $\log_2$ fold change = -23.25, padj = 3.89×10^{-9}), *Bacteroides* sp. (Bacteroidota; $\log_2$ fold change = -22.72, $p_{adj} = 3.00 \times 10^{-8}$), *SepB-3* sp. (Cyanobacteriota; $\log_2$ fold change = -22.67, $p_{adj} = 1.18 \times 10^{-7}$), *Bradyrhizobium* sp. (Pseudomonadota; $\log_2$ fold change = -22.12, $p_{adj} = 2.13 \times 10^{-7}$), and *Desulfovibrio* sp. (Thermodesulfobacteriota; $\log_2$ fold change = -20.88, $p_{adj} = 1.02 \times 10^{-6}$) exhibited significant enrichments in *P. trigonatus*. Conversely, *Ancylothrix_8PC* sp. (Cyanobacteriota; $\log_2$ fold change = 10.28, $p_{adj} = 1.91 \times 10^{-2}$) was significantly enriched in *M. niger*. At the phylum level, Fusobacteriota ($\log_2$ fold change = -20.92, $p_{adj} = 1.28 \times 10^{-6}$), Nitrospirota ($\log_2$ fold change = -7.91, $p_{adj} = 2.16 \times 10^{-2}$), and Deltaproteobacteria (within Pseudomonadota) ($\log_2$ fold change = -7.56, $p_{adj} = 4.38 \times 10^{-2}$) were all significantly more abundant in *P. trigonatus*, with no phyla enriched in *M. niger*.

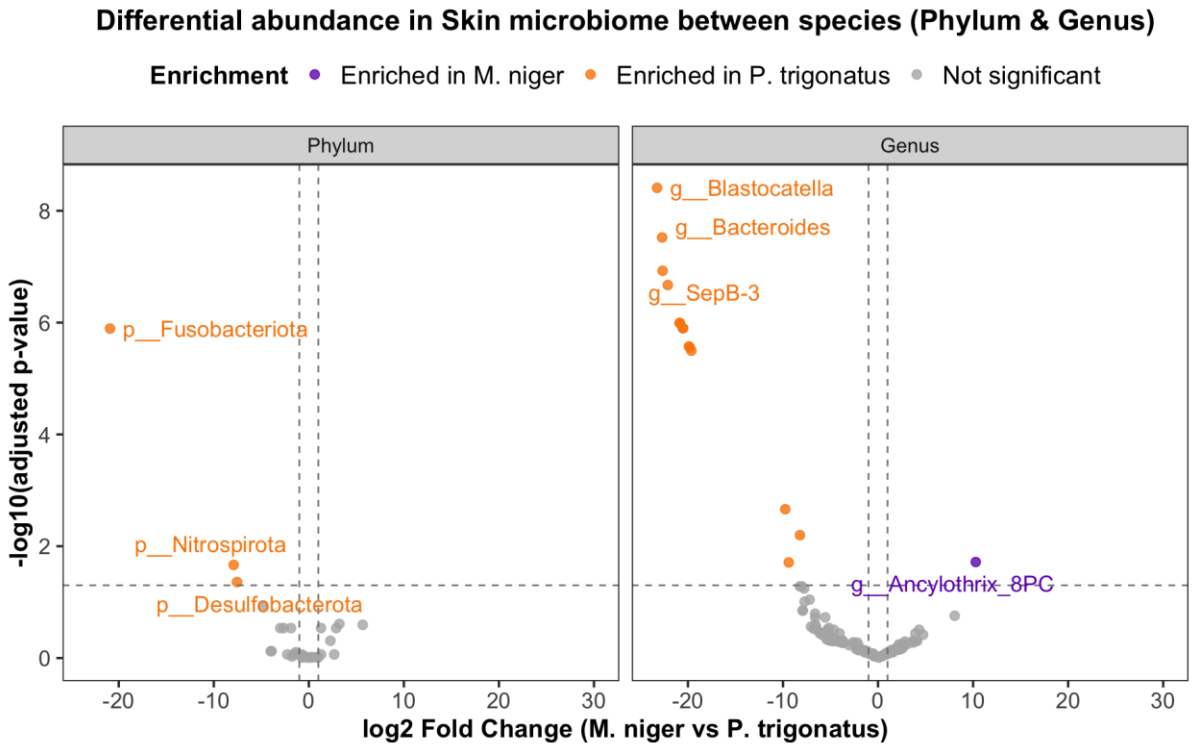

Figure 4: Differential abundance of skin microbiomes at the phylum and genus level between M. niger (purple) and P. trigonatus (orange). Volcano plot showing log_2 fold change (x-axis) and -log_{10} adjusted p-value (y-axis) from DESeq2 analysis. Positive values indicate enrichment in M. niger, negative values enrichment in P. trigonatus.

5.5.3 Soil microbiomes reflect habitat differences between species, with *P. trigonatus* soils enriched in terrestrial lineages and *M. niger* soils in aquatic Cyanobacteriota

In soils, the community was dominated by Pseudomonadota (24.8%), followed by Acidobacteriota (14.1%), Actinomycetota (11.7%), Verrucomicrobiota (7.7%), Chloroflexota (7.7%), Planctomycetota (7.5%), Cyanobacteriota (6.7%), Bacillota (6.5%), Thermoproteota (5.6%), and Bacteroidota (3.1%).

Differential abundance analysis of soil samples associated with *P. trigonatus* soils revealed Actinomycetota ($log_2FC = -3.22$, padj = 1.48×10^{-5}) and Planctomycetota ($log_2FC = -1.61$, padj = 0.044) were enriched at the phylum level. At finer resolution, lineages such as the archaeal *Ca.* Nitrosocosmicus and *Nitrosotalea* sp. were significantly enriched (log_2FC = -9.35 and -9.87; padj < 0.01). *Ca.* Udaeobacter (Verrucomicrobiota; $log_2FC = -8.64$; padj = 0.0026). *Pedomicrobium* sp. (Pseudomonadota; $log_2FC = -8.00$; padj = 0.014), *GOUTA6* (Planctomycetota; $log_2FC = -7.78$; padj = 0.018). By contrast, soils near *M. niger*, from a waterlogged riverine habitat, showed enrichment of aquatic Cyanobacteriota, including *Aetokthonos* AEL04 and *Cylindrospermum* PMC238.04 (log_2FC = 10.52 and 9.80; padj < 0.05).

5.6 Environmental (soil) microbiomes are organized by mercury and space; host-associated (cloaca, skin) microbiomes are comparatively robust

We evaluated mercury effects on microbial community composition using PERMANOVA, assessed homogeneity of dispersion with PERMDISP, and then quantified explained variance with constrained ordination (RDA) and variation partitioning analysis (VPA).

In skin and cloaca, mercury showed no significant effect on community composition (skin: $R^2 = 0.104$, $p = 0.056$; cloaca: $R^2 = 0.129$, $p = 0.246$), and dispersions were homogeneous in both environments (PERMDISP: skin $p = 0.543$; cloaca $p = 0.129$). In soils, mercury was associated with differences in community composition, but part of the signal coincided with heterogeneous dispersion. Soil communities differed between Hg bins (PERMANOVA: $R^2 = 0.096$, $p = 0.001$), while group dispersions also differed (PERMDISP: $p = 0.040$), indicating that the apparent shift may reflect differences in spread as well as centroid separation (Figure 1). RDA further showed that both spatial context and mercury contributed independently to soil variation. With Zone and Hg_burden as predictors (n = 25), Zone explained 17.86% partial inertia, corresponding to 21.10% of total inertia ($F = 3.087$, $p = 0.001$), and Hg_burden explained 6.04%, corresponding to 7.14% of total inertia ($F = 2.089$, $p = 0.003$)(Figure *5*). Samples separated primarily by Zone in the ordination biplot, with a secondary gradient aligned with mercury, consistent with geography as the dominant organizer and mercury as an additional independent signal.

Restricting the analysis to soils from *P. trigonatus* yielded a significant global RDA (constrained inertia = 0.325; adjusted $R^2 = 0.205$; $F = 2.08$, $p = 0.001$) with significant partial effects of Place (25.60%; $F = 2.05$, $p = 0.001$) and Hg_burden (7.00%; $F = 2.25$, $p = 0.001$)(Figure *6*). VPA in soils corroborated these results, identifying geographic places as a significant factor (Place adjusted $R^2 = 0.214$, $p = 0.001$) and a smaller but significant mercury fraction (adjusted $R^2 = 0.037$, $p = 0.001$).

Host-associated communities exhibited a weaker multivariate response. When skin and cloacal data were analyzed jointly, the overall constrained ordination was significant ($R^2 = 0.25$, $F = 1.17$, $p = 0.036$; Figure 7). However, marginal tests did not identify unique contributions of mercury, body condition, or geography when considered separately (all $p > 0.23$), and looking at skin and cloaca separately likewise did not yield significant unique effects for skin or cloaca (all marginal $p \geq 0.275$).

Overall, the analyses support geography as a principal driver of soil microbiome structure, with mercury contributing a smaller yet independent component. In contrast, host-associated assemblages are comparatively stable, showing a significant overall multivariate response only when analyzed jointly, but without uniquely attributable effects to individual predictors.

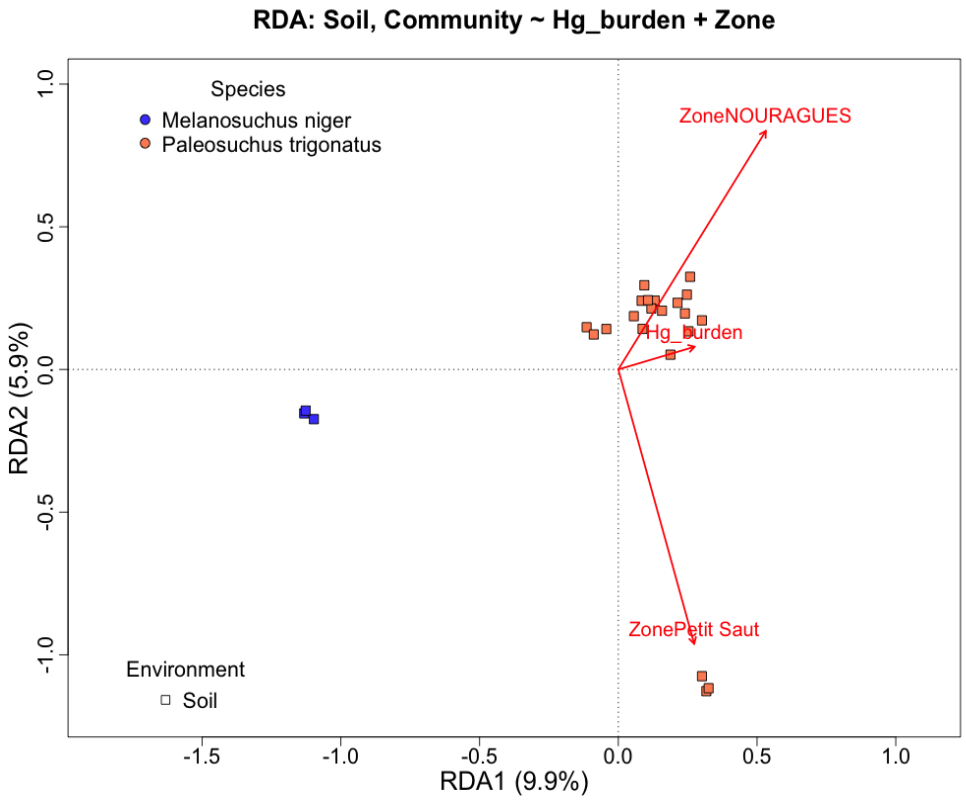

Figure 5: Redundancy analysis (RDA) of soil community composition constrained by mercury burden (Hg_burden) and sampling zone (Zone). Points are samples (color = host species: M. niger purple, P. trigonatus orange). Red vectors show the direction and relative strength of constraining variables; axis labels indicate variance explained (RDA1 = 9.9%, RDA2 = 5.9%). Community structure shifts primarily along RDA1 with increasing Hg burden, with M. niger soil samples separating from the main cluster. Soil RDA constrained by Hg_burden and Place. RDA1 = 29.6%, RDA2 = 23.2%. Vectors for Hg_burden and Place indicate strong structuring effects; points are individual soil samples.

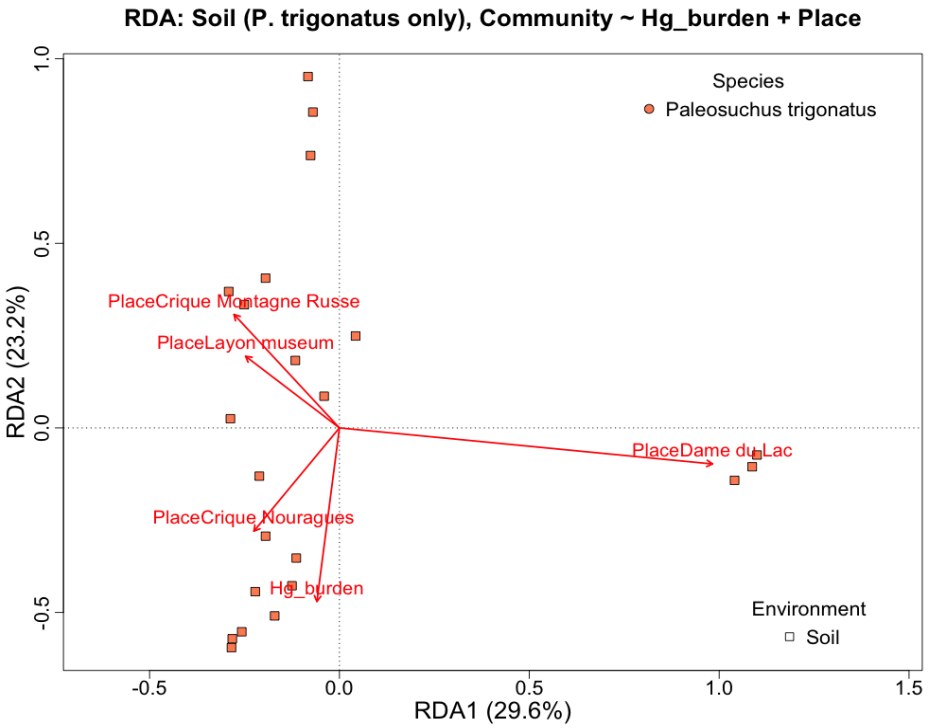

Figure 6: Redundancy analysis (RDA) of soil community composition for P. trigonatus only, constrained by individual mercury burden (Hg_burden) and sampling place (Place). Red vectors indicate the direction and relative influence of constraining variables; axis labels show variance explained (RDA1 = 29.6%, RDA2 = 23.2%). Community structure varies primarily along RDA1, with a strong site effect (notably toward Place: Dame_du_Lac) and a secondary gradient associated with Hg_burden; other sites (e.g., Crique Nouragues, Crique Montagne Russe, Layonne/museum) load in opposing directions.

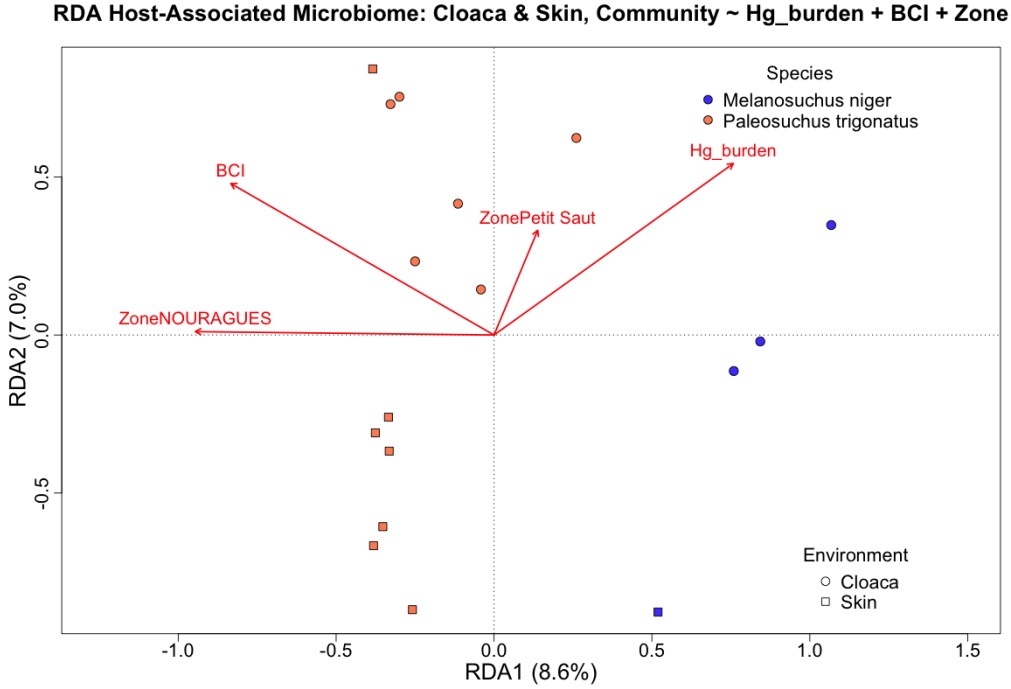

Figure 7: Redundancy analysis (RDA) of host-associated microbiomes (cloaca and skin) constrained by mercury burden (Hg_burden), body-condition index (BCI), and sampling zone. Points are individual samples (color = species: M. niger purple, P. trigonatus orange; shape = body site: skin = square, cloaca = circle). Red vectors indicate the direction and relative influence of constraining variables; axis labels give variance explained (RDA1 = 8.6%, RDA2 = 7.0%). Community composition varies along gradients of Hg_burden, BCI, and zone, with visible structure by species and body site.

6 Results: Evaluating the response of Microbial Communities to Mercury

6.1.1 *MerA* detection showed no relationship with mercury levels at either the site or the individual scale.

Qualitative PCR targeting *merA* showed a lower detection rate in *M. niger* cloacal samples (1/3 positive) compared with *P. trigonatus* (5/9 positive), despite *M. niger* carrying a higher mercury burden in whole blood (Mdn = 0.66 ug g^{-1}) compared to *P. trigonatus* (Mdn = 0.14 ug g^{-1}) (Wilcoxon W = 42, p = 0.013)(Table 1). While the small sample size prevents robust statistical conclusions, this suggests that *P. trigonatus* may harbor greater potential for microbial mercury resistance in the cloaca.

The soil sample associated with *M. niger* (three replicates) all tested negative for *merA* presence whereas *merA* was detected in all of soil samples associated with *P. trigonatus*, in at least 2/3 and 3/4 replicates. Across sites, soil-Hg was not associated with the proportion of *merA*-positive samples (Pearson r = 0.16, p = 0.68; Spearman ρ = 0.36, p = 0.34; n = 9).

For the cloaca samples only 1/3 *M. niger* individuals tested positive for *merA* presence whereas *merA* was detected in cloaca samples of 5/9 *P. trigonatus* individuals. Similar to soil-Hg, whole-blood Hg did not predict *merA* positivity in *M. niger* cloaca (Pearson r = -0.69, p = 0.51; Spearman ρ = -0.87, p = 0.33) or skin (Pearson r = 0.28, p = 0.82; Spearman ρ = 0, p = 1), nor in *P. trigonatus* cloaca (Pearson r = 0.29, p = 0.48; Spearman ρ = 0.28, p = 0.50) or skin (Pearson r = 0.30, p = 0.43; Spearman ρ = 0.21, p = 0.59). Collectively, there was no detectable linear or monotonic association between mercury exposure and *merA* detection within the sampled range.

Table 1: Summary of merA gene detection across soil, skin, and cloacal DNA extracts for each sampled individual, grouped by Species, Zone, and Place. NA means that no sample was collected.

Species	Zone	Place	ID	Soil		Swab	
				Hg (ug g^{-1})	Presence	Skin	Cloaca
M. niger	Kaw	Mare Agami	330	NA	NA	1/1	1/1
			331	NA	NA	0/1	0/1
			333	0.126	0/3	1/1	0/1
P. trigonatus	Nouragues	C. Cascades	298	0.150	2/3	1/1	0/1
			289	NA	NA	1/1	NA
			290	NA	NA	0/1	NA
		C. Montagne Russe	291	0.180	3/4	1/1	1/1
		C. Nouragues	299	0.218	3/3	1/1	0/1
			297	0.175	3/3	1/1	1/1
			300	0.210	3/3	1/1	1/1
		Layon museum	296	0.083	2/3	1/1	1/1
			343	0.015	3/3	0/1	0/1
	Petit Saut	Dame du Lac	336	0.140	3/3	NA	0/1
		Marie Hilaire	335	NA	NA	NA	1/1
		Sud Dame du lac	275	NA	NA	0/1	NA

6.1.2 Phylogenetic analysis of sequenced *merA* variants isolated via cloning revealed clustering of soil and cloacal samples and skin and cloaca but separation of soil and skin.

We PCR-amplified *merA* from skin, cloaca, and soil samples, cloned and plated the product to recover individual colony inserts. Colony PCR followed by Sanger sequencing of these inserts allowed us to identify *merA* sequence variants present in each environment and compare their phylogenetic affiliations. Across nine plated samples we sampled 36 colonies in total, corresponding to 20 isolates from *P. trigonatus* and 16 from *M. niger*. Plate 1M1 (*M. niger* skin) and plate 3P2 (*P. trigonatus* cloaca) produced no colonies. Plate 3P1 (*P. trigonatus* cloaca sample) produced colonies but was conspicuously sparse relative to other plates. Four colonies were sampled from each plate for colony PCR and sent for sequencing. Samples were distributed across as follows: *P. trigonatus* yielded 8 skin, 8 soil, and 4 cloacal isolates. *M. niger* yielded 8 soil and 8 cloacal isolates. PCR of *merA* from colony picks yielded clear single-band amplicons at the expected size (297bp) (Gel in supplementary materials: **Fehler! Verweisquelle konnte nicht gefunden werden.**).

We reconstructed a maximum-likelihood phylogeny of *merA* amplicons from soils and host samples (skin, cloaca) of *P. trigonatus* and *M. niger*, together with reference *merA* sequences. Tips grouped primarily by environment rather than by host species: soil-derived sequences formed distinct clades, whereas skin- and cloaca-derived sequences from both caimans were interspersed with one another, and species-specific subclades were not consistently recovered (Figure 8). A prominent host-associated clade comprising many skin and cloaca sequences showed its top BLAST hit to Psychrobacter *merA* (Gammaproteobacteria).

Moraxellaceae occurred in 20 of 21 host-associated samples (skin = 13, cloaca = 7) and in 1 soil sample. Within skin, relative abundance ranged from 0.05 to 0.76% in *M. niger* and from 0.06 to 5.82% in *P. trigonatus*. In cloaca, *M. niger* carried 0.20 to 0.54% and *P. trigonatus* 0.05 to 2.16%. The single soil-positive sample from *P. trigonatus* was 0.22%.

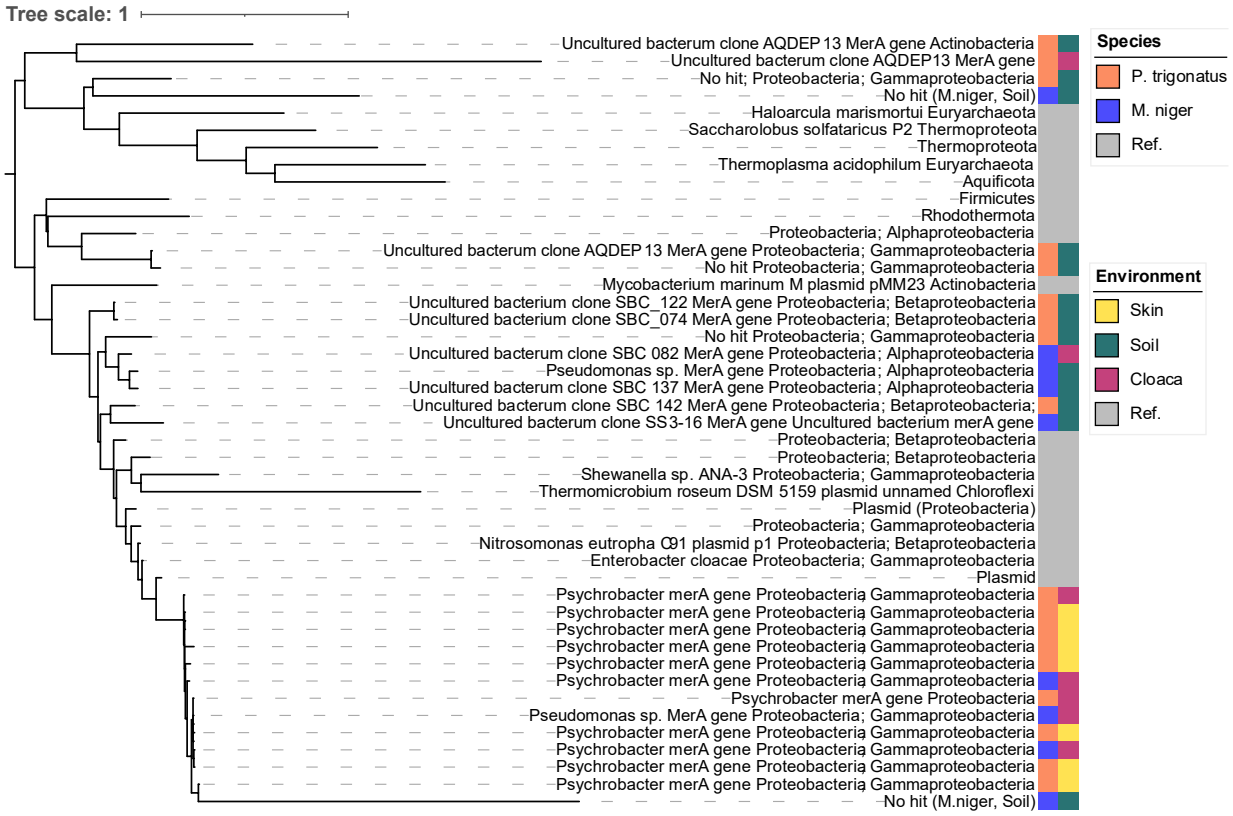

Figure 8: Maximum-likelihood phylogeny inferred with IQ-TREE 2 from the quality-filtered alignment (sequences with >50% gaps removed), midpoint-rooted for display. Tips are labeled by BLAST-derived names. Right-hand color strips annotate each tip by species (P. trigonatus; M. niger; reference sequences) and by environment (skin, soil, cloaca, reference). Scale bar indicates substitutions per site. The tree includes 45 tips; branch support was estimated with SH-aLRT and ultrafast bootstrap (not shown). Plot labels show legacy phylum names; in the text we use the updated NCBI nomenclature: Proteobacteria → Pseudomonadota, Firmicutes → Bacillota, Aquificae → Aquificota, Chloroflexi → Chloroflexota, Euryarchaeota → Methanobacteriota,

6.1.3 *MerA*-linked restructuring diverges between skin and soils with no significant effects in the cloaca.

In skin samples, Clostridia was more abundant in *merA*-negative samples and contributed 4.95% to dissimilarity between *merA*-negative and positive samples ($p = 0.046$)(Figure 9). Across soil samples, *merA*-positive samples were enriched in Bacilli (7.6%), Gammaproteobacteria (3.9%), and Methanobacteria (1.4%)(Figure 9). Cloacal samples showed no consistent class-level signal across species (all $p \geq 0.05$).

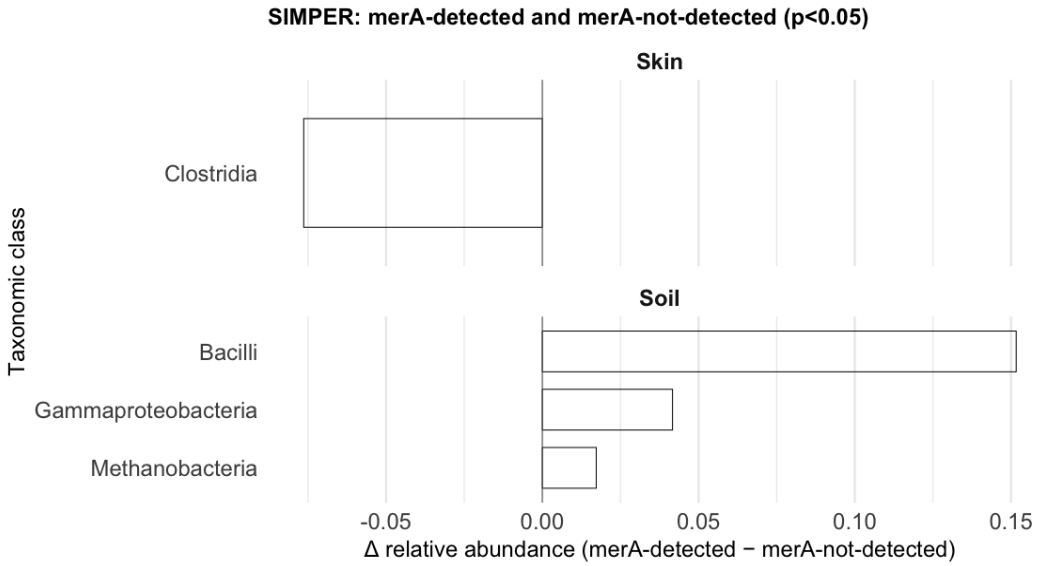

Figure 9: SIMPER analysis of taxonomic classes distinguishing samples where merA was detected versus not detected, shown separately for skin and soil. Bars indicate the mean difference in relative abundance (merA-detected minus merA-not-detected); positive values denote enrichment in merA-detected samples. Only classes with significant contributions are shown ($p < 0.05$; Bray-Curtis dissimilarity, 999 permutations).

Focusing on *P. trigonatus* skin sharpened this signal (Figure 10): Clostridia (6.19%) was more abundant in *merA*-negative than *merA*-positive samples (13.3% vs 2.7%; $p = 0.041$), Alphaproteobacteria (4.34%) increased in *merA*-positive (13.1% vs 5.1%; $p = 0.049$), and Bacteroidia (3.74%) decreased (17.4% vs 13.4%; $p = 0.029$), cumulatively explaining 29.0% of dissimilarity ($p < 0.05$). Restricting to *P. trigonatus* soils, Cyanobacteriia and Bacilli were higher in *merA*-positive, whereas Alphaproteobacteria, Terriglobia, and Planctomycetia were higher in *merA*-negative. Notably, in contrast to the pattern seen in skin samples, Clostridia increased with *merA* in *P. trigonatus* soils. in *P. trigonatus* alone, only small-effect shifts were detected (Thermoplasmata 1.12% higher in *merA*-positive, Verrucomicrobiia and Ca. Kapaibacteriia; each $p < 0.05$).

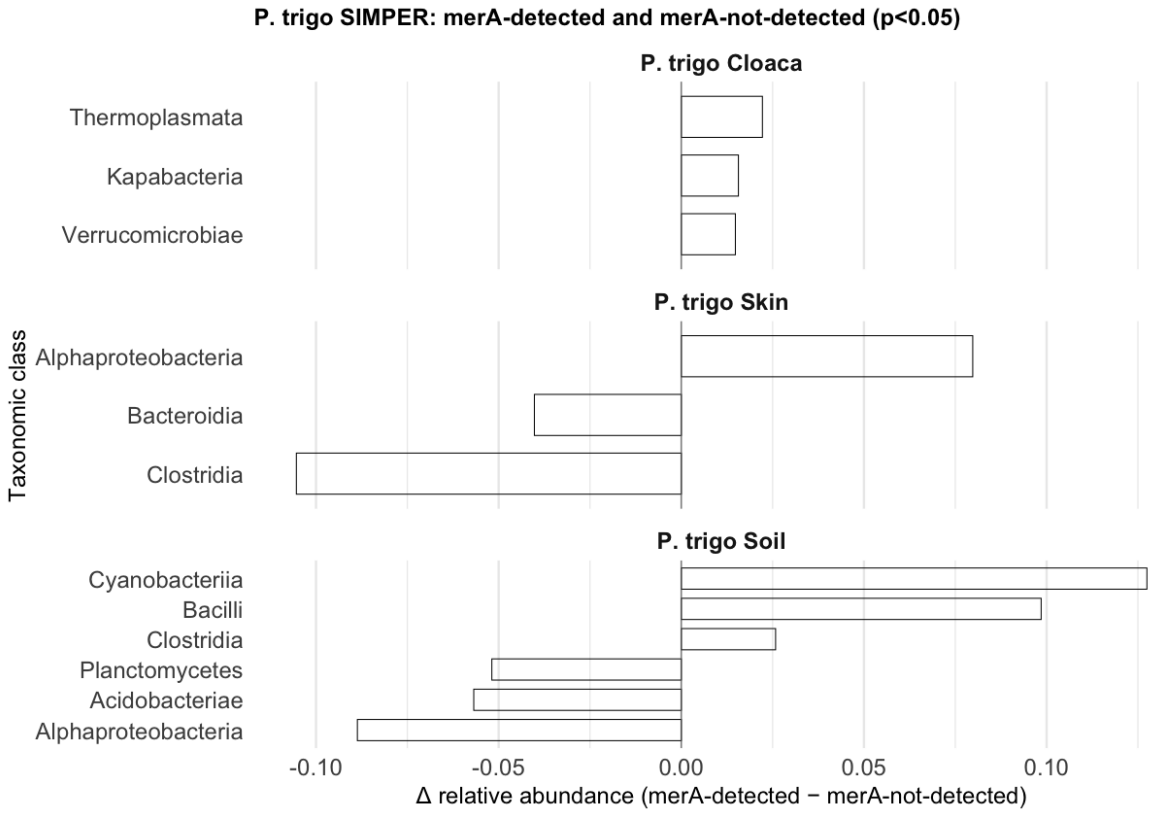

Figure 10: SIMPER results for P. trigonatus *comparing samples with merA detected versus not detected, stratified by compartment (cloaca, skin, soil). Bars show the mean difference in relative abundance (merA-detected − merA-not-detected); positive values indicate enrichment in merA-detected samples. Only taxonomic classes with significant contributions are shown ($p < 0.05$; Bray-Curtis, 999 permutations).*

6.1.4 Alpha diversity remains stable between low and high mercury across cloaca, skin and soil

To assess how the microbial community properties changed between high and low mercury we compared Observed richness, Shannon diversity and Evenness across the cloaca, skin and soil. Wilcoxon tests indicated no statistically significant differences in alpha diversity metrics between low and high mercury groups within any of the environments (Cloaca: observed richness: $p_{adj} = 0.222$; Shannon: $p_{adj} = 0.0952$; evenness: $p_{adj} = 0.0686$; Skin: observed richness: $p_{adj} = 0.222$; Shannon: $p = 0.429$; evenness: $p_{adj} = 0.73$; Soil: observed richness: $p_{adj} = 0.222$; Shannon: $p_{adj} = 0.769$; evenness: $p_{adj} = 0.0686$)(Figure 11). Although not significant, the following trends were observed. Low mercury cloaca samples were more diverse than high in the cloaca and soil (Cloaca: 142 ± 26.0 vs 118 ± 58.6 ASVs; Soil:198 ± 97.4 vs 131 ± 46.3 ASVs). Skin samples showed the opposite trend and increased richness under high mercury (362 ± 111.0 vs 257 ± 123.0 ASVs). Shannon diversity decreased with mercury in the cloaca (Shannon 3.93 ± 0.262 vs 3.24 ± 0.666), remained stable in soil and skin (Soil: Shannon diversity: 4.49 ± 0.857 vs 4.52 ± 0.351; Skin: Evenness 0.835 ± 0.0419 vs 0.799 ± 0.107).

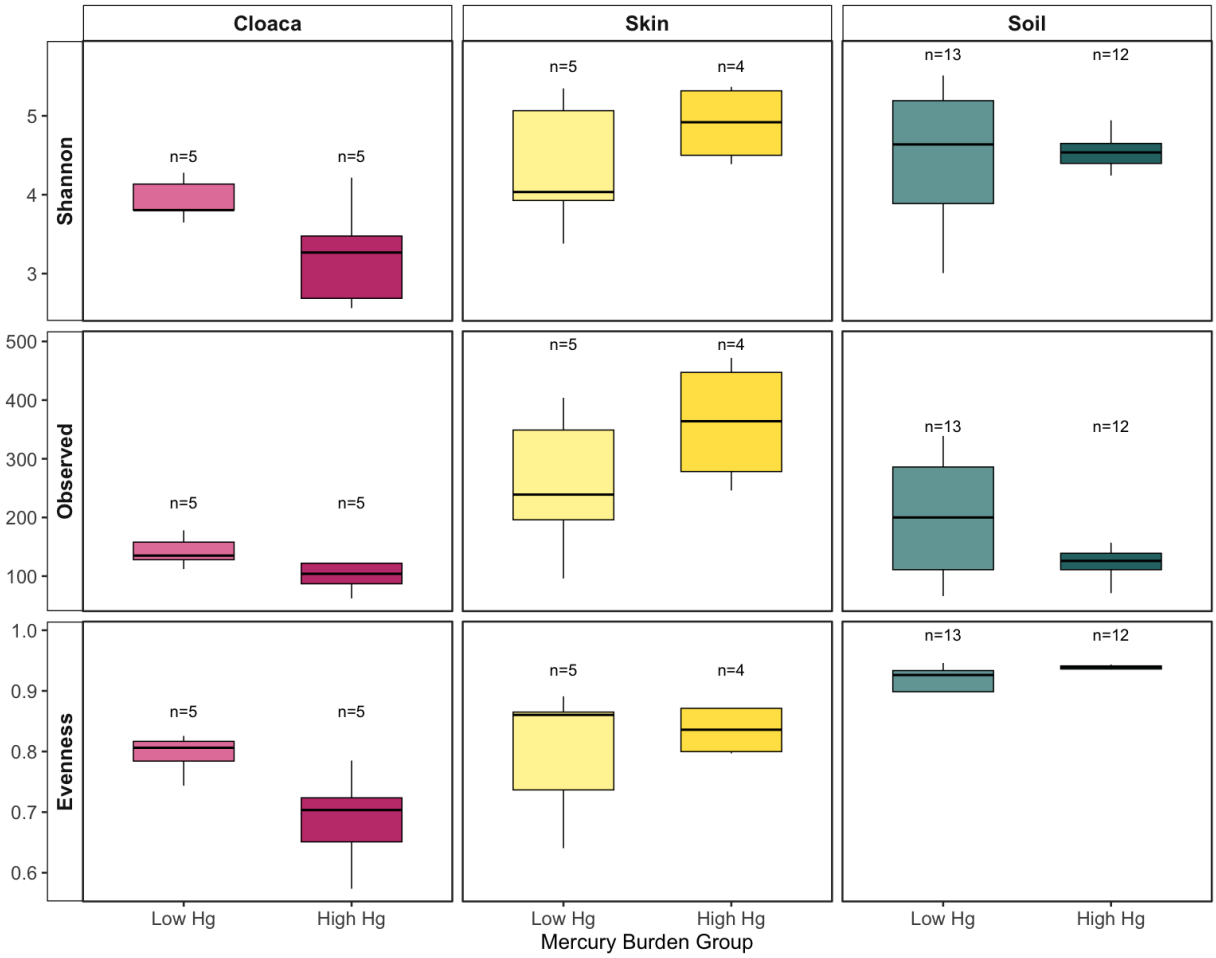

Figure 11: Alpha diversity of cloacal, skin, and soil microbiomes across low- and high-mercury (Hg) burden groups. Boxplots show Shannon diversity, observed amplicon sequence variant (ASV) richness, and Pielou's evenness for each compartment. Boxes indicate medians and interquartile ranges; whiskers extend to 1.5 × IQR. Sample sizes are shown above boxes.

6.1.5 Pseudomonadota, Acidobacteriota and Actinomycetota demonstrate differential response to mercury exposure

We classified ASVs as tolerant if their relative abundance was positively correlated with mercury (Spearman's $\rho > 0$, BH-adjusted $q < 0.05$) and sensitive if negatively correlated ($\rho < 0$, $q < 0.05$); ASVs without significant correlations were not classified.

Across all ASVs classified by tolerance, we identified 42 Hg-tolerant and 54 Hg-sensitive ASVs (Table 3; Figure 12). Pseudomonadota was the most represented phylum in both groups but constituted a larger fraction of Hg-tolerant ASVs (38.1%, n = 16) than Hg-sensitive ASVs (20.4%, n = 11). Hg-tolerant ASVs also included an archaeal component: Thermoproteota (14.3%, n = 6), Methanobacteriota (2.4%, n = 1), and Thermoplasmatota (2.4%, n = 1), totaling 19.0% of the tolerant set, compared with a single archaeal phylum among Hg-sensitive ASVs (Thermoproteota, 1.9%, n = 1). Acidobacteriota (11.9% vs 3.7%) and Chloroflexota (11.9% vs 9.3%) more prevalent in Hg-tolerant ASVs relative to the sensitive set. In contrast, Hg-sensitive ASVs were comparatively enriched in Actinomycetota (14.8% vs 4.8%),

Cyanobacteriota (13.0% vs 0%), and Verrucomicrobiota (13.0% vs 2.4%). Bacillota (5.6%) and Deinococcota (5.6%) appeared only among Hg-sensitive ASVs, whereas Candidate Phylum SAR324 clade (Marine group B; 2.4%) and WPS-2 (2.4%) were unique to the Hg-tolerant set.

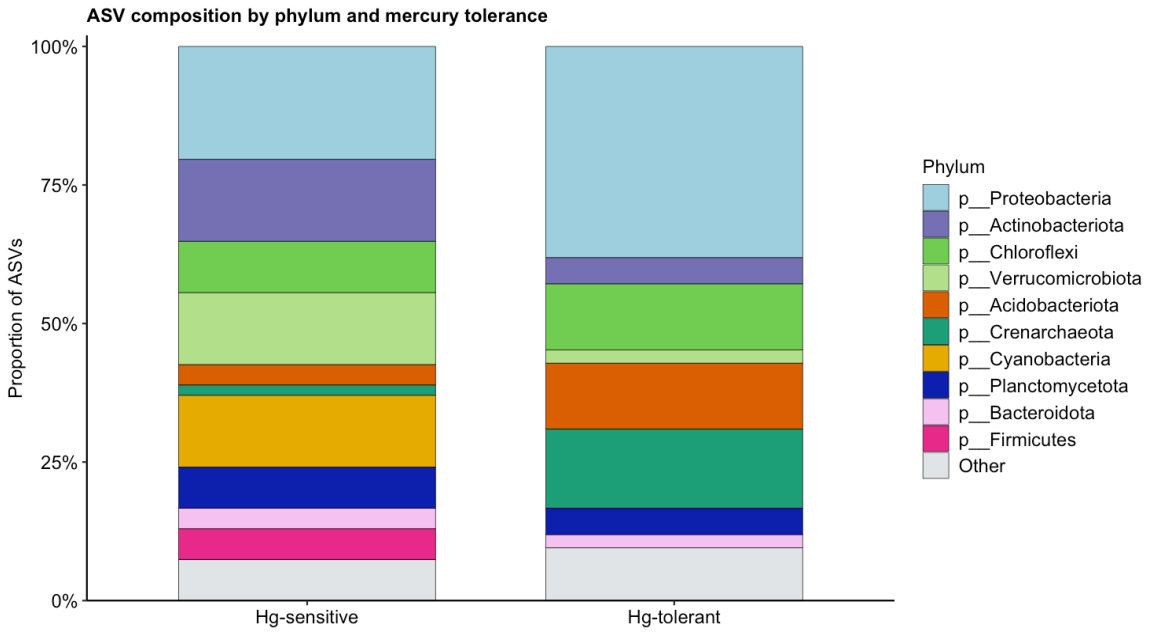

Figure 12: Phylum-level composition of ASVs in Hg-sensitive and Hg-tolerant groups. Each bar shows the within-group proportion of ASVs assigned to each phylum (100% stacked); all remaining phyla are pooled as Other. Note that these proportions reflect counts of unique ASVs, not read-abundance-weighted community composition. Plot labels show legacy phylum names; in the text we use the updated NCBI nomenclature: Proteobacteria → Pseudomonadota; Actinobacteriota → Actinomycetota; Firmicutes → Bacillota; Cyanobacteria → Cyanobacteriota; Chloroflexi → Chloroflexota; Planctomycetes → Planctomycetota; Crenarchaeota → Thermoproteota.

6.2 Mercury reduces Cyanobacteriota and fermentative lineages in soils, host microbiomes remain largely unchanged

DESeq2 was used to determine if there were any significantly different relative abundances of taxa between species and mercury burden groups. Testing was performed separately for soil, cloacal, and skin samples. After filtering to remove taxa present in fewer than four samples, our analyses included 25 soil samples (35 phyla, 150 genera), 11 cloacal samples (24 phyla, 71 genera), and 15 skin samples (26 phyla, 136 genera).

In soil samples, DESeq2 identified five genera and four phyla that differed between high- and low-Hg soils (FDR < 0.05). At the genus level, five taxa were enriched in low-Hg soils: an unclassified genus within the family *Leptolyngbyaceae* (Cyanobacteriota; $\log_2$FC = -21.38, $p_{adj} = 3.54\times10^{-13}$), *Cylindrospermum* sp. (Cyanobacteriota; -22.89, $p_{adj} = 5.17\times10^{-13}$), *Aetokthonos* sp. (Cyanobacteriota; $\log_2$FC = -22.71, 9.81×10^{-13}), *Telmatospirillum* sp. (Pseudomonadota; $\log_2$FC = -21.38, $p_{adj} = 1.68\times10^{-11}$), and *Clostridium sensu stricto 1* sp. (Bacillota ; $\log_2$FC = -8.08, $p_{adj} = 0.0023$), whereas *Pseudolabrys* sp. (Pseudomonadota) was enriched in high-Hg soils ($\log_2$FC = 8.42, $p_{adj} = 1.16\times10^{-6}$).

Telmatospirillum sp., a member of Pseudomonadota reported to tolerate multiple metals including mercury (Frey and Rieder, 2013; Zheng et al., 2022), declined sharply in high-mercury sites, suggesting a toxicity threshold exceeded even at the relatively low contamination levels observed. At the phylum level, Bacillota ($log_2FC = -3.15$, $p_{adj} = 1.08\times10^{-4}$) and Cyanobacteriota ($log_2FC = -3.97$, $p_{adj} = 3.54\times10^{-4}$) were more abundant in low-Hg soils, while Nanoarchaeota ($log_2FC = 3.27$, $p_{adj} = 0.0062$) and Nitrospirota ($log_2FC = 3.31$, $p_{adj} = 0.0081$) were enriched in high-Hg soils. Together, these patterns indicate a loss of several Cyanobacteriota and fermentative/anaerobic lineages under higher Hg, coupled with increases in Nitrospirota and Nanoarchaeota.

In host-associated microbiomes, few taxa respond to mercury burden, with minor genus-level shifts in skin but not cloacal microbiomes. We also conducted differential abundance analysis of the cloaca and skin microbiomes, and the samples categorized as low or high mercury burden. No taxa were significantly differentially abundant in the low and high mercury samples of the cloaca but analysis of the skin microbiome at the genus level revealed two genera that were significantly more abundant in low mercury samples (DESeq2, $p_{adj} < 0.05$). Significant differences were observed for the genera *Roseiarcus* sp. (Pseudomonadota; $log_2FC = -22.85$, $p_{adj} = 3.29x10^{-10}$), and *MND1* (Planctomycetota; $log_2FC = -22.45$, $p_{adj} = 3.95 \times 10^{-10}$). No significant differential abundances were found at the phylum level.

6.3 Drivers of Dissimilarity between Low and High Mercury Burden Samples (SIMPER Analysis)

To complement the taxon-wise DESeq2 results, we investigated which taxa drive the overall difference between low- and high-Hg communities. We used the Similarity Percentage (SIMPER) test (Clarke, 1993) to decompose Bray-Curtis dissimilarity by taxon and rank the main contributors within each compartment. This community-level view shows that the strongest partitioning occurs in skin (SIMPER at phylum level: 45%), followed by cloaca (44%) and soils (37%), indicating where compositional shifts between Hg bins are most pronounced.

6.3.1 Cloacal microbiomes shift toward metal-tolerant taxa under mercury exposure, while skin communities remain stable.

Cloacal communities differed between mercury groups (Bray-Curtis = 0.441), with Pseudomonadota, Bacteroidota, Bacillota, and Actinomycetota together explaining 66.7% of dissimilarity. Pseudomonadota contributed most (10.7%, p = 0.025), nearly doubling in high-Hg individuals (0.376 vs 0.178). At the class level, Gammaproteobacteria were the top contributor (9.1%, p = 0.042), more than doubling in high-Hg samples (0.318 vs 0.161).

Although skin communities differed the most between mercury groups (Bray-Curtis = 0.451), the difference was diffuse and none of the dominant phylum-level contributors such as Cyanobacteriota (10.2%) or Pseudomonadota (7.5%) showed significant differences (all $p > 0.05$). At the class level, only Planctomycetota showed a modest but significant difference between groups (1.6%, $p = 0.030$). These results collectively suggest that Hg exposure exerts a stronger and more selective pressure on the cloacal microbiome, characterized by large, significant shifts in key taxa, while compositional changes in the skin microbiome appear minor and largely non-specific, with the overall community difference spread across many lower-abundance taxa or finer taxonomic levels.

6.3.2 Mercury exposure restructures soil microbiomes, increasing the abundance of Bacillota and Cyanobacteriota and reducing Chloroflexota abundance.

Soil communities showed clear compositional differences between high- and low-mercury groups (Bray-Curtis dissimilarity = 0.377, indicating 62.3% similarity), with seven phyla explaining 65.7% of the dissimilarity. Bacillota (12.4%, $p = 0.008$) and Cyanobacteriota (12.1%, $p = 0.014$) enriched in high-Hg soils (0.103 vs 0.013 and 0.096 vs 0.007, respectively). In contrast, Chloroflexota (8.1%, $p = 0.004$) were more abundant in low-Hg soils. At the class level, Cyanobacteriia (4.4%, $p = 0.019$) were key contributors in high-Hg soils.

6.4 Host-associated co-occurrence network topology remained stable under high Hg, whereas soil networks contracted

Co-occurrence networks at the genus level were built using Spearman's correlations between taxa abundances, keeping all strong positive and negative relationships ($|\rho| \geq 0.65$, $p < 0.05$) to capture both cooperative and competitive interactions. At the genus level, network topology of host-associated microbiomes (cloaca and skin) remained consistent across mercury bins, whereas the soil microbiome network exhibited substantial contraction under high Hg.

For the cloacal microbiome, the low-Hg network comprised 34 genera and 24 edges (global clustering coefficient = 1.0; modularity = 0.885; 15 modules). Under high Hg, the network expanded to 42 nodes and 77 edges with comparable clustering (1.0) and slightly reduced modularity (0.630; 13 modules). Differences in density, clustering, modularity, and positive-edge ratio were not significant (all $p \geq 0.133$). In the skin microbiome, the low-Hg network included 98 genera and 282 edges (clustering = 0.950; modularity = 0.790). The high-Hg network contained 124 genera and 412 edges (clustering = 1.0; modularity = 0.847). No significant differences were detected for any global property (all $p \geq 0.121$). The soil microbiome displayed distinct topological changes between Hg categories. Under low Hg, the network consisted of 118 genera and 383 edges (clustering = 0.629; modularity = 0.537). Under high Hg, it contracted to 44 nodes and 38 edges, with higher clustering (0.857) and modularity (0.878). Node and edge numbers were significantly lower in the high-Hg network ($p = 0.002$ and $p = 0.001$, respectively). Overall, these data indicate that mercury exposure did not affect the global network organization of host-associated microbiomes, whereas soil networks exhibited reduced complexity and connectivity under high Hg conditions.

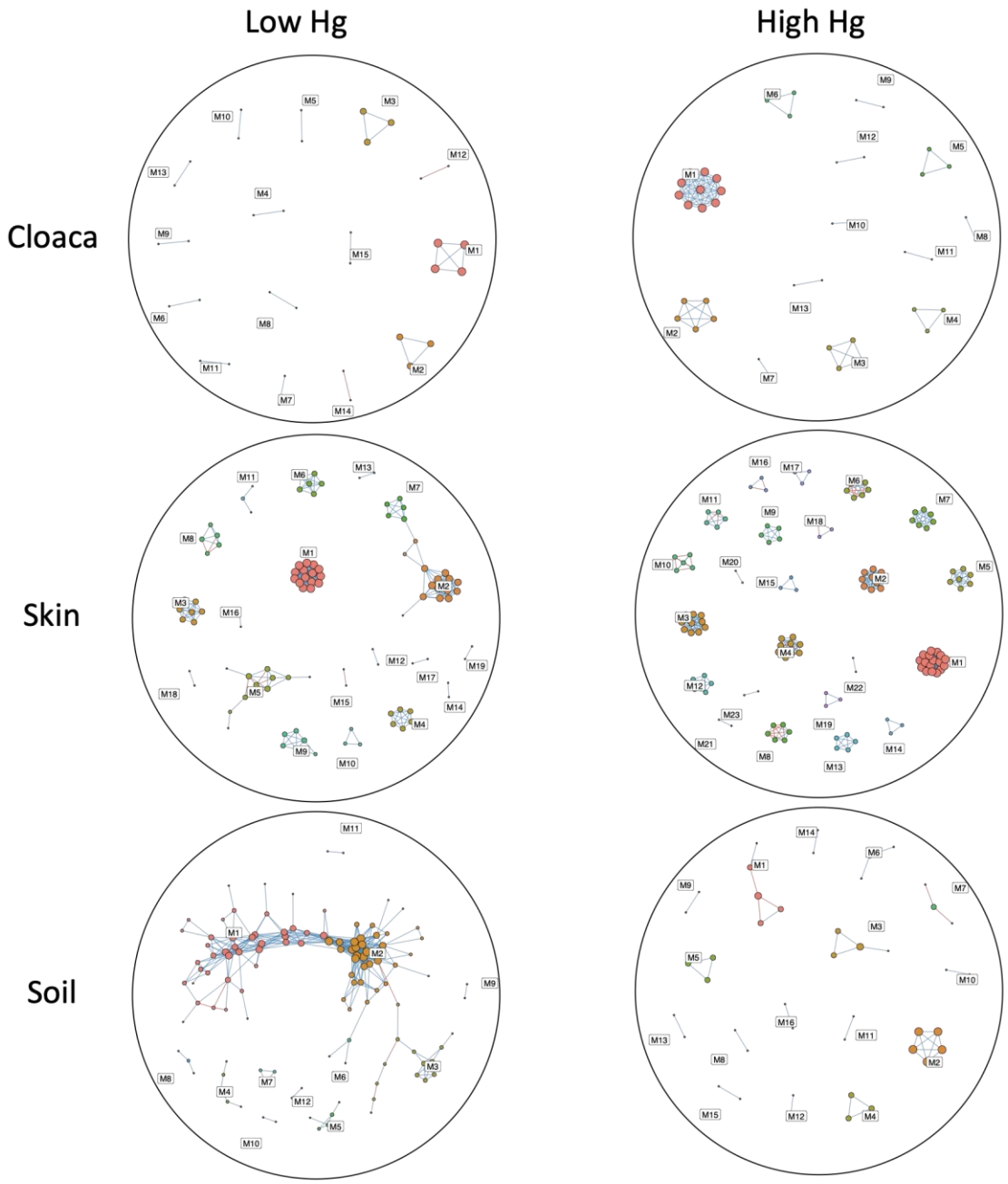

Figure 13: Genus-level co-occurrence network diagrams for cloacal (top panels), skin (middle panels), and soil (bottom panels) microbiomes under low (left panels) and high (right panels) mercury (Hg) exposure. In each panel, nodes represent microbial genera and edges represent significant positive or negative correlations (Spearman's $\rho > |0.65|$, $p < 0.01$) between taxa abundances; colors indicate module membership. Panels for cloaca and skin show consistent network structure between Hg categories, while panels for soil illustrate marked network contraction and reduced connectivity under high Hg conditions

7 Discussion

This study examined the cloacal, skin, and soil microbiomes linked to the caiman species *M. niger* and *P. trigonatus* along a mercury contamination gradient in French Guiana. The results showed that the structure of microbial communities was mostly affected by the environmental compartment (soil, skin, or cloaca) and spatial context. There were also noticeable influences from the host species identity for each compartment. The effects of mercury were specific to each compartment: soil microbial communities showed clear compositional changes along the mercury gradient, while skin and cloacal microbiomes did not demonstrate statistically significant community structure variation attributable to mercury exposure.

Alpha diversity metrics (richness, evenness, Shannon index) did not significantly differ between high- and low-mercury groups in any compartment. However, some trends were noted: cloacal diversity decreased with higher mercury levels, skin microbiomes generally showed increased richness at higher exposures, and soil responses varied depending on the measure used. This difference in alpha diversity responses across compartments suggests the importance of ecological context and exposure routes in affecting stress outcomes. While loss of alpha diversity is often reported under metal contamination stress (Rocca et al., 2019), the increase in skin diversity with Hg exposure may indicate a destabilized surface microbiome that is more vulnerable to environmental changes and opportunistic colonization (review by Huang et al., 2023).

In terms of the genetic factors related to mercury resistance, the *merA* gene was found in samples from both species and all compartments through nested PCR. However, its frequency did not correlate with mercury levels at either the local (sample/site) or individual (host/blood) level. Still, differences in community structure were noted between *merA*-positive and *merA*-negative samples. Network analysis showed that soil co-occurrence connectivity and modularity decreased at high mercury levels, indicating a loss of taxonomic connections and potential key taxa. In contrast, host-associated networks (skin, cloaca) maintained stable, modular structures across exposure levels. This highlights the different ecological support and vulnerability of environmental versus host-associated microbiomes.

Overall, these findings demonstrate that geography and environmental factors are the primary determinants of microbiome composition in this system. Mercury imposes distinct ecological pressures that most strongly affect free-living soil communities, while cloacal and skin microbiomes appear buffered by host physiology and frequent environmental input. Although the *merA* gene was commonly detected, its presence did not reliably reflect environmental mercury exposure, underscoring the need for functional, multi-marker approaches to better assess microbial mercury resistance in complex natural ecosystems.

7.1.1 First integrated microbiome profiles for Neotropical caimans across host and environmental compartments

This study offers the first detailed microbiome profiles for two key Neotropical caiman species, *M. niger* and *P. trigonatus*, filling a knowledge gap in crocodilian host-associated microbial ecology. While prior studies of these species have focused predominantly on tissue contaminant burdens and physiological outcomes (e.g., Lemaire et al., 2020, 2021), this study simultaneously characterizes skin, cloacal, and soil microbiomes using high-throughput sequencing along a natural mercury contamination gradient, providing unique insights into both environmental and host-driven influences on microbial community assembly.

As far as we know, 8 crocodilian species have been examined in wild conditions for the cloacal microbiome: *A. mississippiensis* (Flandry et al. 1989; Johnston et al. 2010; Kieran et al., 2020), A. sinensis (Hu et al., 2022) *Crocodylus acutus* (Cupul-Magaña et al. 2005), *C. niloticus* (Lovely & Leslie 2008), *C. porosus* (Anderson 1999) and *C. johnstoni* (Anderson 1999), *C. moreletii* (Charruau et al., 2012), *C. palustris* (Gholamhosseini et al., 2019), *C. intermedius* (Rudolf et al., 2018). Additionally, the Cloacal mycobiota in wild females of *Caiman latirostris* has been studied (Nunez-Otano et al., 2013) and *Caiman Latriostris* (Silva et al., 2008) in captivity. However, to our knowledge no study has jointly profiled skin, cloaca, and local soils in the wild or evaluated these compartments across a contaminant gradient.

Resolving caiman host-associated microbiota is relevant for wildlife health and risk to humans. Cloacal bacteria can infect eggshells, membranes, and yolks during oviposition, with implications for reproductive success (Huchzermeyer, 2003). In addition, crocodilian-associated bacteria can be transmitted to humans through consumption of meat, bites, or exposure during activities in crocodilian habitats (Suárez et al., 2000; Magnino et al., 2009; Caldicott et al., 2005; Johnston et al., 2010). By linking host-associated communities to environmental sources and mercury exposure, the present dataset addresses these ecological and applied dimensions simultaneously.

7.1.2 Host filtering dominates cloacal microbiome structure, while external factors structure skin and soils

Looking at each microbial environment, we found distinct factors explaining community structure The cloacal microbiome appears to be primarily host-filtered: species identity is the dominant axis of variation and communities are consistently structured, suggesting deterministic assembly in a stable host niche. Body condition index correlated with microbial community structure, but was not significant, which could be due to unmeasured factors like temperature (Moeller et al., 2020), sex (Hu et al., 2022) or seasonal fasting (Tang et al., 2019; Keenan et al., 2013), host genetics (Zhang et al., 2023) and opening their mouths for thermoregulation (Keenan et al., 2013). It is also possible that due

to the pathogen rich environments and carrion feeding lifestyle of crocodilians they have a highly adapted immune system that co-evolved with their microbiomes, thereby limiting toxic health effects (Keenan and Elsey 2015).

External filters dominate microbiome assembly on skin and in soils. For skin, geographic location explains more variance than host species or internal mercury, consistent with the skin's role as a transient interface repeatedly seeded by local water and sediments and with prior evidence that vertebrate skin communities are chiefly shaped by environmental exposure (Ross et al., 2019; Grice et al., 2008; Kueneman et al., 2014). Soil community composition is driven by site-specific geochemistry (habitat, redox status, organic matter, and contaminant load), which explains the spatial clustering of sites and the additional variance attributable to mercury. Although Hg effects in soils depend on total Hg, speciation, and local geochemistry and may only appear beyond site-specific thresholds (Frossard et al., 2017; Zheng et al., 2022; Frey and Rieder, 2013), we nevertheless detected a clear mercury signal on soil microbiome composition across the relatively narrow Hg range sampled in this study.

7.1.3 Between High And Low Mercury Groups, Alpha Diversity Decreases In Cloacal, Increases In Skin Microbiomes And Shows Mixed Responses in Soil

Alpha diversity responded to mercury in opposite directions across matrices. In the cloaca, diversity declined with higher mercury, consistent with selective loss of sensitive symbionts in a host-filtered niche and potential functional narrowing. In contrast, skin diversity increased, and soils displayed mixed responses. Although stressors often reduce diversity (Rocca et al., 2018), increases can also indicate destabilization because as vulnerable species decline, opportunistic and transient species can thrive which can inflate richness without actually improving ecosystem function (Williams et al., 2024). Comparable increases of alpha diversity under stress have been reported for mercury-impacted and industrial soils and for early heat-stressed coral microbiomes, where host control weakens (Frossard et al., 2018; Bourceret et al., 2015; McDevitt-Irwin et al., 2019). Our relatively low Hg levels, together with limited host regulation of crocodilian skin, offer a plausible explanation for increased alpha diversity in the skin microbiomes with increased mercury. The lack of statistical significance for most comparisons indicates mercury levels are either below ecological thresholds or that binning exposure into a simple high/low category is too coarse to detect subtle or nonlinear effects. A design that includes bioavailable Hg metrics and long-term sampling of the microbiome would more effectively test if these trends indicate temporary dynamics or ongoing changes.

7.1.4 Mercury Collapses Soil Microbial Co-occurrence Networks Collapse and Rewiring while host associated networks show no topological changes.

Co-occurrence networks collapsed in soils at higher mercury, with sharp losses in connectivity, redundancy, and putative keystones (e.g., *Clostridium*s sp., *Telmatospirillum* sp.) (Coyte et al., 2015; Bauchinger et al., 2024). Low-Hg soil networks were dominated by densely positive associations that vanished under high Hg. Theoretical models predict that communities stabilized by many weak links are more robust than those dominated by strong positive feedback meaning that weakening interaction strengths actually promotes co-occurrence network stability (Neutel et al., 2002; Coyte et al., 2015). The presence of strongly positively linked modules therefore suggests that low-Hg soils were already unstable, and mercury caused it to collapse. Functionally, the soil network collapse means fewer backup interactions and a higher risk that key processes fail under additional stress. In contrast, skin and cloacal networks showed little topological change across mercury gradients. High modularity with fewer positive ties likely buffers them, supporting the view that exposed soils are more vulnerable to direct stress than host-associated niches and that host-associated niches allow for more stable networks (Frossard et al., 2018). The stable topology accompanied by the turnover of network participants therefore suggests that the host-associated microbiomes can absorb stress without major disruption.

7.1.5 Across compartments, taxa with known metal resistance or detoxification capacity consistently contributed to differences between high and low Hg groups

We identified Pseudomonadota, Acidobacteriota, Actinomycetota, and Chloroflexota as dominant mercury-tolerant phyla consistently present across soil, skin, and cloacal microbiomes. These taxa align with findings from mercury-contaminated environments such as gold mining areas (Sonthiphand et al., 2021) and heavy-metal contaminated rice fields in Guizhou (Vishnivetskaya et al., 2018). The recurrent detection of these phyla in such diverse habitats underscores mercury contamination as a potent environmental filter, promoting the selection of resistant lineages, driving convergence in community composition despite ecological and physiological differences among soil, skin, and cloacal environments. Though less studied, Acidobacteriota and Chloroflexota can contribute to metal tolerance, enhancing microbial survival in contaminated niches (Wang et al., 2020). Their presence within cloacal microbiomes suggests ecological connectivity and gene flow between environmental reservoirs and host-associated communities, facilitating adaptation to mercury toxicity.

In soils, high-mercury sites were enriched in Bacillota (notably Bacilli) and Cyanobacteriota. In host-associated communities, high mercury was linked to higher Pseudomonadota (especially Gammaproteobacteria) and Actinomycetota in the cloaca, and Pseudomonadota and Cyanobacteriota on the skin. These patterns indicate that mercury acts as a selective filter, but its effect depends on local parameters (e.g., redox, DOM quality) and the degree of host control.

7.1.6 Irregular *merA* distribution suggests microhabitat-level selection rather than widespread adaptation

Based on current literature, mercury contamination is expected to select for microbial taxa harboring mercury resistance genes such as *merA*, particularly in environments and hosts exposed to variable mercury burdens like *M. niger* and *P. trigonatus* (Lemaire et al., 2020; Barkay et al., 2003). In line with this expectation, both caiman species' microbiomes contained well-known heavy metal-resistant groups, with Gammaproteobacteria and Actinomycetota more abundant in *M. niger* and Alphaproteobacteria more prevalent in *P. trigonatus*; both clades are recognized carriers of *merA* (Johnson et al., 2001; Radeva et al., 2013; Conteville et al., 2023; Zuo et al., 2023; Boyd and Barkay, 2012). Despite this, detection of the *merA* gene itself was irregular across soils, skin, and cloaca samples and showed no clear correlation with measured mercury levels. For instance, some individuals displayed *merA* presence on skin but absence in adjacent soil and cloacal samples or presence in soil but absence in the host-associated samples, suggesting fine-scale environmental heterogeneity with patchy mercury bioavailability and localized selective pressures driving *merA* presence (Cardona-Marek et al., 2007). Anoxic or hypoxic conditions in soils and cloacal sites could be reducing mercury bioavailability through chemical precipitation thereby reducing selective pressure for *merA* maintenance in these microhabitats (Cardona-Marek et al., 2007).

The class Clostridia was also enriched in *M. niger* and significantly contributed to differences between *merA*-negative and *merA*-positive skin microbiomes, with similar but non-significant trends in cloacal and soil samples. Clostridia depletion in *merA*-positive samples suggests sensitivity or exclusion in environments favoring *merA*-harboring taxa as Clostridia are strict anaerobes found widely in environmental and gut microbiotas and are capable of reducing Hg^{2+} independently of the *mer* operon via alternative metabolic pathways (Morvan et al., 2021; Grégoire et al., 2018). The lack of a strong Clostridia shift in cloaca samples may reflect their adaptation to this anaerobic, mucosal niche, where host factors maintain community stability despite *merA* variations, current research has indeed identified Clostridia as a main component of crocodilian gut microbiomes (Willson et al., 2019). Clostridia have also been identified as mercury methylators in sediments, like genera including *Dethiobacter* sp., *Ethanoligenens* sp. and *Desulfosporosinus* sp. (Yuan et al., 2019). Future work should profile mercury-methylating taxa (e.g., sulfate- and iron-reducing bacteria) and test whether hosts exclude these lineages, since a microbiome-mediated mitigation of Hg toxicity would predict reduced methylator prevalence in host communities relative to surrounding soils (Yuan et al., 2019; Cooper et al., 2005; Fleming et al., 2006).

The inconsistent *merA* detection despite the presence of typical *merA* carriers may also reflect methodological limitations. Although a broad primer set was employed, it may not capture the full genetic diversity of *merA* variants across taxa, or dominant lineages in some samples may genuinely

lack the gene (Felske et al., 2003; Oregaard et al., 2007). Detailed taxonomic analyses of *merA*-negative samples are warranted to distinguish between true absence and methodological detection failure. Additionally, current literature suggests that *merA* presence does not guarantee mercury resistance. Isolates can carry *merA* yet fail to grow under Hg stress outside contaminated contexts (Trojańska et al., 2022; Bogdanova et al., 1992). Robust inference should combine multi-gene screening (e.g., *merA/merB/merR/merT/merP*), expression or activity assays, and non-*mer* operon routes such as fermentative Hg^{2+} reduction (Clostridia) and DOM-mediated chemical reduction of Hg^{2+} (Gu et al., 2010). So, metrics like *merA* presence, differential abundance, or SIMPER alone cannot determine which microbiomes are better equipped to detoxify mercury.

7.1.7 *Psychrobacter*-related *merA* in host skin and cloaca samples despite non-detected 16S rRNA amplicon

We detected a *merA* variant closely related to *Psychrobacter* sp. by colony PCR and Sanger sequencing of *merA* amplicons in host-associated samples (skin and cloaca), but not in adjacent soil. In the corresponding 16S dataset, the genus *Psychrobacter sp.* was not recovered; instead, reads were assigned to Moraxellaceae at the family level, with 36 ASV observations distributed primarily in skin (n = 24), followed by cloaca (n = 11) and soil (n = 1). Moraxellaceae occurred in both host species, *P. trigonatus* and *M. niger*, and positives spanned both skin and cloacal niches.

This pattern is consistent with a predominantly host-associated ecology. *Psychrobacter* sp. is frequently reported from vertebrate skin and mucosa, including horses and marine mammals such as whales and seal pups (O'Shaughnessy-Hunter et al., 2021; Strompfová & Štempelová, 2024; Apprill et al., 2014; Watkins et al., 2022). At the same time, several *Psychrobacter* sp. lineages are soil and rhizosphere associates that promote plant growth and tolerate metals in contaminated soils (Ayala-del-Río et al., 2010; Ma et al., 2011; Pepi et al., 2011). These external reservoirs provide plausible sources for mer-bearing Moraxellaceae that can colonize host surfaces.

The apparent discrepancy between functional detection of *Psychrobacter* sp. *merA*, and the absence of genus-level 16S calls is likely methodological rather than biological. Short 16S regions have limited resolving power, standard classifiers favor conservative assignments at the family level, and *merA* can occur elsewhere within Moraxellaceae through horizontal transfer. Consistent with prior work, *Psychrobacter* sp. carries the *mer* operon and has been discussed as a candidate for mercury bioremediation (Mahbub et al., 2017; Pepi et al., 2011). Our data support a host-associated reservoir of *mer*-bearing Moraxellaceae (possibly *Psychrobacter* sp.) on skin and cloaca. Given that MerA reduces Hg^{2+} to volatile Hg^0, this could lower local Hg^{2+} bioavailability at host surfaces and thus contribute to a microbially mediated detoxification mechanism. However, we have not shown in situ activity or host

benefit, and alternative explanations like transient carriage, or contamination of skin samples from the soil, remain plausible.

7.2 Limitations

Total mercury was measured in the soil however the chemical form of mercury is influenced by environmental factors such as dissolved organic matter, redox conditions, sulfate and sulfide, pH, and salinity (Frey and Rieder, 2013; Frossard et al., 2017; Eagles-Smith et al., 2018). Therefore, abiotic conditions can modulate the selective pressure exerted by mercury in soil and the mostly modest and sometimes non-significant microbiome responses we observed likely reflect this limitation and the relatively narrow mercury ranges in our dataset. Total blood mercury concentrations do not present the same problem as around 80% of measured total mercury is methylmercury (May et al., 1987; Wells et al., 2022). Although soil Hg is a better proxy for skin exposure, using blood mercury quantifies the exposure of the host-associated microbiomes more robustly.

Our study design also places some limits on inference. Sampling was uneven across locations and hosts; for example, only one soil sample was associated with *M. niger*, and cloacal sample sizes were small. Some of the group differences in the PERMANOVA coincided with differences in within-group spread, especially for skin and soil, which makes location effects harder to interpret. Methodological constraints in molecular work limited analysis. Water samples did not yield amplifiable DNA and were excluded, which reduced our ability to compare environmental versus host-associated microbiomes. Several qPCR assays targeting *merA* failed to amplify despite using broad primer panels, so we relied on presence or absence from nested PCR and could not estimate gene copy numbers which could be due to primer mismatches to local tropical lineages. Finally, amplicon sequencing of the 16S rRNA gene has limited functional resolution as we cannot confidently link *merA* or metal resistance traits to individual ASVs.

Analytical choices add another layer of uncertainty. For some comparisons we split mercury into high and low groups at the median to align across datasets. This choice makes results easier to communicate but throws away information and can weaken dose-response signals, especially as the gradient of mercury concentration is narrow. Lastly, the two caiman species occupy different habitats, with *P. trigonatus* in closed-canopy forests and *M. niger* in coastal swamps, which could be responsible for differences observed between species and environment that we could only partly address with species-restricted models.

7.3 Future directions

For future research, mercury assessments should prioritize speciation and bioavailable pools rather than total concentrations. Recording environmental parameters such as soil pH, total and dissolved organic matter, and sulfate would help separate mercury effects from broader geochemical gradients. To characterize resistance mechanisms and community adaptation, sequencing could extend beyond 16S rRNA to shotgun metagenomics and metatranscriptomics. This would allow the diversity and activity of the *mer* operon (including *merA* and *merB*), alternative pathways and detoxification mechanisms to be captured. Metagenomic data would also support the design of environment-specific primers for quantitative *merA* qPCR and allow for more robust comparisons between species and habitats. These molecular tools coupled with more metadata would clarify links among community composition, functional potential, and biogeochemical cycling in caiman habitats.

Sampling should be expanded with larger, balanced designs across host species, habitats, and seasons, with power analyses based on the effect sizes observed here to set targets. Integrating microbiome data with caiman health and conservation metrics is critical under ongoing environmental change and mercury exposure; linking microbial indicators to host condition, stress biomarkers, and demographic outcomes could provide early-warning tools and guide management decisions. Finally, combining high-resolution environmental chemistry with functional genomics and ecological context will clarify how caiman-associated microbiomes respond to mercury and whether they buffer or amplify contaminant risks in Amazonian ecosystems.

8 References

Achá, D., Hintelmann, H., Pavinich-Bertagnolli, L., & Brito, L. F. (2011). Sulfate-reducing bacteria and mercury methylation in tropical wetlands. Environmental Science & Technology, 45(2), 479-485. https://doi.org/10.1021/es1023628

Agency for Toxic Substances and Disease Registry. (2024). Substance Priority List. U.S. Department of Health & Human Services. https://www.atsdr.cdc.gov/spl/

AMAP. (2021). AMAP Assessment 2021: Mercury in the Arctic. Arctic Monitoring and Assessment Programme. https://www.amap.no/

Anderson, J. R. (1999). Characterisation of the oral and cloacal flora of wild and farmed crocodiles (Crocodylus porosus and C. johnstoni) in northern Australia [Honours thesis, James Cook University of North Queensland].

Anderson, M. J. (2001). A new method for non-parametric multivariate analysis of variance. Austral Ecology, 26, 32-46.

Anderson, M. J. (2006). Distance-based tests for homogeneity of multivariate dispersions. Biometrics, 62, 245-253.

Anisimova, M., & Gascuel, O. (2006). Approximate likelihood-ratio test for branches: A fast, accurate, and powerful alternative. Systematic Biology, 55(4), 539-552. https://doi.org/10.1080/10635150600755453

Apprill, A., McNally, S., Parsons, R., & Weber, L. (2015). Minor revision to V4 region SSU rRNA 806R gene primer greatly increases detection of SAR11 bacterioplankton. Frontiers in Microbiology, 6, 1480. https://doi.org/10.3389/fmicb.2015.01480

Bae, H.-S., Dierberg, F. E., & Ogram, A. (2014). Syntrophs dominate sequences associated with the mercury methylation-related gene hgcA in the water conservation areas of the Florida Everglades. Applied and Environmental Microbiology, 80(20), 6517-6526. https://doi.org/10.1128/AEM.01666-14

Barbosa, A. C., Souza, J. D., Dórea, J. G., Jardim, W. F., & Fadini, P. S. (2003). Mercury biomagnification in a tropical black water, Rio Negro, Brazil. Archives of Environmental Contamination and Toxicology, 45(2), 235-246. https://doi.org/10.1007/s00244-003-0207-1

Barkay, T., Kritee, K., Boyd, E., & Geesey, G. (2010). A thermophilic bacterial origin and subsequent constraints by redox, light and salinity on the evolution of the microbial mercuric reductase. Environmental Microbiology, 12(11), 2904-2917. https://doi.org/10.1111/j.1462-2920.2010.02260.x

Barkay, T., Miller, S. M., & Summers, A. O. (2003). Bacterial mercury resistance from atoms to ecosystems. FEMS Microbiology Reviews, 27(2-3), 355-384. https://doi.org/10.1016/S0168-6445(03)00046-9

Barbieri, F. L., & Gardon, J. (2009). Hair mercury levels in Amazonian populations: Spatial distribution and trends. International Journal of Health Geographics, 8, 71. https://doi.org/10.1186/1476-072X-8-71

Bauchinger, F., Seki, D., & Berry, D. (2024). Characteristics of putative keystones in the healthy adult human gut microbiota as determined by correlation network analysis. Frontiers in Microbiology, 15, 1454634. https://doi.org/10.3389/fmicb.2024.1454634

Beijer, K., & Jernelöv, A. (1978). Ecological aspects of mercury-selenium interactions in the marine environment. Environmental Health Perspectives, 25, 43-45. https://doi.org/10.2307/3428707

Bell, M. E., Bernard, K. A., Harrington, S. M., Patel, N. B., Tucker, T. A., Metcalfe, M. G., & McQuiston, J. R. (2016). Lawsonella clevelandensis gen. nov., sp. nov., a new member of the suborder Corynebacterineae isolated from human abscesses. International Journal of Systematic and Evolutionary Microbiology, 66(8), 2929-2935. https://doi.org/10.1099/ijsem.0.001122

Benjamini, Y., & Hochberg, Y. (1995). Controlling the false discovery rate: A practical and powerful approach to multiple testing. Journal of the Royal Statistical Society: Series B (Methodological), 57(1), 289-300.

Benjamini, Y., & Hochberg, Y. (1995). Controlling the false discovery rate. Journal of the Royal Statistical Society: Series B (Methodological), 57(1), 289-300.

Bhat, A., Sharma, R., Desigan, K., Lucas, M. M., Mishra, A., Bowers, R. M., Woyke, T., Epstein, B., Tiffin, P., Pueyo, J. J., & Paape, T. (2024). Horizontal gene transfer of the Mer operon is associated with large effects on the transcriptome and increased tolerance to mercury in nitrogen-fixing bacteria. BMC Microbiology, 24(1), 247. https://doi.org/10.1186/s12866-024-03391-5

Bodenhofer, U., Bonatesta, E., Horejš-Kainrath, C., & Hochreiter, S. (2015). msa: An R package for multiple sequence alignment. Bioinformatics, 31(24), 3997-3999. https://doi.org/10.1093/bioinformatics/btv494

Bogdanova, E. S., Mindlin, S. Z., Pakrová, E., Kocur, M., & Rouch, D. A. (1992). Mercuric reductase in environmental gram-positive bacteria sensitive to mercury. FEMS Microbiology Letters, 76(1-2), 95-100. https://doi.org/10.1016/0378-1097(92)90370-4

Bolyen, E., Rideout, J. R., Dillon, M. R., Bokulich, N. A., Abnet, C. C., Al-Ghalith, G. A., Alexander, H., Alm, E. J., Arumugam, M., Asnicar, F., Bai, Y., Bisanz, J. E., Bittinger, K., Brejnrod, A., Brislawn, C. J., Brown, C. T., Callahan, B. J., Caraballo-Rodríguez, A. M., Chase, J., … Caporaso, J. G. (2019). Reproducible, interactive, scalable and extensible microbiome data science using QIIME 2. Nature Biotechnology, 37(8), 852–857. https://doi.org/10.1038/s41587-019-0209-9

Borcard, D., Legendre, P., & Drapeau, P. (1992). Partialling out the spatial component of ecological variation. Ecology, 73(3), 1045-1055. https://doi.org/10.2307/1940179

Bourceret, A., Cébron, A., Tisserant, E., Poupin, P., Bauda, P., Beguiristain, T., & Leyval, C. (2016). The bacterial and fungal diversity of an aged PAH- and heavy metal-contaminated soil is affected by plant cover and edaphic parameters. Microbial Ecology, 71(3), 711-724. https://doi.org/10.1007/s00248-015-0682-8

Boyd, E. S., & Barkay, T. (2012). The mercury resistance operon: From an origin in a geothermal environment to an efficient detoxification machine. Frontiers in Microbiology, 3, 349. https://doi.org/10.3389/fmicb.2012.00349

Bray, J. R., & Curtis, J. T. (1957). An ordination of the upland forest communities of southern Wisconsin. Ecological Monographs, 27, 325-349.

Brewer, T. E., Handley, K. M., Carini, P., Gilbert, J. A., & Fierer, N. (2016). Genome reduction in an abundant and ubiquitous soil bacterium 'Candidatus Udaeobacter copiosus'. Nature Microbiology, 2(2), 16198. https://doi.org/10.1038/nmicrobiol.2016.198

Briffa, J., Sinagra, E., & Blundell, R. (2020). Heavy metal pollution in the environment and their toxicological effects on humans. Heliyon, 6(9), e04691. https://doi.org/10.1016/j.heliyon.2020.e04691

Buenfil-Rojas, A. M., Álvarez-Legorreta, T., & Cedeño-Vázquez, J. R. (2015). Metals and metallothioneins in Morelet's crocodile (Crocodylus moreletii) from a transboundary river between Mexico and Belize. Archives of Environmental Contamination and Toxicology, 68(2), 265-273. https://doi.org/10.1007/s00244-014-0088-5

Bunker, M. E., & Weiss, S. L. (2022). Cloacal microbiomes of sympatric and allopatric Sceloporus lizards vary with environment and host relatedness. PLOS ONE, 17(12), e0279288. https://doi.org/10.1371/journal.pone.0279288

Cabral, L., Junca, H., & Andreote, F. D. (2016). Anthropogenic impact on mangrove sediments triggers differential responses in the heavy metals and antibiotic resistomes of microbial communities. Applied Microbiology and Biotechnology, 100(12), 5711–5727. https://doi.org/10.1007/s00253-016-7350-y

Callahan, B. J., McMurdie, P. J., Rosen, M. J., Han, A. W., Johnson, A. J. A., & Holmes, S. P. (2016). DADA2: High-resolution sample inference from Illumina amplicon data. Nature Methods, 13(7), 581-583. https://doi.org/10.1038/nmeth.3869

Caldicott, D. G. E., Croser, D., Manolis, C., Webb, G., & Britton, A. (2005). Crocodile attack in Australia: An analysis of its incidence and review of the pathology and management of crocodilian attacks in general. Wilderness & Environmental Medicine, 16(3), 143–159. https://doi.org/10.1580/1080-6032(2005)16[143:CAIAAA]2.0.CO;2

Cardona-Marek, T., Schaefer, J., Ellickson, K., Barkay, T., & Reinfelder, J. R. (2007). Mercury speciation, reactivity, and bioavailability in a highly contaminated estuary, Berry's Creek, New Jersey Meadowlands. Environmental Science & Technology, 41(24), 8268-8274. https://doi.org/10.1021/es070945h

Cedillo-Leal, C. N., Cienfuegos-Rivas, E., & Escobedo-Galván, A. H. (2018). High levels of heavy metals in scutes and eggs of Morelet's crocodiles (Crocodylus moreletii) from northeast Mexico. The Southwestern Naturalist, 63(1), 71-74. https://doi.org/10.1894/0038-4909.63.71

Charruau, P., Pérez-Flores, J., Pérez-Juárez, J., Cedeño-Vázquez, J., & Rosas-Carmona, R. (2012). Oral and cloacal microflora of wild crocodiles Crocodylus acutus and C. moreletii in the Mexican Caribbean. Diseases of Aquatic Organisms, 98(1), 27-39. https://doi.org/10.3354/dao02418

Chen, C. Y., Driscoll, C. T., Eagles-Smith, C. A., Eckley, C. S., Gay, D. A., Hsu-Kim, H., Keane, S. E., Kirk, J. L., Mason, R. P., Obrist, D., Selin, H., Selin, N. E., & Thompson, M. R. (2018). A Critical Time for Mercury Science to Inform Global Policy. Environmental Science & Technology, 52(17), 9556–9561. https://doi.org/10.1021/acs.est.8b02286

Chen, Y., Jiang, Y., Huang, H., Mou, L., Ru, J., Zhao, J., & Xiao, S. (2018). Long-term and high-concentration heavy-metal contamination strongly influences the microbiome and functional genes in Yellow River sediments. Science of the Total Environment, 637-638, 1400-1412. https://doi.org/10.1016/j.scitotenv.2018.05.109

Christakis, C. A., Barkay, T., & Boyd, E. S. (2021). Expanded diversity and phylogeny of mer genes broadens mercury resistance paradigms and reveals an origin for MerA among thermophilic archaea. Frontiers in Microbiology, 12, 682605. https://doi.org/10.3389/fmicb.2021.682605

Christensen, G. A., Gionfriddo, C. M., King, A. J., Moberly, J. G., Miller, C. L., Somenahally, A. C., Callister, S. J., Brewer, H., Podar, M., Brown, S. D., Palumbo, A. V., Brandt, C. C., Wymore, A. M., Brooks, S. C., Hwang, C., Fields, M. W., Wall, J. D., Gilmour, C. C., & Elias, D. A. (2019). Determining the Reliability of Measuring Mercury Cycling Gene Abundance with Correlations with Mercury and

Methylmercury Concentrations. Environmental Science & Technology, 53(15), 8649–8663. https://doi.org/10.1021/acs.est.8b06389
Chu, Z., Song, Y., Li, Y., Shu, L., Li, S., & Yang, Z. (2024). Effects of heavy metals and environmental variables on soil microbial communities in different land-use types of Yellow River Delta (YRD), China. Environmental Earth Sciences, 83(12), 368. https://doi.org/10.1007/s12665-024-11685-0

Clark, D. L., Weiss, A. A., & Silver, S. (1977). Mercury and organomercurial resistances determined by plasmids in Pseudomonas. Journal of Bacteriology, 132(1), 186-196. https://www.ncbi.nlm.nih.gov/pmc/articles/PMC221844/

Clarke, K. R. (1993). Non-parametric multivariate analyses of changes in community structure. Australian Journal of Ecology, 18(1), 117-143. https://doi.org/10.1111/j.1442-9993.1993.tb00438.x

Clarkson, T. W., Magos, L., & Myers, G. J. (2003). The toxicology of mercury—Current exposures and clinical manifestations. New England Journal of Medicine, 349(18), 1731-1737. https://doi.org/10.1056/NEJMra021224

Compeau, G. C., & Bartha, R. (1985). Sulfate-reducing bacteria: Principal methylators of mercury in anoxic estuarine sediment. Applied and Environmental Microbiology, 50(2), 498-502.

Conteville, L. C., Oliveira-Ferreira, J., & Vicente, A. C. P. (2023). Heavy metal resistance in the Yanomami and Tunapuco microbiome. Memórias do Instituto Oswaldo Cruz, 118, e230086. https://doi.org/10.1590/0074-02760230086

Cordeiro, I. F., Lemes, C. G. de C., Sanchez, A. B., da Silva, A. K., de Paula, C. H., de Matos, R. C., Ribeiro, D. F., de Matos, J. P., Garcia, C. C. M., Beirão, M., Becker, C. G., Pires, M. R. S., & Moreira, L. M. (2024). Amphibian tolerance to arsenic: Microbiome-mediated insights. Scientific Reports, 14(1), 10193. https://doi.org/10.1038/s41598-024-60879-w

Coyte, K. J., Schluter, J., & Foster, K. R. (2015). The ecology of the microbiome: Networks, competition, and stability. Science, 350(6261), 663-666. https://doi.org/10.1126/science.aad2602

Cupul-Magaña, F. G., Rubio-Delgado, A., & Reyes-Juárez, A. (2005). La mordida del cocodrilo americano (Crocodylus acutus), ¿es potencialmente séptica? Revista Biomédica, 16(1), 65–67.

Das, S., Najar, I. N., Sherpa, M. T., Kumar, S., Sharma, P., Mondal, K., Tamang, S., & Thakur, N. (2023). Baseline metagenome-assembled genome (MAG) data of Sikkim hot springs from Indian Himalayan geothermal belt (IHGB) showcasing its potential CAZymes, and sulfur-nitrogen metabolic activity. World Journal of Microbiology and Biotechnology, 39(7), 179. https://doi.org/10.1007/s11274-023-03631-2

DeSantis, T. Z., Hugenholtz, P., Larsen, N., Rojas, M., Brodie, E. L., Keller, K., ... & Andersen, G. L. (2006). Greengenes, a chimera-checked 16S rRNA gene database and workbench. Applied and Environmental Microbiology, 72(7), 5069-5072. https://doi.org/10.1128/AEM.03006-05

Diringer, S. E., Roulet, M., Guimarães, J. R. D., Sousa Passos, C. J., Mergler, D., & Lavoie, R. (2015). River transport of mercury from artisanal and small-scale gold mining in the Madre de Dios River Basin, Peru. Environmental Science: Processes & Impacts, 17(2), 478–487. https://doi.org/10.1039/C4EM00567H

Drewniak, L., Krawczyk, P. S., Mielnicki, S., Adamska, D., Sobczak, A., Lipinski, L., Burec-Drewniak, W., & Sklodowska, A. (2016). Physiological and Metagenomic Analyses of Microbial Mats Involved in Self-Purification of Mine Waters Contaminated with Heavy Metals. Frontiers in Microbiology, 7. https://doi.org/10.3389/fmicb.2016.01252

Driscoll, C. T., Mason, R. P., Chan, H. M., Jacob, D. J., & Pirrone, N. (2013). Mercury as a global pollutant: Sources, pathways, and effects. Environmental Science & Technology, 47(10), 4967-4983. https://doi.org/10.1021/es305071v

Eagles-Smith, C. A., Silbergeld, E. K., Basu, N., Bustamante, P., Diaz-Barriga, F., Hopkins, W. A., Kidd, K. A., & Nyland, J. F. (2018). Modulators of mercury risk to wildlife and humans in the context of rapid global change. Ambio, 47(2), 170–197. https://doi.org/10.1007/s13280-017-1011-x

Escapa, I. F., Chen, T., Huang, Y., Gajare, P., Dewhirst, F. E., & Lemon, K. P. (2018). New insights into human nostril microbiome from the expanded Human Oral Microbiome Database (eHOMD): A resource for the microbiome of the human aerodigestive tract. mSystems, 3(6), e00187-18. https://doi.org/10.1128/mSystems.00187-18

Escallón, C., Belden, L. K., & Moore, I. T. (2019). The cloacal microbiome changes with the breeding season in a wild bird. Integrative Organismal Biology, 1(1), oby009. https://doi.org/10.1093/iob/oby009

Esdaile, L. J., & Chalker, J. M. (2018). The mercury problem in artisanal and small-scale gold mining. Chemistry - A European Journal, 24(27), 6905-6916. https://doi.org/10.1002/chem.201704840

Faith, D. P. (1992). Conservation evaluation and phylogenetic diversity. Biological Conservation, 61(1), 1-10. https://doi.org/10.1016/0006-3207(92)91201-3

Fierer, N. (2017). Embracing the unknown: Disentangling the complexities of the soil microbiome. Nature Reviews Microbiology, 15(10), 579-590. https://doi.org/10.1038/nrmicro.2017.87

Fierer, N., Hamady, M., Lauber, C. L., & Knight, R. (2008). The influence of sex, handedness, and washing on the diversity of hand surface bacteria. Proceedings of the National Academy of Sciences, 105(46), 17994-17999. https://doi.org/10.1073/pnas.0807920105

Flandry, F., Lisecki, E. J., Domingue, G. J., Nichols, R. L., Greer, D. L., & Haddad, R. J. (1989). Initial antibiotic therapy for alligator bites: Characterization of the oral flora of Alligator mississippiensis. Southern Medical Journal, 82(2), 262–266. https://doi.org/10.1097/00007611-198902000-00021

Fosmire, G. J. (1990). Zinc toxicity. The American Journal of Clinical Nutrition, 51(2), 225–227. https://doi.org/10.1093/ajcn/51.2.225

Franco, M. W., Mendes, L. A., Windmöller, C. C., Moura, K. A. F., Oliveira, L. A. G., & Barbosa, F. A. R. (2018). Mercury methylation capacity and removal of Hg species from aqueous medium by cyanobacteria. Water, Air, & Soil Pollution, 229(4), 127. https://doi.org/10.1007/s11270-018-3782-5

Frey, B., & Rieder, S. R. (2013). Response of forest soil bacterial communities to mercury chloride application. Soil Biology and Biochemistry, 65, 329-337. https://doi.org/10.1016/j.soilbio.2013.06.001

Frossard, A., Donhauser, J., Mestrot, A., Gygax, S., Bååth, E., & Frey, B. (2018). Long- and short-term effects of mercury pollution on the soil microbiome. Soil Biology and Biochemistry, 120, 191-199. https://doi.org/10.1016/j.soilbio.2018.01.028

Fulton, T. W. (1904). The rate of growth of fishes. 22nd Annual Report of the Fishery Board for Scotland, 3, 141-241.

Ge, L., Yuan, X., Zhang, L., Li, H., Liu, X., & Zhu, X. (2024). Uncovering the relationship between soil bacterial community and heavy metals in a copper waste pile. Minerals, 14(12), 1237. https://doi.org/10.3390/min14121237

Gholamhosseini, A., Banaee, M., Soltanian, S., & Sakhaie, F. (2022). Heavy metals in the blood serum and feces of Mugger crocodile (Crocodylus palustris) in Sistan and Baluchistan Province, Iran. Biological Trace Element Research, 200(7), 3336-3345. https://doi.org/10.1007/s12011-021-02916-7

Gholamhosseini, A., Sharifiyazdi, H., Rakhshaninejad, M., Soltanian, S., Salighehzadeh, R., & Kordestani, H. (2021). A study on the oral and cloacal bacterial flora of Mugger crocodiles (Crocodylus palustris) in the Negour protected area, Iran. Veterinary Research Forum, 12(3), 361-367. https://doi.org/10.30466/vrf.2019.108417.2571

Ghosh, S., Mohapatra, S., & Ram, A. (2015). Distribution of mercury resistance genes in estuarine sediments and their association with anthropogenic activities. Marine Pollution Bulletin, 93(1-2), 200-207. https://doi.org/10.1016/j.marpolbul.2015.01.033

Gilmour, C. C., Podar, M., Bullock, A. L., Graham, A. M., Brown, S. D., Somenahally, A. C., ... & Elias, D. A. (2013). Mercury methylation by novel microorganisms from new environments. Environmental Science & Technology, 47(20), 11810-11820. https://doi.org/10.1021/es403075t

Good, P. (2005). Permutation, parametric and bootstrap tests of hypotheses (3rd ed.). Springer. https://doi.org/10.1007/b138696

Gower, J. C. (1966). Some distance properties of latent root and vector methods. Biometrika, 53, 325-338.

Grice, E. A., Kong, H. H., Renaud, G., Young, A. C., Bouffard, G. G., Blakesley, R. W., ... & Segre, J. A. (2008). A diversity profile of the human skin microbiota. Genome Research, 18(7), 1043-1050. https://doi.org/10.1101/gr.075549.107

Griffiths, E., & Gupta, R. S. (2007). Identification of signature proteins that are distinctive of the Deinococcus-Thermus phylum. International Microbiology, 10(3), 201-208.

Grégoire, D. S., Lavoie, N. C., & Poulain, A. J. (2018). Heliobacteria reveal fermentation as a key pathway for mercury reduction in anoxic environments. Environmental Science & Technology, 52(7), 4145-4153. https://doi.org/10.1021/acs.est.8b00320

Gu, B., Bian, Y., Miller, C. L., Dong, W., Jiang, X., & Liang, L. (2011). Mercury reduction and complexation by natural organic matter in anoxic environments. Proceedings of the National Academy of Sciences, 108(4), 1479–1483. https://doi.org/10.1073/pnas.1008747108

Guo, H., Nasir, M., Lv, J., Dai, Y., & Gao, J. (2017). Understanding the variation of microbial community in heavy metals contaminated soil using high throughput sequencing. Ecotoxicology and Environmental Safety, 144, 300-306. https://doi.org/10.1016/j.ecoenv.2017.06.048

Guo, Y., Cheng, S., Fang, H., Geng, J., Li, Y., Shi, F., ... & Zhou, Y. (2024). Copper and cadmium co-contamination increases the risk of nitrogen loss in red paddy soils. Journal of Hazardous Materials, 479, 135626. https://doi.org/10.1016/j.jhazmat.2024.135626

Gupta, P., & Diwan, B. (2017). Bacterial exopolysaccharide mediated heavy metal removal: A review on biosynthesis, mechanism and remediation strategies. Environmental Technology & Innovation, 5, 336-353. https://doi.org/10.1016/j.eti.2017.07.007

Handy, R. D., Clark, N. J., Hutt, L. P., & Bescós, R. (2023). The microbiomes of wildlife and chemical pollution: Status, knowledge gaps and challenges. Current Opinion in Toxicology, 36, 100428. https://doi.org/10.1016/j.cotox.2023.100428

Hao, X., Zhu, J., Rensing, C., Liu, Y., Gao, S., Chen, W., ... & Liu, Y. R. (2020). Recent advances in exploring the heavy metal(loid) resistant microbiome. Computational and Structural Biotechnology Journal, 19, 94-109. https://doi.org/10.1016/j.csbj.2020.12.006

Harrison, X. A., Price, S. J., Hopkins, K., Leung, W. T. M., Sergeant, C., & Garner, T. W. J. (2017). Host microbiome richness predicts resistance to disturbance by pathogenic infection in a vertebrate host [Preprint]. bioRxiv. https://doi.org/10.1101/158428

Harrell, F. E., Jr. (2024). Hmisc: Harrell miscellaneous (Version 5.x) [R package]. CRAN. https://CRAN.R-project.org/package=Hmisc

Heaton-Jones, T. G., Homer, B. L., Heaton-Jones, D. L., & Sundlof, S. F. (1997). Mercury distribution in American alligators (Alligator mississippiensis) in Florida. Journal of Zoo and Wildlife Medicine, 28(1), 62-70.

Hoang, D. T., Chernomor, O., von Haeseler, A., Minh, B. Q., & Vinh, L. S. (2018). UFBoot2: Improving the ultrafast bootstrap approximation. Molecular Biology and Evolution, 35(2), 518-522. https://doi.org/10.1093/molbev/msx281

Holum, J. R. (1983). Elements of General and Biological Chemistry (7th ed.). Wiley.

Hu, M. Y., Yu, Q. Z., Lin, J. Q., & Fang, S. G. (2022). Sexual dimorphism of the gut microbiota in the Chinese alligator and its convergence in the wild environment. International Journal of Molecular Sciences, 23(20), 12140. https://doi.org/10.3390/ijms232012140

Huchzermeyer, F. W. (2003). Crocodiles: Biology, husbandry and diseases. CABI. ISBN 978-0-85199-656-1.

Huang, C., Zhuo, F., Han, B., Li, W., Jiang, B., Zhang, K., Jian, X., Chen, Z., Li, H., Huang, H., Dou, X., & Yu, B. (2023). The updates and implications of cutaneous microbiota in acne. Cell & Bioscience, 13(1), 113. https://doi.org/10.1186/s13578-023-01072-w

Isberg, S. (2018). Possible chinks in the crocodile armour: Defining skin microflora. AgriFutures Australia.

Islam, W., Noman, A., Naveed, H., Huang, Z., & Chen, H. Y. H. (2020). Role of environmental factors in shaping the soil microbiome. Environmental Science and Pollution Research, 27(33), 41225-41247. https://doi.org/10.1007/s11356-020-10471-2

Jaccard, P. (1912). The distribution of the flora in the alpine zone. New Phytologist, 11(2), 37-50. https://doi.org/10.1111/j.1469-8137.1912.tb05611.x

Jiang, H., Luo, S., Zhou, J., Huang, W., Li, L., Zhang, X., ... & Chen, J. (2022). Skin microbiota was altered in crocodile lizards (Shinisaurus crocodilurus) with skin ulcer. Frontiers in Veterinary Science, 9, 817490. https://doi.org/10.3389/fvets.2022.817490

Jiang, H., Lv, M., He, T., Xie, M., Zhao, Z., He, J., ... & Chen, J. (2025). Effects of ex situ conservation on commensal bacteria of crocodile lizard and conservation implications. Veterinary Quarterly, 45(1), 1-14. https://doi.org/10.1080/01652176.2025.2463704

Johnson, H., Cho, H., & Choudhary, M. (2019). Bacterial heavy metal resistance genes and bioremediation potential. Computational Molecular Bioscience, 9(1), 1-12. https://doi.org/10.4236/cmb.2019.91001

Johnston, M. A., Porter, D. E., & Scott, G. I. (2010). Isolation of faecal coliform bacteria from the American alligator (Alligator mississippiensis). Journal of Applied Microbiology, 108(3), 965–973. https://doi.org/10.1111/j.1365-2672.2009.04498.x

Kalyaanamoorthy, S., Minh, B. Q., Wong, T. K. F., von Haeseler, A., & Jermiin, L. S. (2017). ModelFinder: Fast model selection for accurate phylogenetic estimates. Nature Methods, 14(6), 587-589. https://doi.org/10.1038/nmeth.4285

Kane, A. L., Al-Shayeb, B., Holec, P. V., Rajan, S., Le Mieux, N. E., Heinsch, S. C., & Naviaux, R. K. (2016). Toward bioremediation of methylmercury using silica-encapsulated Escherichia coli harboring the mer operon. PLOS ONE, 11(1), e0147036. https://doi.org/10.1371/journal.pone.0147036

Keenan, S. W., & Elsey, R. M. (2015). The good, the bad, and the unknown: Microbial symbioses of the American alligator. Integrative and Comparative Biology, 55(6), 972-985. https://doi.org/10.1093/icb/icv006

Keenan, S. W., Engel, A. S., & Elsey, R. M. (2013). The alligator gut microbiome and implications for archosaur symbioses. Scientific Reports, 3, 2877. https://doi.org/10.1038/srep02877

Kembel, S. W., Cowan, P. D., Helmus, M. R., Cornwell, W. K., Morlon, H., Ackerly, D. D., ... & Webb, C. O. (2010). Picante: R tools for integrating phylogenies and ecology. Bioinformatics, 26(11), 1463-1464.

Kerin, E. J., Gilmour, C. C., Roden, E., Suzuki, M. T., Coates, J. D., & Mason, R. P. (2006). Mercury methylation by dissimilatory iron-reducing bacteria. Applied and Environmental Microbiology, 72(12), 7919-7921. https://doi.org/10.1128/AEM.01602-06

Khan, B., & Tansel, B. (2000). Mercury bioconcentration factors in American alligators (Alligator mississippiensis) in the Florida Everglades. Ecotoxicology and Environmental Safety, 47(1), 54-58. https://doi.org/10.1006/eesa.2000.1923

Khan, I., Huang, Z., Liang, L., Li, N., Ali, Z., Ding, L., ... & Shi, H. (2021). Ammonia stress influences intestinal histomorphology, immune status and microbiota of Chinese striped-neck turtle (Mauremys sinensis). Ecotoxicology and Environmental Safety, 222, 112471. https://doi.org/10.1016/j.ecoenv.2021.112471

Kieran, T. J., Goodman, S. J., Finger, J. W., Thomas, J. C., Hamilton, M. T., Tuberville, T. D., & Glenn, T. C. (2020). Microbiota of four tissue types in American alligators (Alligator mississippiensis) following extended dietary selenomethionine exposure. Bulletin of Environmental Contamination and Toxicology, 105(3), 381-386. https://doi.org/10.1007/s00128-020-02961-3

Kirsch, M. R., Smith, S. N., McMillan, B. R., & Lanier, H. C. (2024). Family shapes microbiome differences in Oklahoma salamanders. Frontiers in Microbiomes, 3, 1277645. https://doi.org/10.3389/frmbi.2024.1277645

Kocman, D., Wilson, S. J., Amos, H. M., Telmer, K. H., Steenhuisen, F., Sunderland, E. M., ... & Horvat, M. (2017). Toward an assessment of the global inventory of present-day mercury releases to freshwater environments. International Journal of Environmental Research and Public Health, 14(2), 138. https://doi.org/10.3390/ijerph14020138

Kolde, R. (2019). pheatmap: Pretty Heatmaps (Version 1.0.12) [R package]. https://CRAN.R-project.org/package=pheatmap

Kou, B., He, Y., Wang, Y, Qu, C., Tang, J., Wu, Y., ... & Yu, T. (2023). The relationships between heavy metals and bacterial communities in a coal gangue site. Environmental Pollution, 322, 121136. https://doi.org/10.1016/j.envpol.2023.121136

Krout, I. N., Polacco, B. J., Skoglund, C. M., Williams, K. H., Barkay, T., & Elias, D. A. (2022). Organomercurial lyase (MerB)–mediated demethylation decreases bacterial methylmercury resistance in the absence of mercuric reductase (MerA). Applied and Environmental Microbiology, 88(7), e00010-22. https://doi.org/10.1128/aem.00010-22

Kruskal, J. B. (1964). Nonmetric multidimensional scaling. Psychometrika, 29, 1-27.

Kruskal, W. H., & Wallis, W. A. (1952). Use of ranks in one-criterion variance analysis. Journal of the American Statistical Association, 47, 583-621.

Kueneman, J. G., Parfrey, L. W., Woodhams, D. C., Archer, H. M., Knight, R., & McKenzie, V. J. (2014). The amphibian skin-associated microbiome across species, space and life history stages. Molecular Ecology, 23(6), 1238-1250. https://doi.org/10.1111/mec.12510

Kuo, J., Liu, D., Wen, W. H., Chiu, C. Y., Chen, W., Wu, Y. W., ... & Lin, C. H. (2023). Different microbial communities in paddy soils under organic and nonorganic farming. Brazilian Journal of Microbiology, 55(1), 777-788. https://doi.org/10.1007/s42770-023-01218-5

Lal, D., & Lal, R. (2010). Evolution of mercuric reductase (merA) gene: A case of horizontal gene transfer. Microbiology, 79(4), 500-508. https://doi.org/10.1134/S0026261710040120

Lavoie, R. A., Jardine, T. D., Chumchal, M. M., Kidd, K. A., & Campbell, L. M. (2013). Biomagnification of mercury in aquatic food webs: A worldwide meta-analysis. Environmental Science & Technology, 47(23), 13385-13394. https://doi.org/10.1021/es403103t

Legendre, P., & Legendre, L. (2012). Numerical ecology (3rd English ed.). Elsevier.

Legendre, P., & Gallagher, E. D. (2001). Ecologically meaningful transformations for ordination of species data. Oecologia, 129, 271-280.

Legg, K., Ouboter, P., et al. (2015). Mercury in the aquatic environment of the Guiana Shield. Ambio, 44(S2), 692-702.

Lemaire, J. (2023). Using crocodylians for monitoring mercury in the tropics. Ecotoxicology, 32(8), 977-993. https://doi.org/10.1007/s10646-023-02703-1

Lemaire, J., Brischoux, F., Marquis, O., Mangione, R., Caut, S., Brault-Favrou, M., ... & Bustamante, P. (2022). Relationships between stable isotopes and trace element concentrations in the crocodilian community of French Guiana. Science of the Total Environment, 837, 155846. https://doi.org/10.1016/j.scitotenv.2022.155846

Lemaire, J., Bustamante, P., & Shirley, M. H. (2024). Preliminary assessment of blood mercury contamination in four African crocodile species. Environment International, 190, 108877. https://doi.org/10.1016/j.envint.2024.108877

Lemaire, J., Bustamante, P., Marquis, O., Caut, S., & Brischoux, F. (2021). Influence of sex, size and trophic level on blood Hg concentrations in Black caiman, Melanosuchus niger (Spix, 1825) in French Guiana. Chemosphere, 262, 127819. https://doi.org/10.1016/j.chemosphere.2020.127819

Lemaire, J., Mangione, R., Caut, S., & Bustamante, P. (2024). Mercury biomagnification in the food web of Agami Pond, Kaw-Roura Nature Reserve, French Guiana. Heliyon, 10(7), e28859. https://doi.org/10.1016/j.heliyon.2024.e28859

Lenntech. (2004). Heavy metals. https://www.lenntech.com/

Letunic, I., & Bork, P. (2021). Interactive Tree Of Life (iTOL) v5: An online tool for phylogenetic tree display and annotation. Nucleic Acids Research, 49(W1), W293-W296. https://doi.org/10.1093/nar/gkab301

Li, D., Li, X., Tao, Y., Yan, Z., & Ao, Y. (2022). Deciphering the bacterial microbiome in response to long-term mercury contaminated soil. Ecotoxicology and Environmental Safety, 229, 113062. https://doi.org/10.1016/j.ecoenv.2021.113062

Li, Y., & Cai, Y. (2013). Progress in the study of mercury methylation and demethylation in aquatic environments. Chinese Science Bulletin, 58(2), 177-185. https://doi.org/10.1007/s11434-012-5416-4

Lin, M., Zeng, C., Li, Z., Ma, Y., & Jia, X. (2019). Comparative analysis of the composition and function of fecal-gut bacteria in captive juvenile Crocodylus siamensis between healthy and anorexic individuals. MicrobiologyOpen, 8(12), e929. https://doi.org/10.1002/mbo3.929

Lin, X., Zhao, J., Zhang, W., He, L., Wang, L., Chang, D., ... & Li, Y.-F. (2020). Acute oral methylmercury exposure perturbs the gut microbiome and alters gut-brain axis related metabolites in rats. Ecotoxicology and Environmental Safety, 190, 110130. https://doi.org/10.1016/j.ecoenv.2019.110130

Lin, Y., Wang, L., Xu, K., Li, K., & Ren, H. (2021). Revealing taxon-specific heavy metal-resistance mechanisms in denitrifying phosphorus removal sludge using genome-centric metaproteomics. Microbiome, 9, 67. https://doi.org/10.1186/s40168-021-01016-x

Lin, Y., Ye, Y., Hu, Y., & Shi, H. (2019). The variation in microbial community structure under different heavy metal contamination levels in paddy soils. Ecotoxicology and Environmental Safety, 180, 557-564. https://doi.org/10.1016/j.ecoenv.2019.05.057

Lin, Z., He, M., Zhong, C., Li, Y., Tang, S., Kang, X., & Wu, Z. (2023). Responses of gut microbiota in crocodile lizards (Shinisaurus crocodilurus) to changes in temperature. Frontiers in Microbiology, 14, 1263917. https://doi.org/10.3389/fmicb.2023.1263917

Liu, J., Chen, J., Poulain, A. J., Pu, Q., Hao, Z., Meng, B., & Feng, X. (2023). Mercury and sulfur redox cycling affect methylmercury levels in rice paddy soils across a contamination gradient. Environmental Science & Technology, 57(21), 8149-8160. https://doi.org/10.1021/acs.est.3c02676

Liu, Y.-R., Delgado-Baquerizo, M., Bi, L., Zhu, J., & He, J.-Z. (2018). Consistent responses of soil microbial taxonomic and functional attributes to mercury pollution across China. Microbiome, 6, 183. https://doi.org/10.1186/s40168-018-0572-7

Liu, Y.-R., Wang, J.-J., Zheng, Y.-M., Zhang, L.-M., & He, J.-Z. (2014). Patterns of bacterial diversity along a long-term mercury-contaminated gradient in paddy soils. Microbial Ecology, 68(3), 575-583. https://doi.org/10.1007/s00248-014-0430-5

Liu, Y., Wang, F., Zhang, X., & Song, N. (2010). Effects of mercury on nitrification in wastewater treatment. Journal of Hazardous Materials, 175(1-3), 122-128. https://doi.org/10.1016/j.jhazmat.2009.10.050

Locatelli, F. M., Goo, K. S., & Ulanova, D. (2016). Effects of trace metal ions on secondary metabolism and the morphological development of streptomycetes. Metallomics, 8(5), 469-480. https://doi.org/10.1039/c5mt00324e

Love, M. I., Huber, W., & Anders, S. (2014). Moderated estimation of fold change and dispersion for RNA-seq data with DESeq2. Genome Biology, 15(12), 550. https://doi.org/10.1186/s13059-014-0550-8

Lovely, C. J., & Leslie, A. J. (2008). Normal intestinal flora of wild Nile crocodiles (Crocodylus niloticus) in the Okavango Delta, Botswana. Journal of the South African Veterinary Association, 79(2), 67-70. https://journals.jsava.aosis.co.za/index.php/jsava/article/view/246

Magnino, S., Colin, P., Dei-Cas, E., Madsen, M., McLauchlin, J., Nöckler, K., Prieto Maradona, M., Tsigarida, E., Vanopdenbosch, E., & Van Peteghem, C. (2009). Biological risks associated with consumption of reptile products. International Journal of Food Microbiology, 134(3), 163–175. https://doi.org/10.1016/j.ijfoodmicro.2009.07.001

Mahbub, K. R., King, W. L., Siboni, N., Nguyen, V. K., Rahman, M. M., Megharaj, M., ... & Labbate, M. (2020). Long-lasting effect of mercury contamination on the soil microbiota and its co-selection of antibiotic resistance. Environmental Pollution, 265, 115057. https://doi.org/10.1016/j.envpol.2020.115057

Mahbub, K. R., Subashchandrabose, S. R., Krishnan, K., Naidu, R., & Megharaj, M. (2017). Mercury alters the bacterial community structure and diversity in soil even at concentrations lower than the guideline values. Applied Microbiology and Biotechnology, 101(5), 2163-2175. https://doi.org/10.1007/s00253-016-7965-y

Marupakula, S., Mahmood, S., & Finlay, R. D. (2016). Analysis of single root tip microbiomes suggests that distinctive bacterial communities are selected by Pinus sylvestris roots colonized by different ectomycorrhizal fungi. Environmental Microbiology, 18(5), 1470-1483. https://doi.org/10.1111/1462-2920.13102

Mason, R. P., & Sheu, G.-R. (2002). Role of the ocean in the global mercury cycle. Global Biogeochemical Cycles, 16(4), 40-1-40-14. https://doi.org/10.1029/2001GB001440

Mathema, V. B., Thakuri, B. C., & Sillanpää, M. (2011). Bacterial mer operon-mediated detoxification of mercurial compounds: A short review. Archives of Microbiology, 193(12), 837-844. https://doi.org/10.1007/s00203-011-0751-4

May, K., Stoeppler, M., & Reisinger, K. (1987). Studies in the ratio total mercury/methylmercury in the aquatic food chain. Toxicological & Environmental Chemistry, 13(3-4), 153-159. https://doi.org/10.1080/02772248709357178

McDevitt-Irwin, J. M., Garren, M., McMinds, R., Vega Thurber, R., & Baum, J. K. (2019). Variable interaction outcomes of local disturbance and El Niño-induced heat stress on coral microbiome alpha and beta diversity. Coral Reefs, 38(2), 331–345. https://doi.org/10.1007/s00338-019-01780-3

Mildvan, A. S. (1970). Enzymes. In P. Boyer (Ed.), The Enzymes (3rd ed.). Academic Press.

Minh, B. Q., Schmidt, H. A., Chernomor, O., Schrempf, D., Woodhams, M. D., von Haeseler, A., & Lanfear, R. (2020). IQ-TREE 2: New models and efficient methods for phylogenetic inference in the genomic era. Molecular Biology and Evolution, 37(5), 1530-1534. https://doi.org/10.1093/molbev/msaa015

Mitchell, H. M., Rocha, G. A., Kaakoush, N. O., O'Rourke, J. L., & Queiroz, D. M. M. (2014). The family Helicobacteraceae. In E. Rosenberg et al. (Eds.), The Prokaryotes (pp. 337-392). Springer. https://doi.org/10.1007/978-3-642-39044-9_275

Moeller, A. H., Ivey, K., Cornwall, M. B., Herr, K., Rede, J., Taylor, E. N., & Gunderson, A. R. (2020). The lizard gut microbiome changes with temperature and is associated with heat tolerance. Applied and Environmental Microbiology, 86(17), e01181-20. https://doi.org/10.1128/AEM.01181-20

Morvan, C., Folgosa, F., Kint, N., Teixeira, M., & Martin-Verstraete, I. (2021). Responses of Clostridia to oxygen: From detoxification to adaptive strategies. Environmental Microbiology, 23(8), 4112-4125. https://doi.org/10.1111/1462-2920.15665

Müller, A. K., Westergaard, K., Christensen, S., & Sørensen, S. J. (2001). The effect of long-term mercury pollution on the soil microbial community. FEMS Microbiology Ecology, 36(1), 11-19. https://doi.org/10.1111/j.1574-6941.2001.tb00821.x

Narita, M., Chiba, K., Nishizawa, H., Ishii, H., Huang, C.-C., Kawabata, Z.-I., Silver, S., & Endo, G. (2003). Diversity of mercury resistance determinants among Bacillus strains isolated from sediment of Minamata Bay. FEMS Microbiology Letters, 223(1), 73-82. https://doi.org/10.1016/S0378-1097(03)00325-2

Nascimento, A. M. A., & Chartone-Souza, E. (2003). Operon mer: Bacterial resistance to mercury and potential for bioremediation of contaminated environments. Genetics and Molecular Research, 2(1), 92-101.

Neutel, A. M., Heesterbeek, J. A. P., & de Ruiter, P. C. (2002). Stability in real food webs: Weak links in long loops. Science, 296(5570), 1120-1123. https://doi.org/10.1126/science.1068326

Nies, D. H. (2003). Efflux-mediated heavy metal resistance in prokaryotes. FEMS Microbiology Reviews, 27(2-3), 313-339. https://doi.org/10.1016/S0168-6445(03)00048-2

Nies, D. H. (1999). Microbial heavy-metal resistance. Applied Microbiology and Biotechnology, 51, 730-750. https://doi.org/10.1007/s002530051457

Núñez-Otaño, N. B., Ignacio Piña, C., Gonçalves Portelinha, T. C., & Margarita Arambarri, A. (2013). Cloacal mycobiota in wild females of Caiman latirostris (Crocodylia: Alligatoridae). Revista Mexicana de Biodiversidad, 84(2), 722–726. https://doi.org/10.7550/rmb.32425

Oksanen, J., Simpson, G. L., Blanchet, F. G., Kindt, R., Legendre, P., Minchin, P. R., ... & Wagner, H. (2024). vegan: Community Ecology Package (Version 2.6-x) [R package]. https://CRAN.R-project.org/package=vegan

Osborn, A. M., Bruce, K. D., Strike, P., & Ritchie, D. A. (1997). Distribution, diversity and evolution of the bacterial mercury resistance (mer) operon. FEMS Microbiology Reviews, 19(4), 239-262. https://doi.org/10.1111/j.1574-6976.1997.tb00300.x

O'Shaughnessy-Hunter, L. C. (2021). Longitudinal study of the cutaneous microbiota of healthy horses (Master's thesis, University of Guelph)

Oregaard, G., & Sørensen, S. J. (2007). High diversity of bacterial mercuric reductase genes from surface and sub-surface floodplain soil (Oak Ridge, USA). The ISME Journal, 1(5), 453–467. https://doi.org/10.1038/ismej.2007.56

Padfield, D., Kay, S., Vos, R., Quince, C., & Vos, M. (2024). Macroevolutionary dynamics in micro-organisms: Generalists give rise to specialists across biomes in the ubiquitous bacterial phylum

Myxococcota. Molecular Biology and Evolution, 41(5), msae088. https://doi.org/10.1093/molbev/msae088

Pagès, H., Aboyoun, P., Gentleman, R., & DebRoy, S. (2024). Biostrings: Efficient manipulation of biological strings (Version 2.76.0) [R package]. Bioconductor. https://bioconductor.org/packages/Biostrings

Pal, C., Bengtsson-Palme, J., Kristiansson, E., & Larsson, D. G. J. (2015). Co-occurrence of resistance genes to antibiotics, biocides and metals reveals novel insights into their co-selection potential. BMC Genomics, 16, 964. https://doi.org/10.1186/s12864-015-2153-5

Panahi, P., Afsharnia, M., Nazmara, S., & Jafari, S. (2022). Relationship between mer genes and methylmercury in sediments: A review. Science of the Total Environment, 827, 154361. https://doi.org/10.1016/j.scitotenv.2022.154361

Parada, A. E., Needham, D. M., & Fuhrman, J. A. (2016). Every base matters: Assessing small subunit rRNA primers for marine microbiomes with mock communities, time series and global field samples. Environmental Microbiology, 18(5), 1403-1414. https://doi.org/10.1111/1462-2920.13023

Paranjape, A. R., & Hall, B. D. (2017). Recent advances in the study of mercury methylation in aquatic ecosystems. FACETS, 2(1), 85–119. https://doi.org/10.1139/facets-2016-0027

Parks, D. H., Chuvochina, M., Waite, D. W., Rinke, C., Skarshewski, A., Chaumeil, P.-A., & Hugenholtz, P. (2018). A standardized bacterial taxonomy based on genome phylogeny substantially revises the tree of life. Nature Biotechnology, 36(10), 996-1004. https://doi.org/10.1038/nbt.4229

Parks, J. M., Johs, A., Podar, M., Bridou, R., Hurt, R. A., Smith, S. D., ... & Liang, L. (2013). The genetic basis for bacterial mercury methylation. Science, 339(6125), 1332-1335. https://doi.org/10.1126/science.1230667

Pepi, M., Gaggi, C., Bernardini, E., Focardi, S., Lobianco, A., Ruta, M., ... & Focardi, S. E. (2011). Mercury-resistant bacterial strains Pseudomonas and Psychrobacter spp. isolated from sediments of Orbetello Lagoon (Italy) and their possible use in bioremediation processes. International Biodeterioration & Biodegradation, 65(1), 85-91. https://doi.org/10.1016/j.ibiod.2010.09.006

Peres-Neto, P. R., Legendre, P., Dray, S., & Borcard, D. (2006). Variation partitioning of species data matrices: Estimation and comparison of fractions. Ecology, 87(10), 2614-2625. https://doi.org/10.1890/0012-9658(2006)87[2614:VPOSDM]2.0.CO;2

Pielou, E. C. (1966). The measurement of diversity in different types of biological collections. Journal of Theoretical Biology, 13, 131-144.

Pirrone, N., Cinnirella, S., Feng, X., Finkelman, R. B., Friedli, H. R., Leaner, J., Mason, R., Mukherjee, A. B., Stracher, G. B., Streets, D. G., & Telmer, K. (2010). Global mercury emissions to the atmosphere from anthropogenic and natural sources. Atmospheric Chemistry and Physics, 10(13), 5951–5964. https://doi.org/10.5194/acp-10-5951-2010

Podar, M., Gilmour, C. C., Brandt, C. C., Soren, A., Brown, S. D., Crable, B. R., ... & Elias, D. A. (2015). Global prevalence and distribution of genes and microorganisms involved in mercury methylation. Science Advances, 1(9), e1500675. https://doi.org/10.1126/sciadv.1500675

Polti, M. A., Amoroso, M. J., & Abate, C. M. (2007). Chromium(VI) resistance and removal by actinomycete strains isolated from sediments. Chemosphere, 67(4), 660-667. https://doi.org/10.1016/j.chemosphere.2006.11.008

Poulain, A. J., Aris-Brosou, S., Blais, J. M., Brazeau, M., Keller, W., & Paterson, A. M. (2015). Microbial DNA records historical delivery of anthropogenic mercury. The ISME Journal, 9(12), 2541-2550. https://doi.org/10.1038/ismej.2015.86

Quast, C., Pruesse, E., Yilmaz, P., Gerken, J., Schweer, T., Yarza, P., ... & Glöckner, F. O. (2013). The SILVA ribosomal RNA gene database project: Improved data processing and web-based tools. Nucleic Acids Research, 41(D1), D590-D596. https://doi.org/10.1093/nar/gks1219

Radeva, G., Kenarova, A., Bachvarova, V., Flemming, K., Popov, I., Vassilev, D., SelenskaPobell, S., 2013. Bacterial diversity at abandoned uranium mining and milling sites in Bulgaria as revealed by 16s RRNA genetic diversity stud

Ralston, N. V. C., & Raymond, L. J. (2010). Dietary selenium's protective effects against methylmercury toxicity. Toxicology, 278(1), 112-123. https://doi.org/10.1016/j.tox.2010.06.004

Ralston, N. V. C., Ralston, C. R., Blackwell, J. L., & Raymond, L. J. (2008). Dietary and tissue selenium in relation to methylmercury toxicity. Neurotoxicology, 29(5), 802-811. https://doi.org/10.1016/j.neuro.2008.07.007

Ranchou-Peyruse, M., Monperrus, M., Bridou, R., Duran, R., Amouroux, D., Salvado, J.-C., & Guyoneaud, R. (2009). Overview of mercury methylation capacities among anaerobic bacteria including representatives of the sulphate-reducers: Implications for environmental studies. Geomicrobiology Journal, 26(1), 1-8. https://doi.org/10.1080/01490450802599227

Ravichandran, M. (2004). Interactions between mercury and dissolved organic matter in the aquatic environment: A review. Chemosphere, 55(3), 319-331. https://doi.org/10.1016/j.chemosphere.2003.11.011

Rocca, J. D., Simonin, M., Blaszczak, J. R., Ernakovich, J. G., Gibbons, S. M., Midani, F. S., & Washburne, A. D. (2019). The Microbiome Stress Project: Toward a global meta-analysis of environmental stressors and their effects on microbial communities. Frontiers in Microbiology, 9, 3272. https://doi.org/10.3389/fmicb.2018.03272

Ross, A. A., & Neufeld, J. D. (2015). Microbial biogeography of a university campus. Microbiome, 3, 66. https://doi.org/10.1186/s40168-015-0135-0

Ross, A. A., Rodrigues Hoffmann, A., & Neufeld, J. D. (2019). The skin microbiome of vertebrates. Microbiome, 7, 79. https://doi.org/10.1186/s40168-019-0694-6

Rowland, I., Gibson, G., Heinken, A., Scott, K., Swann, J., Thiele, I., & Tuohy, K. (2018). Gut microbiota functions: Metabolism of nutrients and other food components. European Journal of Nutrition, 57(1), 1-24. https://doi.org/10.1007/s00394-017-1445-8

Rudolf, C. A., Jaimes, A., Espinosa-Blanco, A. S., Contreras, M., & García-Amado, M. A. (2018). Oral and cloacal Helicobacter detection in wild and captive Orinoco crocodiles (Crocodylus intermedius) in Venezuela. Vector-Borne and Zoonotic Diseases, 18(10), 567-569. https://doi.org/10.1089/vbz.2017.2210

Rumbold, D., Laine, K. A., Niemczyk, S. L., Fink, L. E., Robertson, W. B., & Cox, C. (2002). Levels of mercury in alligators (Alligator mississippiensis) collected along a transect through the Florida Everglades. Science of the Total Environment, 297(1-3), 99-110. https://doi.org/10.1016/S0048-9697(02)00132-8

Sanfeliu, C., Sebastià, J., Cristòfol, R., & Rodríguez-Farré, E. (2003). Neurotoxicity of organomercurial compounds. Neurotoxicity Research, 5(4), 283-305. https://doi.org/10.1007/BF03033386

Schaefer, J. K., Letowski, J., & Barkay, T. (2002). mer-mediated resistance and volatilization of Hg(II) under anaerobic conditions. Geomicrobiology Journal, 19(1), 87-102. https://doi.org/10.1080/014904502317246192

Schaefer, J. K., Yagi, J., Reinfelder, J. R., Cardona, T., Ellickson, K. M., Tel-Or, S., & Barkay, T. (2004). Role of the bacterial organomercury lyase (MerB) in controlling methylmercury accumulation in mercury-contaminated natural waters. Environmental Science & Technology, 38(16), 4304-4311. https://doi.org/10.1021/es049895w

Schliep, K. P. (2011). phangorn: Phylogenetic analysis in R. Bioinformatics, 27, 592-593.

Selin, N. E. (2009). Global biogeochemical cycling of mercury: A review. Annual Review of Environment and Resources, 34, 43–63. https://doi.org/10.1146/annurev.environ.051308.084314

Shannon, C. E. (1948). A mathematical theory of communication. Bell System Technical Journal, 27, 379-423.

Sharma, P., & Agrawal, M. (2005). Biological effects of heavy metals: An overview. Journal of Environmental Biology, 26(2), 301-313.

Silva, J. S. A., Mota, R. A., Pinheiro Júnior, J. W., Almeida, M. C. S., Silva, D. R., Ferreira, D. R. A., & Azevedo, J. C. N. (2009). Aerobic bacterial microflora of Broad-snouted caiman (Caiman latirostris) oral cavity and cloaca, originating from Parque Zoológico Arruda Câmara, Paraíba, Brazil. Brazilian Journal of Microbiology, 40(1), 194-198. https://doi.org/10.1590/S1517-838220090001000034

Silva, S. M., Trigo, S., Cardoso, G. C., & Xavier, R. (2022). Cloaca- and feather-associated bacteria communities in common waxbills Estrilda astrild. Journal of Avian Biology, 2022(7), e02910. https://doi.org/10.1111/jav.02910

Silver, S., & Phung, L. T. (2005). A bacterial view of the periodic table: Genes and proteins for toxic inorganic ions. Journal of Industrial Microbiology & Biotechnology, 32(11-12), 587-605. https://doi.org/10.1007/s10295-005-0019-6

Smith, P. N., Cobb, G. P., Godard-Codding, C., Hoff, D., McMurry, S. T., Rainwater, T. R., & Reynolds, K. D. (2007). Contaminant exposure in terrestrial vertebrates. Environmental Pollution, 150(1), 41-64. https://doi.org/10.1016/j.envpol.2007.06.009

Smith, S. D., Bridou, R., Johs, A., Parks, J. M., Elias, D. A., Hurt, R. A., ... & Wall, J. D. (2015). Site-directed mutagenesis of HgcA and HgcB reveals amino acid residues important for mercury methylation. Applied and Environmental Microbiology, 81(9), 3205-3217. https://doi.org/10.1128/AEM.00217-15

Smith, S. N., Colston, T. J., & Siler, C. D. (2021). Venomous snakes reveal ecological and phylogenetic factors influencing variation in gut and oral microbiomes. Frontiers in Microbiology, 12, 657754. https://doi.org/10.3389/fmicb.2021.657754

Sonthiphand, P., Kraidech, S., Polart, S., Chotpantarat, S., Kusonmano, K., Uthaipaisanwong, P., Rangsiwutisak, C., & Luepromchai, E. (2021). Arsenic speciation, the abundance of arsenite-oxidizing bacteria, and microbial community structures in groundwater, surface water, and soil from a gold mine. *Journal of Environmental Science and Health, Part A*, *56*(7), 769-785. https://doi.org/10.1080/10934529.2021.192742

Sotero-Martins, A., de Jesus, M. S., Lacerda, M., Moreira, J. C., Filgueiras, A. L. L., & Barrocas, P. R. G. (2008). A conservative region of the mercuric reductase gene (merA) as a molecular marker of

bacterial mercury resistance. Brazilian Journal of Microbiology, 39(2), 307-310. https://doi.org/10.1590/S1517-838220080002000020

Spearman, C. (1904). The proof and measurement of association between two things. The American Journal of Psychology, 15(1), 72-101. https://doi.org/10.2307/1412159

Stackebrandt, E., Chertkov, O., Lapidus, A., Nolan, M., Lucas, S., Hammon, N., ... & Klenk, H.-P. (2013). Genome sequence of the free-living aerobic spirochete Turneriella parva type strain (HT), and emendation of the species Turneriella parva. Standards in Genomic Sciences, 8(2), 228-238. https://doi.org/10.4056/sigs.3617113

Strompfová, V., & Štempelová, L. (2024). Composition and diversity of 16S rRNA based skin bacterial microbiome in healthy horses. Veterinary Research Communications, 48(4), 2847-2855. https://doi.org/10.1007/s11259-024-10444-7

Su, R., Zhang, S., Zhang, X., Wang, S., & Zhang, W. (2023). Neglected skin-associated microbial communities: A unique immune defense strategy of Bufo raddei under environmental heavy metal pollution. Environmental Science and Pollution Research, 30(9), 22330-22342. https://doi.org/10.1007/s11356-022-23803-1

Sun, K., Li, W., Fan, G., Yang, L., Zhang, H., Shu, Y., Zhou, Y., Tu, G., Zhang, S., Yi, P., Ayub, M., Wu, X., & Pan, T. (2024). Ecological Networks of Allometric Growth, Feeding Behavior and Gut Microbiota in Chinese Alligator Hatchlings. Asian Herpetological Research, 15(2), 104–114. https://doi.org/10.3724/ahr.2095-0357.2024.0010

Tan, S., Xu, X., Cheng, H., Wang, J., & Wang, X. (2022). The alteration of gut microbiome community plays an important role in mercury biotransformation in largemouth bass. Environmental Research, 204(Pt A), 112026. https://doi.org/10.1016/j.envres.2021.112026

Tavaré, S. (1986). Some probabilistic and statistical problems in the analysis of DNA sequences. In Lectures on Mathematics in the Life Sciences (Vol. 17, pp. 57-86).

Thermo Fisher Scientific. (2012). NanoDrop Spectrophotometers: Nucleic Acid Concentration and Purity. Application Note. https://assets.thermofisher.com/

Thompson, J. D., Higgins, D. G., & Gibson, T. J. (1994). CLUSTAL W: Improving the sensitivity of progressive multiple sequence alignment through sequence weighting, position-specific gap penalties and weight matrix choice. Nucleic Acids Research, 22(22), 4673-4680. https://doi.org/10.1093/nar/22.22.4673

Trojańska, A., Felis, E., Wróbel, J., & Bajkacz, S. (2022). Phenotypic mercury resistance versus merA presence—A review. Microorganisms, 10(5), 988. https://doi.org/10.3390/microorganisms10050988

Turutoglu, H., Ercelik, S., & Corlu, M. (2005). Aeromonas hydrophila-associated skin lesions and septicaemia in a Nile crocodile (Crocodylus niloticus). Journal of the South African Veterinary Association, 76(1), 40-42. https://doi.org/10.4102/jsava.v76i1.393

Ullrich, S. M., Tanton, T. W., & Abdrashitova, S. A. (2001). Mercury in the aquatic environment: A review of factors affecting methylation. Critical Reviews in Environmental Science and Technology, 31(3), 241-293. https://doi.org/10.1080/20016491111730

van Dongen, W. F., White, J., Brandl, H. B., Moodley, Y., Merkling, T., Leclaire, S., Blanchard, P., Danchin, É., Hatch, S. A., & Wagner, R. H. (2013). Age-related differences in the cloacal microbiota of a wild bird species. BMC Ecology, 13, 11. https://doi.org/10.1186/1472-6785-13-11

Veiga, M. M., Maxson, P. A., & Hylander, L. D. (2014). Review of barriers to reduce mercury use in artisanal gold mining. The Extractive Industries and Society, 1(2), 351–361. https://doi.org/10.1016/j.exis.2014.03.004

Vishnivetskaya, T. A., Hu, H., Van Nostrand, J. D., Wymore, A. M., Xu, X., Qiu, G., et al. (2018). Microbial community structure with trends in methylation gene diversity and abundance in mercury-contaminated rice paddy soils in Guizhou, China. Environ. Sci. Process. Impacts 20, 673-685. doi: 10.1039/c7em 00558j

von Canstein, H., Li, Y., Timmis, K. N., & Deckwer, W. D. (1999). Removal of mercury from chlor-alkali electrolysis wastewater by a mercury-resistant Pseudomonas putida strain. Applied and Environmental Microbiology, 65(12), 5271-5275.

Wang, X., Mi, J., Yang, K., & Wang, L. (2023). Environmental cadmium exposure perturbs gut microbial dysbiosis in ducks. Veterinary Sciences, 10(11), 649. https://doi.org/10.3390/vetsci10110649

Wang, Y., Boyd, E., Crane, S., Lu-Irving, P., Krabbenhoft, D., King, S., Dighton, J., Geesey, G., & Barkay, T. (2011). Environmental Conditions Constrain the Distribution and Diversity of Archaeal merA in Yellowstone National Park, Wyoming, U.S.A. Microbial Ecology, 62(4), 739–752. https://doi.org/10.1007/s00248-011-9890-z

Watkins, C. A., Gaines, T., Strathdee, F., Baily, J. L., Watson, E., Hall, A. J., Free, A., & Dagleish, M. P. (2022). A comparative study of the fecal microbiota of gray seal pups and yearlings - a marine mammal sentinel species. MicrobiologyOpen, 11(3), e1281. https://doi.org/10.1002/mbo3.1281

Wells, E. M., Kopylev, L., Nachman, R., Radke, E. G., Congleton, J., & Segal, D. (2022). Total blood mercury predicts methylmercury exposure in fish and shellfish consumers. Biological Trace Element Research, 200(8), 3867-3875. https://doi.org/10.1007/s12011-021-02968-9

Wilcoxon, F. (1945). Individual comparisons by ranking methods. Biometrics Bulletin, 1, 80-83.

Williams, C. E., Hammer, T. J., & Williams, C. L. (2024). Diversity alone does not reliably indicate the healthiness of an animal microbiome. The ISME Journal, 18(1), wrae133. https://doi.org/10.1093/ismejo/wrae133

Williams, T. J., Allen, M. A., Berengut, J. F., & Cavicchioli, R. (2021). Shedding light on microbial 'dark matter': Insights into novel Cloacimonadota and Omnitrophota from an Antarctic lake. Frontiers in Microbiology, 12, 741077. https://doi.org/10.3389/fmicb.2021.741077

Willson, N. L., Van, T. T. H., Lever, J., Moore, R. J., & Stanley, D. (2019). Characterisation of the intestinal microbiota of commercially farmed saltwater crocodiles, Crocodylus porosus. Applied Microbiology and Biotechnology, 103(21), 8977-8985. https://doi.org/10.1007/s00253-019-10143-3

Wright, E. S. (2015). DECIPHER: Harnessing local sequence context to improve protein multiple sequence alignment. BMC Bioinformatics, 16, 322.

Xiao, S., Zhang, Q., Chen, X., Dong, F., Chen, H., Liu, M., & Ali, I. (2019). Speciation distribution of heavy metals in uranium mining impacted soils and impact on bacterial community revealed by high-throughput sequencing. Frontiers in Microbiology, 10, 1867. https://doi.org/10.3389/fmicb.2019.01867

Yanochko, G. M., Jagoe, C. H., & Brisbin, I. L. (1997). Tissue mercury concentrations in alligators (Alligator mississippiensis) from the Florida Everglades and the Savannah River Site, South Carolina. Archives of Environmental Contamination and Toxicology, 32(3), 323-328. https://doi.org/10.1007/s002449900192

Yu, K. B., Chandra, F., Coley-O'Rourke, E. J., Paulson, E. T., Novoselov, A., Zhang, D., Finnigan, D., Paramo, J., Lopez-Romero, A., Dong, T. S., Schartup, A. T., & Hsiao, E. Y. (2025). An engineered gut bacterium protects against dietary methylmercury exposure in pregnant mice. Cell Host & Microbe, 33(5), 621-631.e7. https://doi.org/10.1016/j.chom.2025.04.009

Yu, Q.-Z., Hu, M.-Y., Wang, L., Lin, J.-Q., & Fang, S.-G. (2022). Incubation determines favorable microbial communities in Chinese alligator nests. Frontiers in Microbiology, 13, 983808. https://doi.org/10.3389/fmicb.2022.983808

Zhang, H., Li, W., Tu, G., Sun, K., Yang, L., Wang, Z., Wu, Z., Zhou, Y., Zhang, S., Sun, H., Sheng, C., Wang, X., Zhang, R., Wu, X., & Pan, T. (2023). Host Genetic Background Impacts Microbiome Composition in Newborn Alligator. Asian Herpetological Research, 14(3), 237–245. https://doi.org/10.3724/ahr.2095-0357.2023.0007

Zhang, Y., Zhang, P., & Li, Y. (2022). Gut microbiota-mediated ferroptosis contributes to mercury exposure-induced brain injury in common carp. Metallomics, 14(1), mfab072. https://doi.org/10.1093/mtomcs/mfab072

Zhao, X., Huang, J., Lu, J., & Sun, Y. (2020). Ecological effects of heavy metal pollution on soil microbial community structure and diversity in Karamay, China. Toxics, 8(3), 58. https://doi.org/10.3390/toxics8030058

Zheng, X., Cao, H., Liu, B., Zhang, M., Zhang, C., Chen, P, & Yang, B. (2022). Effects of mercury contamination on microbial diversity of different kinds of soil. Microorganisms, 10(5), 977. https://doi.org/10.3390/microorganisms10050977

Zhou, F., Zhang, J., Gong, L., Wang, G., Khan, A., & Cui, H. (2023). Infection caused by Lawsonella clevelandensis after breast augmentation with autologous fat grafting: A case report. BMC Infectious Diseases, 23(1), 124. https://doi.org/10.1186/s12879-022-07812-6

Zuo, Y., Li, Y., Chen, H., Ran, G., & Liu, X. (2023). Effects of multi-heavy metal composite pollution on microorganisms around a lead–zinc mine in typical karst areas, southwest China. Ecotoxicology and Environmental Safety, 262, 115190. https://doi.org/10.1016/j.ecoenv.2023.115190